Laboratory Testing of Historic Mortars: Part 1 - A Close Look to a 200-year-old Historic Clay-Lime Mortar

Dipayan Jana[1] and Shubham N. Mahajan[2]

INTRODUCTION

Built originally in 1820s Wetherill Barn (Figure 1) in the Valley Forge National Historic Park is a stone masonry structure with interior timber framing located on the former Pawling Farm where George Washington's Valley Forge winter encampment and commissary were located. The barn measures approximately 116 ft. × 40 ft. (35.3 m. × 12.2 m.), three stories in height, and constructed post-encampment in two building campaigns. The original eastern portion was constructed by Sam Wetherill, with a later addition constructed to the west in 1845. The barn has been progressively deteriorating since the National Park Service took possession of the Walnut Hill farm property in 1984 on which the barn is situated.

SAMPLE

As part of the renovation and stabilization of the barn, a small 90 mm × 60 mm × 40 mm dimension and 180-gram weight brown-colored original bedding mortar fragment was provided (Figure 2) for detailed laboratory studies to determine the composition and mix proportion of the mortar so that a suitable repointing mortar can be formulated. Although the sample provided was reportedly 'representative' of the original bedding mortar, due to the examination of only one sample let alone considering the effects of natural weathering of mortar during service, the study can at best provide an idea of the original bedding mortar composition; collection of multiple mortar samples from different depths and elevations would be advisable to assure the original mortar composition for assessment of the best restoration mortar. Compared to many traditional lime mortars that are usually very soft, fragile, and dusty, the sample for its age was relatively dense, hard, and intact. Scattered throughout the mortar are white, angular, soft, unmixed lumps of lime many noticeably coarser than sand (up to 10 mm in size) resembling remnant lime clasts traditionally found in many hot-mixed mortars to immediately confirm its lime-based binder composition consistent with its age. The harder nature of samples than many traditional lime mortars indicated the potential presence of a pozzolanic and/or hydraulic component, whereas the brown color tone indicated the potential presence of an iron oxide-based pigment or some other ferruginous components.

1. TMS Member, President and Petrographer, Construction Materials Consultants, Inc., Greensburg, PA, info@cmc-concrete.com

2. Petrographer, Construction Materials Consultants, Inc., Greensburg, PA, info@cmc-concrete.com

Figure 1 - Field Photos of Wetherill Barn at the Valley Forge National Historic Park Showing Location of Bedding Mortar Sample

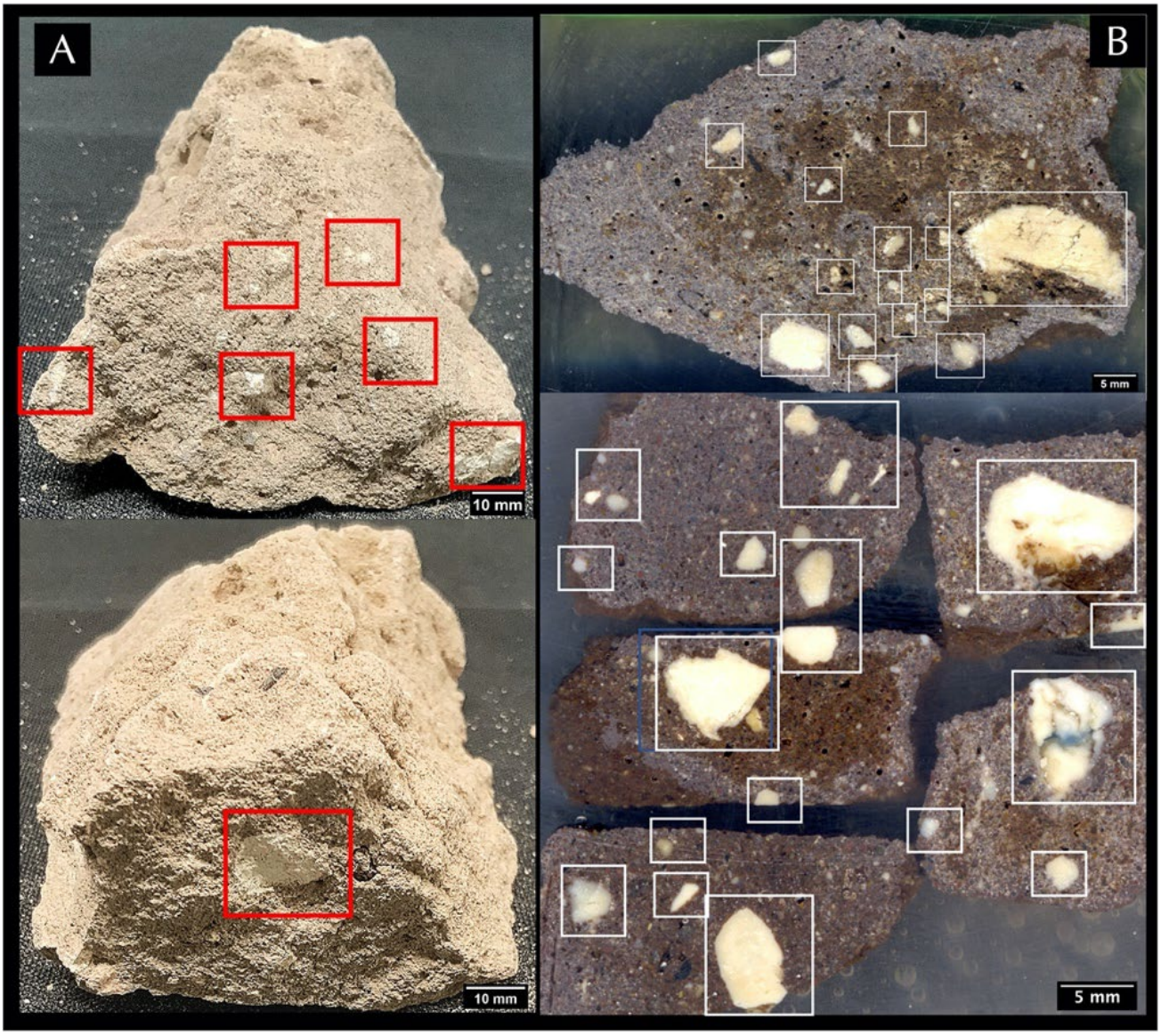

Figure 2 - Shown are A - actual mortar fragment as received viewed from two sides; B – lapped cross sections of mortar fragment where white lumps of unmixed dolomitic lime are seen scattered over pigmented brown mortar most of which are angular, noticeably coarser than sand (up to 10 mm) and resemble lime clasts often found in many hot-mixed mortars where quicklime is slaked during mixing with wet sand. Average composition of white lumps in boxes determined from SEM-EDS studies is 53.8% CaO, 41.1% MgO, (94.9% lime and magnesia), 3.6% SiO_2, 0.4% Al_2O_3, 0.75% Fe_2O_3, 0.22% TiO_2, and negligible alkalis, indicating their derivation from slaking of quicklime derived from calcination of relatively pure dolomitic limestone feed. Field widths of sample images (in A) are 100 mm and lapped cross sections (in B) are 75 mm (top) and 50 mm (bottom).

ANALYTICAL TECHNIQUES

Currently, there are two standardized procedures available that describe various laboratory techniques for analyses of masonry mortars with special emphasis on historic mortars. One is ASTM C 1324 "Standard Test Method for Examination and Analysis of Hardened Masonry Mortar," which includes detailed petrographic examinations (optical microscopy), followed by chemical analyses, along with various ancillary techniques, e.g., SEM-EDS, XRD and thermal analysis. The second one is the RILEM method, which also included both petrography and chemical analysis as the two primary methods of testing along with other ancillary methods described in ASTM C 1324 and described in a series of publications from Middendorf, et al. (2000, 2004 a, b, 2005 a, b), Valek, et al. (2012), and Bartos, et al. (2000). The present mortar was tested by both methods. Both methods are essentially destructive techniques, which involve sectioning, grinding, pulverizing, and acid digestion of a mortar sample. Many traditional non-destructive testing and damage assessment of masonry structures (e.g., rebound hardness, stress wave transmission, impact-echo, surface

penetrating radar, tomographic imaging, infrared thermography) despite their powerful applications in condition survey and identifications of internal features such as voids or areas of distress, they still cannot assess the original mortar ingredients or their mix proportions.

The mortar sample was first photographed with a digital camera, then scanned on a flatbed scanner, and viewed through a low-power stereomicroscope for the preliminary examinations, e.g., to separate any unusual pieces having different appearances, perhaps representing contaminants from later pointing episodes, or the remains of host masonry units.

Four representative subset pieces of interest were then carefully sectioned with a water-cooled thin diamond saw from the original fragment for: (a) epoxy-impregnation for optical and electron microscopy, (b) acid digestion for extraction of acid-insoluble component representing mostly the siliceous component of sand, (c) first-stage pulverization to finer than US No. 50 sieve (0.3 mm) for gravimetric analyses (i.e., insoluble residue, soluble silica, and loss on ignition from ambient to 950°C) and ion chromatography, and (d) second-stage pulverization of an aliquot from the first pulverized batch to finer than US No. 325 (44-micron) size for XRD, XRF, FTIR, and thermal analysis. Due to the small sample size usually collected during retrieval of historic mortars and inherent soft nature, typical physical tests such as compressive strengths cannot be done directly, which can only be assessed from mix proportions determined from combinations of microscopy and chemical methods.

Grain-Size Distribution of Sand

The portion selected for sand extraction was first gently broken down into < 5 mm size pieces in a porcelain mortar and rubber-tipped pestle making sure not to reduce the inherent grain-size of sand during this initial size-reduction process. Subsequent smaller pieces are then placed in a 250-ml glass beaker completely immersed in dilute (1+4) hydrochloric acid and stirred with a magnetic stirring rod over a stirrer for a period of at least 24 hours to several days with intermitted decantation of liquid (without losing the suspended solids, if any, by filtration of solution), washings of residue with tap water, and re-immersion in fresh dilute acid for complete dissolution of binder fractions and settlement of dominantly siliceous and some argillaceous fractions of sand at the bottom of beaker to be eventually filtered out and oven-dried for sieve analysis. Sand particles, thus extracted, were sieved in an automatic mini sieve shaker (e.g., from Gilson) through various U.S. Sieves from No. 4 (4.75 mm opening) through 8 (2.36 mm), 16 (1.18 mm), 30 (0.6 mm), 50 (0.3 mm), 100 (0.15 mm), and 200 (0.075 mm) for determination of the size, shape, angularity, and color of sands retained on various sieves. Photomicrographs of sand retained on each sieve are then taken with a stereomicroscope to record the sand size, shape, and color variations. Figure 3 shows grain-size distribution of extracted sand and micrographs of dominant sand populations retained on US Nos. 50 and 100 sieves.

Optical Microscopy

Optical microscopy is the most powerful method in mortar investigation (Erlin and Hime (1987), Elsen (2006), Elsen et al. (2012), Goins (2004), Jana (2005), Hughes et al. (2001), Doebley and Spitzer (1996), Leslie and Hughes (2001)). Steps followed during sample preparation for optical microscopy are as follows:

Steps followed during sample preparation for optical microscopy are as follows: First, portion selected for microscopy was oven-dried at 40 to 60°C to a constant mass and placed in a flexible (e.g., molded silicone) sample holder where one part was encapsulated with a clear epoxy and another part with a colored (blue) dye-mixed low-viscosity (100-110 cps) epoxy under vacuum to effectively replace all air-filled capillary pores and voids, cracks etc. with epoxy. Then both clear and colored epoxy-encapsulated parts were encapsulated in one solid block to improve the overall integrity of the sample during thin sectioning, and, for the dyed sample, to highlight porous areas, voids, and cracks. The block was then demolded after 6 hours in ambient air, sectioned or ground in a medium to coarse grid metal-bonded diamond disc to exposed the sample from under epoxy, oven-dried, exposed sectioned mortar was then impregnated with a thin film of clear and dyed epoxy, cured, processed through a series of coarse to fine grinding on metal and resin-bonded diamond grinding discs with water or a lubricant for a precision flat clean ground surface to be glued to a frosted large-area (50 ´ 75 mm) glass slide with a UV-cure adhesive. Careful precision sectioning and precision grinding of the sample was then done in a thin-sectioning machine (e.g., Buehler Petrothin) till the thickness was down to 50 to 60 microns. Final thinning down to 25-to-30-micron thickness was done on a glass plate with fine (5-15 microns) alumina abrasive. Thin section is eventually polished with various fine (1 micron to 0.25-micron size) diamond abrasives on polishing wheels suitable for examinations in a petrographic microscope (Olympus BX51 POL, Nikon Eclipse E600 POL, and Leica DMLP), and eventually in SEM-EDS. Residue block left after thin sectioning was further polished (after oven drying and light impregnation of sectioned surface with epoxy, if needed) for examination in a stereomicroscope, metallurgical microscope, and SEM. Details on step-by-step procedure of sample preparation can be found in Jana (2006).

The prepared thin section was then (a) scanned on a flatbed transparent office scanner with one and two perpendicular linear polarizing filters to create whole-slide high-resolution digital images in plane and cross polarized light (PPL and XPL) modes; (b) examined in a high-power stereozoom microscope up to 100X magnifications having transmitted-light (in PPL and XPL) facilities with attached rotating polarizer and analyzer to capture large-area images (often stitching of overlapped images and various image analyses steps) to further compliment the whole-slide scanned image; and (c) examined in a petrographic microscope equipped with transmitted, reflected, PPL/XPL, and fluorescent (UV)-light facilities (from 4x/5x for sand to 10x/20x for paste microstructure to 40/60x for residual hydraulic phases to 100x with immersion oil for any particular

phase/feature of interest). Adequate micrographs were captured during each stage of microscopy via high-resolution, high frame rate, digital microscope cameras with appropriate image analyses software (Basler camera with Pylon and Micromanager software, Jenoptik Progres camera with Capture Pro software, Lumenera camera with Infinity software, etc.). Such digital archiving is an integral part of optical microscopy.

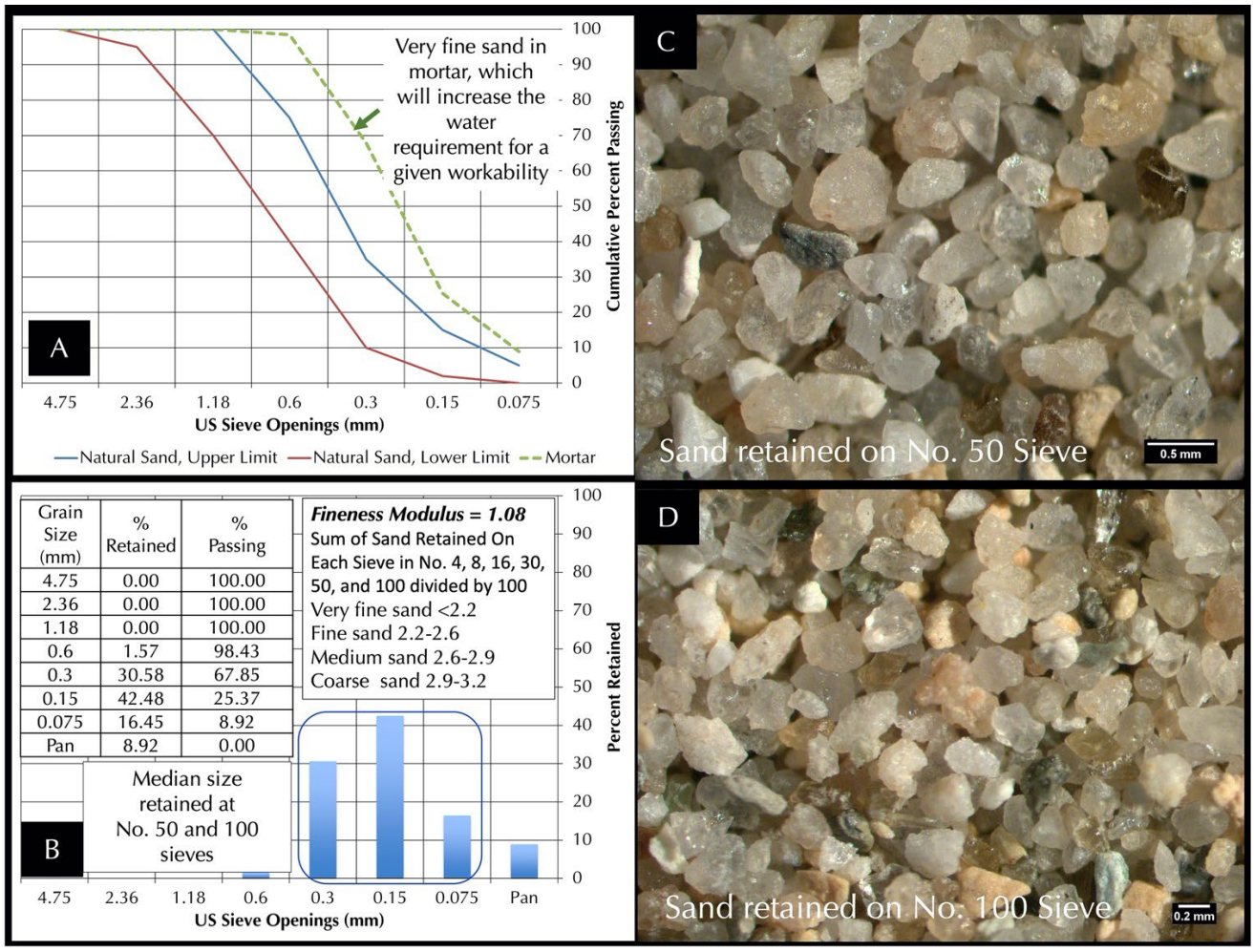

Figure 3 - Shown are: A - grain size distribution of sand extracted from mortar after acid digestion (in dashed green line) plotted with upper (in blue) and lower (in red) limits of ASTM C 144 natural sand; B – percent of extracted sand retained on different sieves and histogram; C – micrographs of sand particles from two dominant size populations retained on US No. 50 (0.30 mm) sieve, and D – particles retained on US No. 100 (0.15 mm) sieve. Sand particles are angular, clear, transparent to translucent, off-white, light to medium gray, and a few occasional darker-toned grains. Field widths of micrographs are 4.75 mm.

Scanning Electron Microscopy and Energy-Dispersive X-ray microanalysis (SEM-EDS)

SEM-EDS analysis was done in a CamScan Series 2 scanning electron microscope equipped with a high-resolution column 40Å tungsten, 40 kV electron optics zoom condenser focusing lens operating at 20 kV, equipped with a variable geometry secondary electron detector, backscatter electron detector, EDS detector for observations of microstructures at high-resolution, compositional analysis, and quantitative determinations of major element oxides from various areas of interest, respectively. Revolution 4Pi software was used for digital storage of secondary electron and backscatter electron images, elemental mapping, and compositional analysis along a line, or on a point or an area of interest. Portion(s) of interest on the polished 50 mm × 75 mm size thin section used for optical microscopy were subsequently coated with carbon or gold-palladium film and placed on a custom-made aluminum sample holder to fit inside the large multiported chamber of CamScan SEM equipped with the eucentric 50 × 100 mm motorized stage. Usually, features of interest from optical microscopy are marked on the thin section with a fine-tipped conductive marker pen for further observations in SEM. Alternately, solid polished section or grain mount from phases or areas of interest can also be examined. Procedures for SEM

examinations are described in ASTM C 1723 and Sarkar et al. (2000).

Gravimetric Analysis

Three common gravimetric techniques followed are (a) hydrochloric acid-insoluble residue content to determine the siliceous sand content; (b) losses on ignition due to release of free water, hydrate water, and CO_2; and (c) soluble silica content to determine the hydraulic binder contents from an assumed soluble silica content of the binder.

Acid Digestion

Until 1970-1980, characterization of masonry mortars was mostly based on traditional wet chemical analysis (Jedrzejewska (1960), Stewart and Moore (1981)), where interpretation of results were often difficult if not impossible without a good knowledge of the nature of the different ingredients.

Acid digestion was done to (a) extract insoluble component of sand from as-received mortar for grain-size distribution of siliceous component of sand; (b) determine insoluble (siliceous) sand content from 1.00 gram of pulverized sample (finer than 0.3 mm size) digested in 50-ml dilute (1+3) HCl (heated rapidly but below boiling for 15 min); and (c) as the first step for determination of soluble silica content from the hydraulic components in binder.

Soluble Silica from Hydraulic Binder

Soluble silica content contributed from the hydraulic component of binder is determined from: (a) digestion of a pulverized mortar (finer than 0.3 mm size, without excessive fines) in a 100-mL cold (at 3 to 5°C) HCl followed by; (b) further digestion of the filtered residue in a hot (below boiling) 75-ml NaOH alkali hydroxide solution, where cold acid digestion usually dissolves most of the binder without affecting the sand, followed by hot alkali hydroxide digestion to dissolve remaining soluble silica from calcium silicate hydrate component of paste or in mortars containing hydraulic binders. The two filtrates from acid and alkali digestions are then combined, re-filtered twice with 2.5-micron and then through 0.45-micron filter paper to remove any suspended silica fines, brought to 250 ml volume with deionized water, and then used for soluble silica determination by an appropriate instrumental technique (e.g., XRF). The soluble silica content corresponds to the silica mostly contributed from the hydraulic binder components (and a minor amount from any soluble silica component in the aggregates).

Loss on Ignition

Losses in weight of pulverized mortar on stepwise heating from ambient to 110°C, 550°C, and 950°C temperatures liberate free water from capillary pore spaces by 110°C, combined water from dehydration/dehydroxylation of various hydrous phases (calcium silicate hydrate, calcium hydroxide, etc.) by 550°C, and liberation of carbon dioxide from decomposition of carbonated paste and carbonate minerals by 950°C. Weight losses are measured by heating 1.00 gram of pulverized mortar (finer than 0.3 mm) in an alumina crucible in a muffle furnace at a heating rate of 10°C/min.

X-ray Fluorescence Spectroscopy (XRF)

An energy-dispersive bench-top X-ray fluorescence unit from Rigaku Americas Corporation (NEX-CG) was used, which was calibrated by using various certified (CCRL, NIST, GSA, and Brammer) reference standards of cements and rocks. The < 44-micron pulverized fraction of mortar was pressed into a pellet with a 15-ton Spex hydraulic press for XRF. Unlike conventional EDXRF analyzers, the NEX-CG was engineered with a unique close-coupled Cartesian Geometry (CG) optical kernel that dramatically increased signal-to-noise. By using monochromatic secondary target excitation, instead of conventional direct excitation, sensitivity was further improved.

X-ray Diffraction (XRD)

X-ray diffraction was done on the pulverized (to finer than 45-micron size) fraction of mortar in a Bruker D2 Phaser benchtop powder diffractometer equipped with a Lynxeye 1D detector, a θ-θ goniometer, a Cu X-ray tube (Cu K-alpha radiation of 1.54 angstroms), a primary slit of 1 mm, a receiving slit of 3 mm, a position sensitive 1D Lynxeye XE-T detector, generator settings used are 30 kV and 10 mA (300 watt, scanned at 2θ from 4° to 64° with a step of 0.05° 2θ integrated at 0.05 sec. step^{-1} dwell time). The resulting diffraction patterns are collected by Bruker Diffrac. Suite software and analyzed by MDI Jade with ICDD PDF4 Minerals database of diffraction data. Phase identification, and quantitative analyses were carried out with MDI Jade's Search/Match with Rietveld Whole Pattern Fitting.

Thermal Analysis

Simultaneous thermogravimetric analysis (TGA) and differential scanning calorimetry (DSC) analyses were done in Mettler Toledo TGA/DSC 1 and Perkin Elmer STA 6000 units on 30-70 mg of finely ground (< 45-micron) sample in alumina crucible (70 µl, no lid) from 30°C to 1000°C at a heating rate of 10°C/min with high purity nitrogen as purge gas at a flow rate of 75.0 ml/min. Both TGA/DSC 1 and STA 6000 instruments simultaneously measure heat flow in addition to weight change and offer high-resolution (ultra-microgram resolution over the whole measurement range),

efficient automation (with a reliable sample robot for high sample throughput), wide measurement range (measure small and large sample masses and volumes) broad temperature scale, superior ultra-micro balance and, as mentioned, simultaneous DSC heat flow measurements, e.g., for polymorphic alpha-to-beta transition of quartz and determination of quartz content.

Fourier Transform Infrared Spectroscopy (FTIR)

FTIR measurements were done in a Perkin Elmer Spectrum 100 FT-IR spectrophotometer running with Spectrum 10 software. Finely pulverized mortar (< 45-micron size) was measured using attenuated total reflection (ATR) on a single bounce diamond ATR crystal between a frequency range of 4000 to 650 cm^{-1}. Each run is collected at 4 cm^{-1} resolution with Strong Beer-Norton apodization. Data are collected with a temperature-stabilized deuterated triglycine sulfate (DTGS) detector by placing the sample in contact with the ATR crystal and by applying force from the pressure applicator supplied with the ATR accessory. The application of pressure enables the sample to be in intimate contact with the ATR crystal, ensuring achievement of a high-quality spectrum. Additionally, more conventional KBr pellet was also prepared by thoroughly mixing finely pulverized mortar with KBr powder in an agate mortar at 1:10 ratio, by mass.

Ion Chromatography (IC)

IC methods are described in ASTM D 4327 "Standard Test Method for Anions in Water by Chemically Suppressed Ion Chromatography." Briefly, an aliquot of 1 gram of pulverized mortar (passing No. 50 sieve) was digested in 50 ml deionized water for 30 minutes at a temperature below boiling, followed by continued digestion in water at the ambient laboratory condition for 24 hours on a magnetic stirrer at a temperature below the boiling point of water. The thoroughly digested sample is then filtered through two 2.5-micron filter papers under vacuum, followed by a second filtration through micro-filter (0.45-micron) paper, then the filtrate is either used directly or diluted to 100 to 250 ml with deionized water depending on the concentration of anions, and used for analysis to get ppm-level fluoride, chloride, nitrite, bromide, nitrate, phosphate, and sulfate in the water-digested sample in various automated IC instruments from Metrohm that were previously calibrated against various custom-made anion standard solutions of all these anions covering the observed concentrations. Weight percent concentrations were obtained from ppm-results times original filtrate volume times dilution factor divided by sample weight.

RESULTS

Mortar Sand

Mortar contains very fine (< 1 mm size) crushed siliceous sand, where majority of sand sizes are between 0.15-mm and 0.30-mm, having a fineness modulus of 1.08 (Figures 3 to 5). Use of such a fine crushed sand usually increases water requirement of freshly mixed mortar containing dry hydrated lime binder at a given workability, which, in turn, increases the potential for drying shrinkage and related microcracking. Increased water requirement, however, is readily compensated by a matured lime putty commonly used in historic mortars as opposed to dry powder of hydrated lime. Grain size distribution of sand after acid digestion representing the insoluble (i.e., mostly siliceous) fraction shows noticeably finer sizes at all size fractions than an ASTM C 144 masonry sand (Figure 3).

Siliceous sand particles are variably colored from clear, light gray to off-white, brown, transparent to translucent, subangular to angular, mostly equidimensional to a few elongated, dense, hard, well-graded, well-distributed, and present in sound conditions without any evidence of potentially deleterious reactions (e.g., alkali-aggregate reactions) or any unsoundness. Particles are mostly quartz with a subordinate quartzite and feldspar. A trace amount of scattered opaque (e.g., Fe-Ti-oxide) grains are noticed in SEM studies. No calcareous component was found in sand, which has helped straightforward determination of sand content from the acid-insoluble residue content (argillaceous residue from clay was present in insignificant amount to affect the overall sand content).

Binder Compositions and Microstructure

Sand particles are scattered in an overall fine-grained, porous, and carbonated lime matrix, which is the typical characteristic matrix found in most historic lime mortars. A reddish-brown appearance of the matrix found in many iron oxide-based pigmented mortars, however, was imparted from use of ferruginous clay particles (Figures 4 and 5).

Figure 4 (A and B) shows clear-epoxy impregnated thin section of mortar fragment scanned in a flatbed transparency scanner with one or two perpendicular linear polarizing filters to recreate plane and cross polarized-light modes (PPL and XPL, respectively) of a polarizing microscope. Scattered throughout the section are any ultrafine (< 0.1 mm) reddish brown angular to subrounded particles of ferruginous clay some of which have approached and even exceeded the maximum sand size of 1 mm. The XPL image shows many coarse fragments of unmixed lime (boxed). In an attempt to calculate volumetric proportions of clay particles, image analysis (by Image J) of the central yellow boxed area of PPL image of thin section in Figure 4A was done by highlighting such particles in a binary image, which showed 5% by area occupied by clay particles. Figure 4D shows another sectioned fragment that was impregnated with a blue dye-

mixed epoxy to highlight porous areas, voids, and cracks. The XPL images at 4B and D showed the overall carbonated nature of lime matrix characterized by the overall golden yellow interference color of paste, which is a typical microstructure of a historic lime mortar.

Evidence of leaching of lime paste is found, which is not unexpected for a mortar exposed to a moist outdoor environment for two centuries. Leaching, however, was localized and created a near-isotropic nature of leached areas when observed in cross polarized light mode in a petrographic microscope. SEM-EDS studies of those areas showed consistently higher silica and alumina at the expense of lime compared to the pristine non-leached areas. The clay-lime mortar was denser than traditional non-hydraulic lime-only mortar to restrict lime leaching in the moist service environment.

Distributed throughout the matrix are white, angular to rounded lumps (in carbonated form) of unmixed slaked lime as fine-grained calcium-magnesium carbonate of sizes varying from very fine (< 0.5 mm) to coarser than sand (e.g., up to 7 mm × 20 mm in size, Figure 2). Such unmixed lime lumps occur either in (a) dense massive-texture, or (b) in variably porous pelleted or clotted appearance with (c) fine shrinkage microcracks and (d) with sharp or diffused interfaces with mortar paste are indeed very common in historic lime mortars that are helpful for direct determination of the original lime binder composition as well as manufacturing process. They can be formed through: (a) traditional hot mixing process, where quicklime is added directly with wet sand (dry slaked), or (b) in matured putty form. Lime lumps sometime contain: (a) relict or pseudomorph textures of original limestone feed and (b) regions of unburnt limestone to permit identification of limestone provenance.

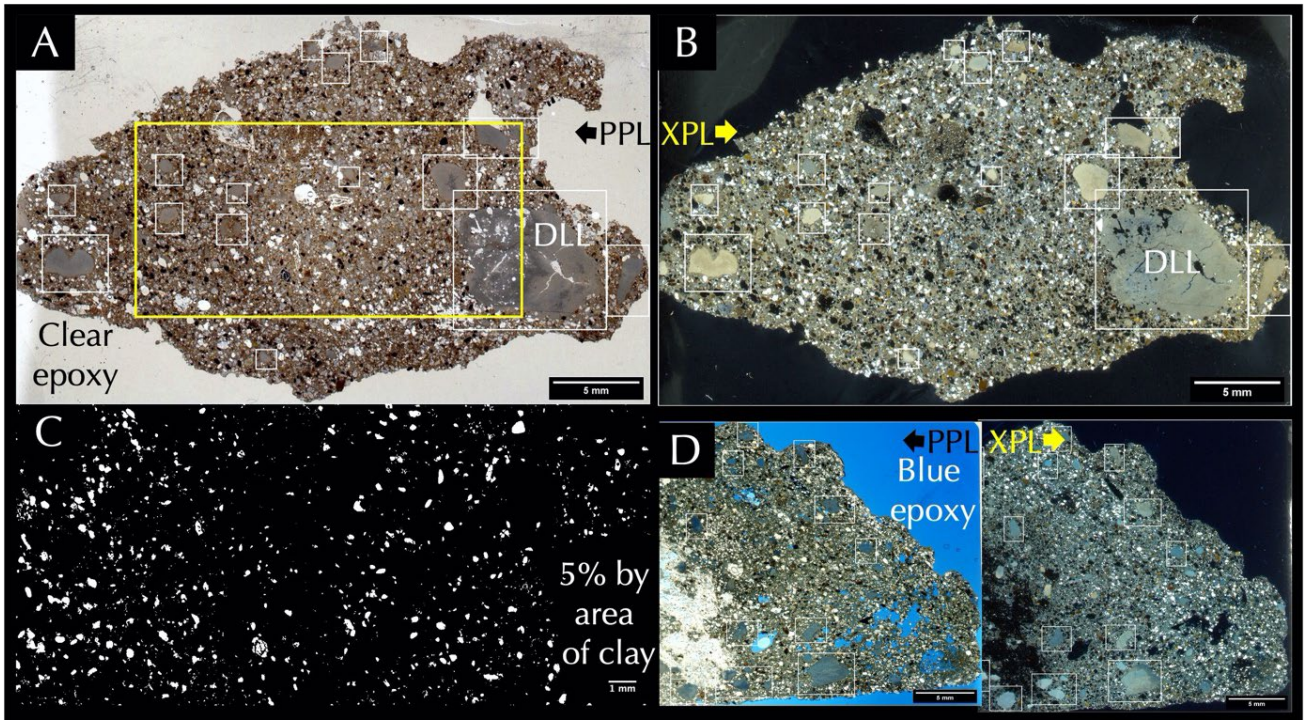

Figure 3 - A - Thin section of mortar impregnated with clear epoxy and scanned on a flatbed transparent office scanner with a linear polarizing filter for PPL view where white boxed areas enclose unmixed dolomitic lime lumps (DLLs), B – same thin section sandwiched between two perpendicular polarizing filters during scanning for XPL view; C – image analysis of the large yellow boxed area in "A" to highlight very fine, evenly distributed clay particles in white in a binary black and white image; D – blue dye-mixed epoxy-impregnated thin section of another mortar fragment in PPL and XPL views. Field widths of scans (in A and B) are 36.5 mm and micrographs are 25 mm (in C and D).

Figure 5 shows micrographs of blue dye-mixed epoxy-impregnated thin section of mortar where scattered angular dolomitic lime lumps (DLLs) are boxed, whereas dark reddish brown clay lumps are circled both of which show particles noticeably coarser than fine (< 1 mm) size of sand.

Lime lumps in Figure 5 are free of any residual hydraulic phases to indicate non-hydraulic nature of the lime binder produced from calcination of relatively pure dolomitic/magnesian limestone feed. Residual hydraulic phases (e.g., belite, Ca-Si-Al-based crystalline and amorphous phases) are commonly found within the unmixed lumps if the original limestone raw feed used for calcination and production of quicklime contained clay or silica impurities. No such evidence, however, is found in the present lumps, all of which showed very consistent similar compositions of lime and magnesia. The average composition determined from about a dozen of such white lumps boxed in Figure 2 by SEM-EDS showed 53.8% CaO, 41.1% MgO, (94.9% lime and magnesia), 3.6% SiO_2, 0.4% Al_2O_3, 0.75% Fe_2O_3, 0.22% TiO_2 and negligible alkalis, indicating their derivation from slaking of quicklime derived from calcination of relatively pure dolomitic limestone feed.

Lime lumps can have multiple origins and modes of occurrences all of which are commonly found in many historic lime mortars (Hughes et al. (2001)), e.g., (a) as unburnt or overburnt lime often occur in darker black or brown color tones, respectively where former can potentially permit identification of limestone provenance, (b) as denser massive-textured unmixed clumps of very fine-grained slaked lime (e.g., Figures 5 A, B) from traditional matured lime putty (may also occur in dry hydrated lime) now variably carbonated during service and often maintain distinct rounded to subrounded to angular shapes with distinct boundaries (e.g., Figure 5 A-D) or may have partially or completely diffused boundary to the surrounding lime matrix, and may show massive to pelleted or clotted appearance or texture with internal porosity (e.g., Figure 5C), or concentric color zoning over distinct granular texture with silicate inclusions from original limestone feed, sometimes contain pseudomorphs of original limestone texture to help potential detection of limestone provenance, or residual hydraulic phases if original calcined limestone was impure, or (c) as lime clasts as subangular to angular coarse-grained aggregates from slaked quicklime left from hot mixing process. All modes and origins of lime lumps/clasts can show fine discontinuous shrinkage microcracks developed either during initial stage from loss of moisture or during subsequent carbonation. Microcracks in clasts from hot-mixed mortar are more common as also in matured lime putty than dry hydrated lime (Valek and Matas (2010)).

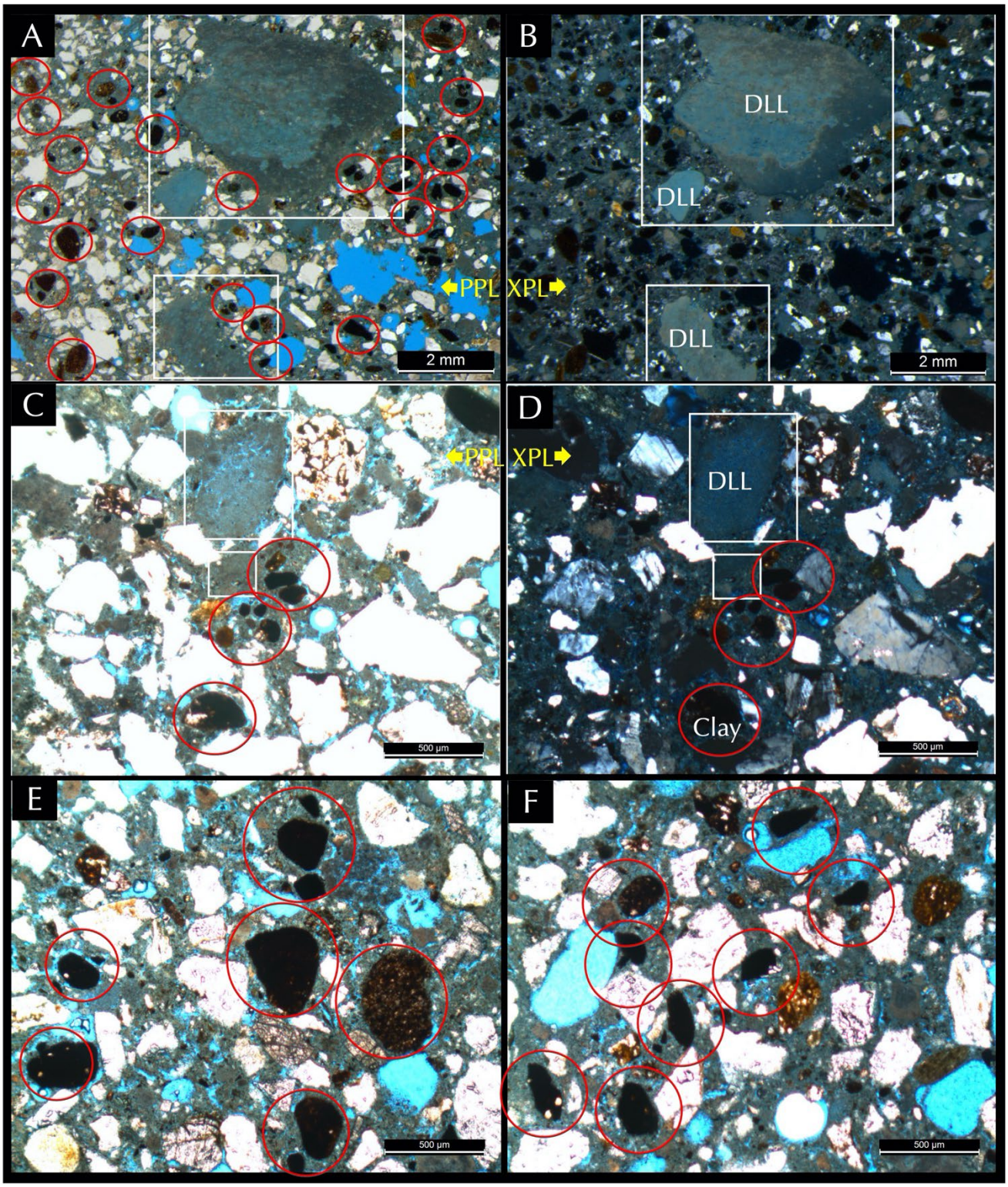

Figure 5 - Micrographs of blue dye-mixed epoxy-impregnated thin section of mortar in PPL and XPL showing: (a) dolomitic lime lumps/clasts (DLLs, boxed), which are subangular (A, B) to rounded (C, D), both massive-textured (A, B), or mottled (C, D) with relatively sharp boundaries, (b) subangular to rounded, dark reddish brown ferruginous clay lumps (circled), (c) very fine (< 1 mm, mostly 0.15-0.3 mm) crushed angular siliceous sand (quartz > quartzite, feldspar), (d) relatively porous and leached lime paste with fine, discontinuous shrinkage microcracks and irregular-shaped voids (all PPL images), and (e) some coarse entrapped voids (A, F). Field widths of micrographs are 10 mm (in A and B), and 2.5 mm (in C to F).

In the main matrix body outside the lime lumps/clasts, paste often shows: (a) severely carbonated, porous, fine-grained calcium carbonate, (b) short, discontinuous shrinkage microcracks, and (c) residual hydraulic phase (e.g., belite) if the original limestone contained silica, alumina, iron impurities to form a calcium silicate-aluminate hydraulic phase during calcination (which is not seen in the present case). All these are telltale microstructural features of historic lime mortars. Paste in the examined mortar, however, has undergone lime leaching process during service to be enriched in silica, alumina, and magnesia compared to lime, which is determined in SEM-EDS studies, where silica and alumina are mostly contributed from clay. As a result, XPL images in Figures 5B and D show near-isotropic appearance as opposed to typical golden yellow interference color of carbonated paste commonly seen in lime mortars.

As mentioned, ultrafine particles to sand-size angular to rounded reddish-brown clay lumps (circled in Figure 5) have imparted the overall brown color tone of mortar and provided some pozzolanic character to densify the paste. Clay is most probably added separately as a binder component than part of crushed sand.

Figure 6 shows backscatter electron images and corresponding chemical (oxide) compositions in boxed areas or at the tips of callouts from sand, lime lump, clay particles, and paste, whose respective compositions are color coded in various rows of the Tables beneath (dominant components for each phase are marked in bold).

SEM-EDS studies in Figure 7 determined: (a) the characteristic high-magnesia composition of lime (Figures 7A to D), (b) K-Al-Si-Fe based compositions of clay particles (Figures 7 A and D), which are further detected from XRD studies as illite, and (c) an intermediate large compositional range for lime-leached paste (Mg, Si, Al >> Ca, Figures 7E and F). Unlike calcined clay as a separate binder to offer pozzolanic properties, clay was probably added in pristine form though partly calcined nature of clay cannot be overruled.

Microchemical Variations

Major element oxide compositions of siliceous sand, unmixed lime lumps, clay particles, and overall paste when plotted in various binary and ternary oxide variation diagrams showed systematic variations in line with the compositions of endmember phases. An excellent linear mixing trend was found in Figure 8 when lime plus magnesia contents of all phases were plotted against silica plus alumina contents where dolomitic lime lump and clay (plus sand) occupied the end members with a large range of paste compositions in between from various proportions of clay in the fine-grained, porous, carbonated lime matrix. SEM-EDS analysis of unmixed lime lumps showed high-magnesian, relatively non-hydraulic (low silica) composition typical of a non-hydraulic dolomitic lime commonly used in matured putty and/or hot mix form.

Alterations

SEM-EDS studies of paste showed evidence of leaching of lime resulting in increased silica-alumina-magnesia components at the expense of lime, which was not unexpected for a historic mortar exposed to a moist, outdoor environment in Pennsylvania. Leaching, however, did not soften the paste by turning into a gelatinous mass to affect the overall integrity of the mortar thanks to the pozzolanic contributions of clay in densifying the overall matrix with lime, magnesia, silica and alumina.

Air

Mortar is non-air-entrained, which is typical of most historic mortars (Jana (2005)) formulated before the advent of air entrainment. Air content is estimated to be 4 to 6 percent, which are coarse, irregular-shaped entrapped voids.

Chemical Composition

Bulk oxide chemical composition of mortar is determined from XRF (in Figure 9 below the XRD pattern). A silica content of 48.45 percent reflects contribution from silica sand, and some from clay addition, as also seen in optical microscopy and XRD analysis of the mortar. Lime content (11.5%) and magnesia (8.8%) are consistent with derivation from a dolomitic lime putty binder. Alumina (7.15%), iron (3.66%), and alkalis (1.28% potassium and 0.95% sodium) are contributed from sand, clay, and paste. A trace amount of Ti (0.61%), and P (0.12%) were detected. A balance of 17.6 percent is contributed from volatiles (H_2O and CO_2). No detectable sulfur (as sulfate) was found as noted in XRD studies.

Acid-insoluble residue content of 65.9% is determined after digesting pulverized (< 0.3 mm size) fragment of mortar in hydrochloric acid. The result indicates contribution from crushed silica component of sand.

Loss on ignition of a separate aliquot of pulverized mortar during heating in a muffle furnace to 110°C, 550°C, and 950°C at 10°C/min rate showed 0.5%, 7.5%, and 7.2% mass losses corresponding to loss of free water, combined (hydrate) water, and CO_2 from decarbonation, respectively. The loss on ignition at 550°C corresponds to the water contents from dehydration of clay and paste. The loss on ignition at 950°C corresponds to degree of carbonation of carbonated paste.

Mineralogical Composition

XRD studies of pulverized mortar showed 52.2% quartz and 21.2% feldspar (albite) from sand, 13.8% illitic clay, and 12.8% calcite from carbonated lime matrix. No sulfate (e.g., gypsum), chloride (e.g., halite) or other salts were found.

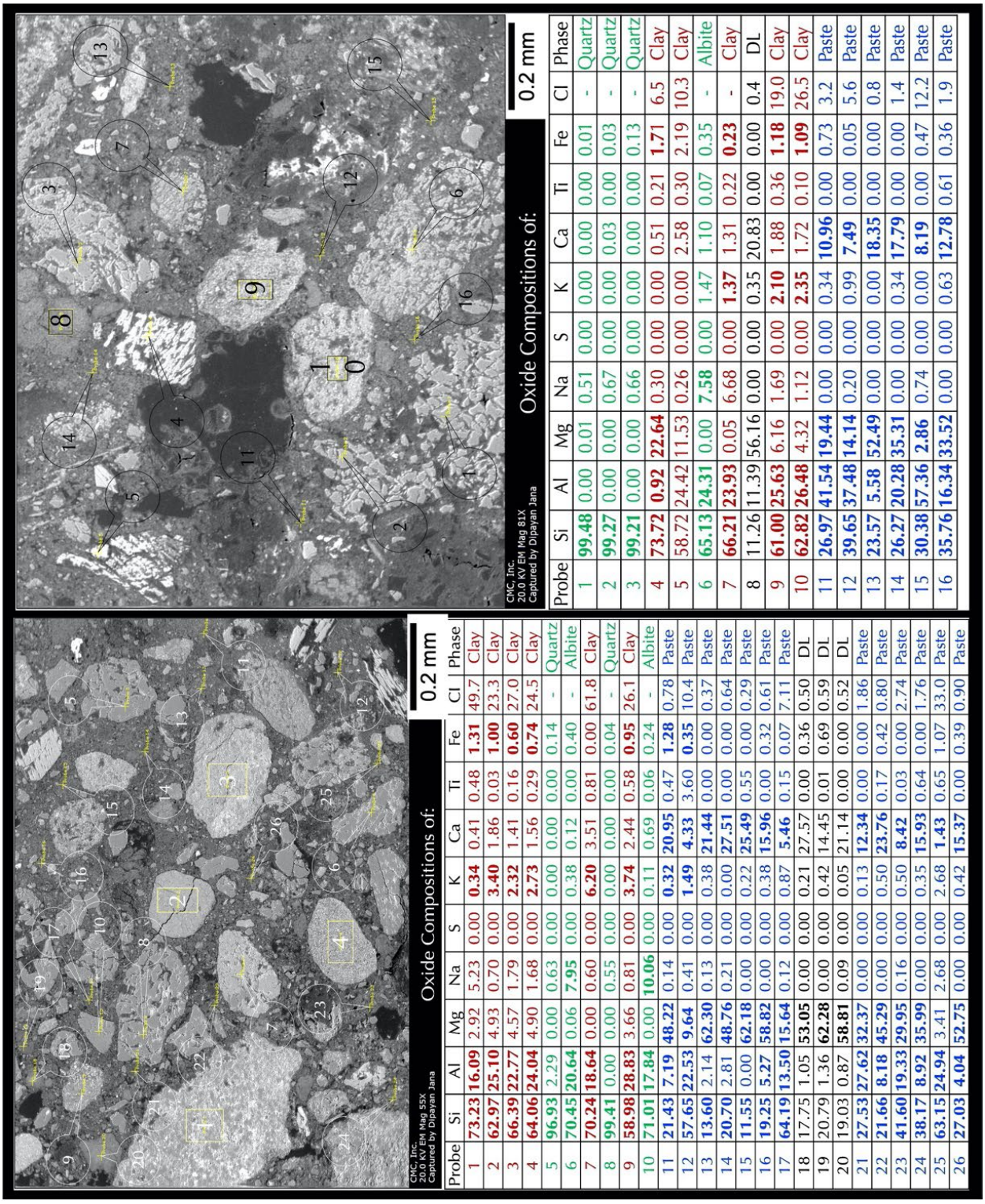

Oxide Compositions of:

Probe	Si	Al	Mg	Na	S	K	Ca	Ti	Fe	CI	Phase
1	**73.23**	**16.09**	2.92	5.23	0.00	**0.34**	0.41	0.48	**1.31**	49.7	Clay
2	**62.97**	**25.10**	4.93	0.70	0.00	**3.40**	1.86	0.03	**1.00**	23.3	Clay
3	**66.39**	**22.77**	4.57	1.79	0.00	**2.32**	1.41	0.16	**0.60**	27.0	Clay
4	**64.06**	**24.04**	4.90	1.68	0.00	**2.73**	1.56	0.29	**0.74**	24.5	Clay
5	**96.93**	2.29	0.00	0.63	0.00	0.00	0.00	0.00	0.14	-	Quartz
6	**70.45**	**20.64**	0.06	**7.95**	0.00	0.38	0.12	0.00	0.40	-	Albite
7	**70.24**	**18.64**	0.00	0.60	0.00	**6.20**	3.51	0.81	0.00	61.8	Clay
8	**99.41**	0.00	0.00	0.55	0.00	0.00	0.00	0.00	0.04	-	Quartz
9	**58.98**	**28.83**	3.66	0.81	0.00	**3.74**	2.44	0.58	**0.95**	26.1	Clay
10	**71.01**	**17.84**	0.00	**10.06**	0.00	0.11	0.69	0.06	0.24	-	Albite
11	**21.43**	**7.19**	**48.22**	0.14	0.00	**0.32**	**20.95**	0.47	**1.28**	0.78	Paste
12	**57.65**	**22.53**	**9.64**	0.41	0.00	**1.49**	**4.33**	3.60	**0.35**	10.4	Paste
13	**13.60**	2.14	**62.30**	0.13	0.00	0.38	**21.44**	0.00	0.00	0.37	Paste
14	**20.70**	2.81	**48.76**	0.21	0.00	0.00	**27.51**	0.00	0.00	0.64	Paste
15	**11.55**	0.00	**62.18**	0.00	0.00	0.22	**25.49**	0.55	0.00	0.29	Paste
16	**19.25**	**5.27**	**58.82**	0.00	0.00	0.38	**15.96**	0.00	0.32	0.61	Paste
17	**64.19**	**13.50**	**15.64**	0.12	0.00	0.87	**5.46**	0.15	0.07	7.11	Paste
18	17.75	1.05	**53.05**	0.00	0.00	0.21	27.57	0.00	0.36	0.50	DL
19	20.79	1.36	**62.28**	0.00	0.00	0.42	14.45	0.01	0.69	0.59	DL
20	19.03	0.87	**58.81**	0.09	0.00	0.05	21.14	0.00	0.00	0.52	DL
21	**27.53**	**27.62**	**32.37**	0.00	0.00	0.13	**12.34**	0.00	0.00	1.86	Paste
22	**21.66**	**8.18**	**45.29**	0.00	0.00	0.50	**23.76**	0.17	0.42	0.80	Paste
23	**41.60**	**19.33**	**29.95**	0.16	0.00	0.50	**8.42**	0.03	0.00	2.74	Paste
24	**38.17**	**8.92**	**35.99**	0.00	0.00	0.35	**15.93**	0.64	0.00	1.76	Paste
25	**63.15**	**24.94**	3.41	2.68	0.00	2.68	**1.43**	0.65	1.07	33.0	Paste
26	**27.03**	**4.04**	**52.75**	0.00	0.00	0.42	**15.37**	0.00	0.39	0.90	Paste

Oxide Compositions of:

Probe	Si	Al	Mg	Na	S	K	Ca	Ti	Fe	CI	Phase
1	**99.48**	0.00	0.01	0.51	0.00	0.00	0.00	0.00	0.01	-	Quartz
2	**99.27**	0.00	0.00	0.67	0.00	0.00	0.03	0.00	0.03	-	Quartz
3	**99.21**	0.00	0.00	0.66	0.00	0.00	0.00	0.00	0.13	-	Quartz
4	**73.72**	**0.92**	**22.64**	0.30	0.00	0.00	0.51	0.21	**1.71**	6.5	Clay
5	58.72	24.42	11.53	0.26	0.00	0.00	2.58	0.30	2.19	10.3	Clay
6	**65.13**	**24.31**	0.00	**7.58**	0.00	1.47	1.10	0.07	0.35	-	Albite
7	**66.21**	**23.93**	0.05	6.68	0.00	**1.37**	1.31	0.22	**0.23**	-	Clay
8	11.26	11.39	56.16	0.00	0.00	0.35	20.83	0.00	0.00	0.4	DL
9	**61.00**	**25.63**	6.16	1.69	0.00	**2.10**	1.88	0.36	**1.18**	19.0	Clay
10	**62.82**	**26.48**	4.32	1.12	0.00	**2.35**	1.72	0.10	**1.09**	26.5	Clay
11	**26.97**	**41.54**	**19.44**	0.00	0.00	0.34	**10.96**	0.00	0.73	3.2	Paste
12	**39.65**	**37.48**	**14.14**	0.20	0.00	0.99	**7.49**	0.00	0.05	5.6	Paste
13	**23.57**	**5.58**	**52.49**	0.00	0.00	0.00	**18.35**	0.00	0.00	0.8	Paste
14	**26.27**	**20.28**	**35.31**	0.00	0.00	0.34	**17.79**	0.00	0.00	1.4	Paste
15	**30.38**	**57.36**	**2.86**	0.74	0.00	0.00	**8.19**	0.00	0.47	12.2	Paste
16	**35.76**	**16.34**	**33.52**	0.00	0.00	0.63	**12.78**	0.61	0.36	1.9	Paste

Figure 6 - Backscatter electron images and energy-dispersive X-ray microanalysis at the tips of callouts and in boxed areas of sand, lime lump, clay particles, and paste, whose respective compositions are color coded in various rows of the Tables. CI = Cementation Index (after Eckel (1922)), which is a measure of hydraulicity of binder, and calculated as $[(2.8 \times SiO_2) + (1.1 \times Al_2O_3) + (0.7 \times Fe_2O_3)]/[(CaO) + (1.4 \times MgO)]$ CI is commonly < 0.5 for non-hydraulic lime mortar but characteristically higher for hydraulic lime and still higher for Portland cement or masonry cement-based binders.

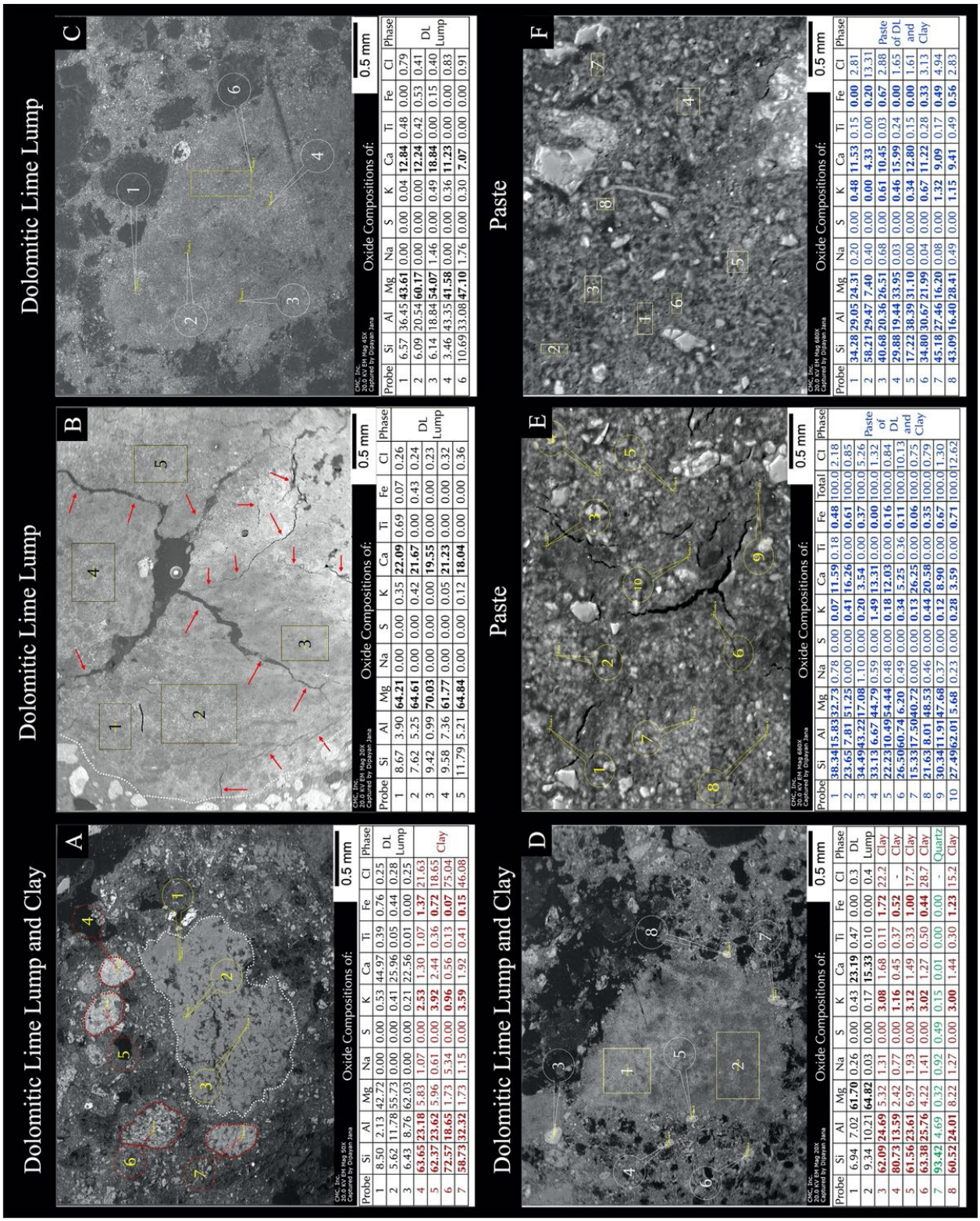

Probe	Si	Al	Mg	Na	S	K	Ca	Ti	Fe	Cl	Phase
1	8.50	2.13	42.72	0.00	0.53	44.97	0.39	0.76	0.25		DL
2	5.62	11.78	55.73	0.00	0.00	0.41	25.96	0.05	0.44	0.28	
3	6.43	8.76	62.03	0.00	0.00	0.21	22.56	0.01	0.00	0.25	Lump
4	**63.65**	**23.18**	5.83	1.07	0.00	**2.53**	1.30	1.07	**1.37**	21.63	
5	**62.37**	**23.62**	5.96	0.61	0.00	**3.92**	2.44	0.36	**0.72**	18.65	Clay
6	**72.57**	**18.65**	1.73	5.34	0.00	**0.96**	0.56	0.13	**0.07**	75.04	
7	**58.73**	**32.32**	1.73	1.15	0.00	**3.59**	1.92	0.41	**0.15**	46.08	

Probe	Si	Al	Mg	Na	S	K	Ca	Ti	Fe	Cl	Phase
1	8.67	3.90	**64.21**	0.00	0.00	0.35	**22.09**	0.69	0.07	0.26	
2	7.62	5.25	**64.61**	0.00	0.00	0.42	**21.67**	0.00	0.43	0.24	DL
3	9.42	0.99	**70.03**	0.00	0.00	0.00	**19.55**	0.00	0.00	0.23	
4	9.58	7.36	**61.77**	0.00	0.00	0.05	**21.23**	0.00	0.00	0.32	Lump
5	11.79	5.21	**64.84**	0.00	0.00	0.12	**18.04**	0.00	0.00	0.36	

Probe	Si	Al	Mg	Na	S	K	Ca	Ti	Fe	Cl	Phase
1	6.57	36.45	**43.61**	0.00	0.00	0.04	**12.84**	0.48	0.00	0.79	
2	6.09	20.54	**60.17**	0.00	0.00	0.00	**12.24**	0.42	0.53	0.41	DL
3	6.14	18.84	**54.07**	1.46	0.00	0.49	**18.84**	0.00	0.15	0.40	Lump
4	3.46	43.35	**41.58**	0.00	0.00	0.36	**11.23**	0.00	0.00	0.83	
6	10.69	33.08	**47.10**	1.76	0.00	0.30	**7.07**	0.00	0.00	0.91	

Probe	Si	Al	Mg	Na	S	K	Ca	Ti	Fe	Cl	Phase
1	6.94	7.02	**61.70**	0.26	0.00	0.43	**23.19**	0.47	0.00	0.3	DL
2	9.34	10.21	**64.82**	0.03	0.00	0.17	**15.33**	0.10	0.00	0.4	Lump
3	**62.09**	**24.69**	5.32	1.31	0.00	**3.08**	1.68	0.11	**1.72**	22.2	Clay
4	**80.73**	**13.59**	2.42	0.77	0.00	**1.16**	0.45	0.37	**0.52**	-	Clay
5	**61.56**	**23.61**	6.97	1.93	0.00	**3.12**	1.49	0.33	**1.00**	17.7	Clay
6	**63.38**	**25.76**	4.22	1.41	0.00	**3.02**	1.27	0.50	**0.44**	28.7	Clay
7	**93.42**	4.69	0.32	0.92	0.49	0.15	0.01	0.00	0.00	-	Quartz
8	**60.52**	**24.01**	8.22	1.27	0.00	**3.00**	1.44	0.30	**1.23**	15.2	Clay

Probe	Si	Al	Mg	Na	S	K	Ca	Ti	Fe	Total	Cl	Phase
1	**38.34**	**15.83**	**32.73**	0.78	0.00	**0.07**	**11.59**	0.18	**0.48**	100.0	2.18	
2	**23.65**	**7.81**	**51.25**	0.00	0.00	**0.41**	**16.26**	0.00	**0.61**	100.0	0.85	
3	**34.49**	**43.22**	**17.08**	1.10	0.00	**0.20**	**3.54**	0.00	**0.37**	100.0	5.26	Paste
4	**33.13**	**6.67**	**44.79**	0.59	0.00	**1.49**	**13.31**	0.00	**0.00**	100.0	1.32	of
5	**22.23**	**10.49**	**54.44**	0.48	0.00	**0.18**	**12.03**	0.00	**0.16**	100.0	0.84	DL
6	**26.50**	**60.74**	**6.20**	0.49	0.00	**0.34**	**5.25**	0.36	**0.11**	100.0	0.13	and
7	**15.33**	**17.50**	**40.72**	0.00	0.00	**0.13**	**26.25**	0.00	**0.06**	100.0	0.75	Clay
8	**21.63**	**8.01**	**48.53**	0.46	0.00	**0.44**	**20.58**	0.00	**0.35**	100.0	0.79	
9	**30.34**	**11.91**	**47.68**	0.37	0.00	**0.12**	**8.90**	0.00	**0.67**	100.0	1.30	
10	**27.49**	**62.01**	**5.68**	0.23	0.00	**0.28**	**3.59**	0.00	**0.71**	100.0	12.62	

Probe	Si	Al	Mg	Na	S	K	Ca	Ti	Fe	Cl	Phase
1	**34.28**	**29.05**	**24.31**	0.20	0.00	**0.48**	**11.53**	0.15	**0.00**	2.81	
2	**58.21**	**29.47**	**7.40**	0.40	0.00	**0.00**	**4.33**	0.00	**0.20**	13.31	
3	**40.68**	**20.36**	**26.51**	0.68	0.00	**0.61**	**10.45**	0.03	**0.67**	2.88	Paste
4	**29.88**	**19.44**	**33.95**	0.03	0.00	**0.46**	**15.99**	0.24	**0.00**	1.65	of DL
5	**17.22**	**38.39**	**31.10**	0.00	0.00	**0.34**	**12.80**	0.15	**0.00**	1.61	and
6	**34.80**	**30.67**	**21.99**	0.04	0.00	**0.67**	**11.22**	0.28	**0.33**	3.13	Clay
7	**45.18**	**27.46**	**16.20**	0.08	0.00	**1.32**	**9.09**	0.17	**0.49**	4.94	
8	**43.09**	**16.40**	**28.41**	0.49	0.00	**1.15**	**9.41**	0.49	**0.56**	2.83	

Figure 7 - Backscatter electron images and energy-dispersive X-ray microanalysis at the tips of callouts and in boxed areas of various mortar phases, e.g., from unmixed dolomitic lime lumps (in A to D) to clay particles (in A and D) to paste (in E and F). Results are given in Tables where different phases are color coded.

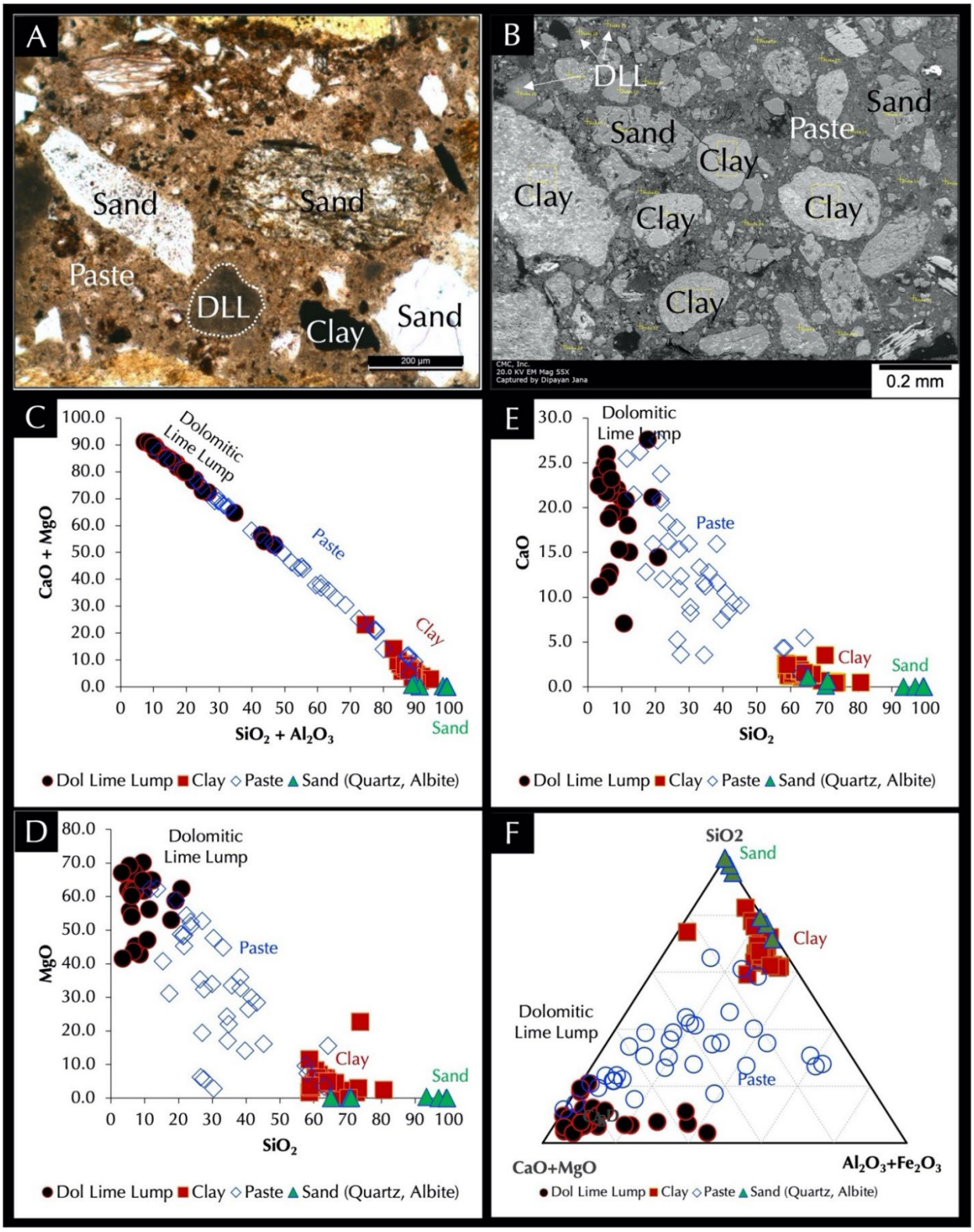

Figure 8 - Oxide chemical variations of various components of mortar from siliceous sand to dolomitic lime to clay plotted in binary and ternary plots of relevant oxides of lime, silica, alumina, and iron. An excellent linear trend is found when lime plus magnesia contents were plotted against silica plus alumina contents of various binder, clay, and sand phases where dolomitic lime lump and clay (plus sand) occupied the end members with a large range of paste compositions in between from various proportions of clay in the fine-grained, porous, carbonated lime matrix. Field width of micrograph in A is 1 mm and backscatter electron image in B is 1.25 mm.

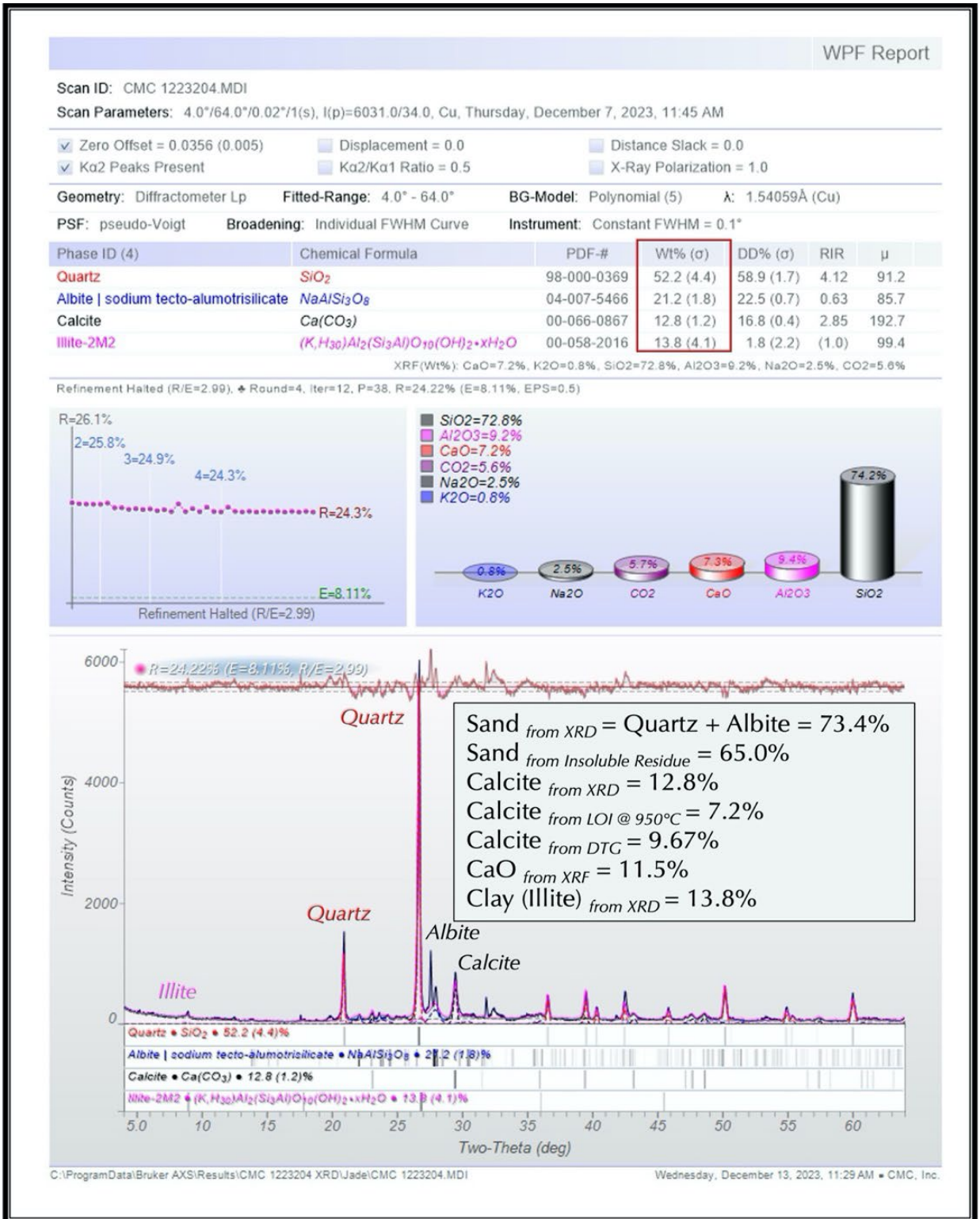

XRF											Gravimetry			
SiO_2	Al_2O_3	Fe_2O_3	CaO	MgO	Na_2O	K_2O	TiO_2	P_2O_5	SO_3	(LOI)	IR	Loss on Ignition @		
												110°C	550°C	950°C
48.45	7.15	3.66	11.54	8.79	0.95	1.28	0.61	0.12	ND	17.57	65.92	0.5	7.5	7.2

Figure 9 - X-ray diffraction pattern of bulk mortar sample showing the dominance of quartz from silica sand, and subordinate clay (illite), calcite, and feldspar (albite) from clay lumps, paste, and sand, respectively. Results of Rietveld analysis are marked in a box and corresponding XRF chemical (oxide %) data are shown in a bar graph. Bottom table summarizes results from XRF and gravimetry.

Hydrates, Clay, and Carbonates from Thermal Studies

Thermal analysis produced results comparable to gravimetric weight losses from loss of water (0.78%), dehydroxylation of clay and lime (6.84%), and decarbonation of carbonated lime paste (6.32%) along with distinct characteristic endothermic peaks at 81.3°C, 504.4°C and 745.4°C for loss of free and combined water, dehydroxylation of illitic clay and hydrated lime, and decarbonation of carbonated lime paste (including scattered lumps), respectively. A peak at 574.53°C corresponds to polymorphic transition of quartz from alpha to beta form where a quartz content of 48.1% showed a close match to 52.2% quartz from XRD. A small endotherm at 325°C corresponds to dehydration of brucite and hydromagnesite from dolomitic lime. An illite content of 15.1% calculated from dehydroxylation at 504.4°C shows comparable result to 13.8% from XRD. Calcite content from DTG is 9.5% as opposed to 12.8% calcite from XRD.

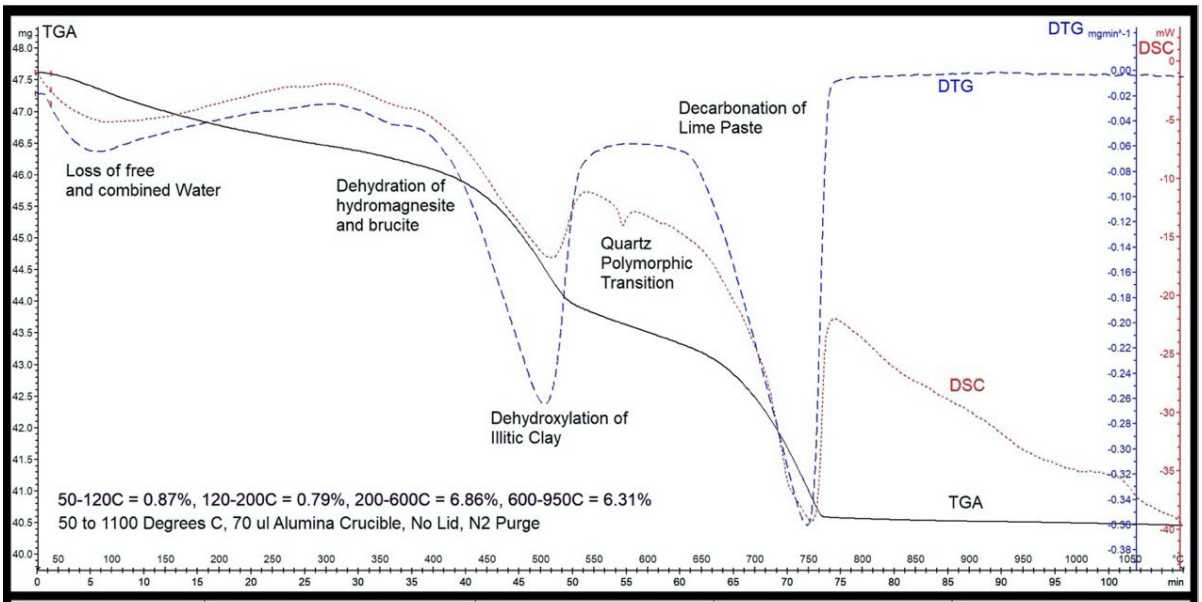

T(°C)	Up to 120°C	120°C to 200°C	200°C to 600°C	> 600°C
Phases	Hygroscopic Water	Water from Hydrated Salts	Structural Water From Hydraulic Components	CO_2 from decomposition of carbonates
Mass Loss From TGA	0.79	0.78	6.84	6.32
Mass Loss (%) From Gravimetry	0.50	-	7.50	7.20

Peaks#	Peak Position (°C)	Phase
1 (DTG)	81.36	Loss of Free & Combined Water
2 (DTG)	325	Dehydration of Hydromagnesite, Brucite
3 (DTG)	504.40	Dehydroxylation of Portlandite and Clay
4 (DSC)	574.53	Polymorphic Transition of Quartz
5 (DTG)	745.36	Decarbonation of Calcite

Figure 10 - TGA (in bold black), DSC (in dotted red), and DTG (in dashed blue) curves of mortar showing losses in weights due to decompositions (loss of water and carbon dioxide) of various phases during controlled heating from 30°C to 1100°C in a ceramic crucible (alumina 70µl, no lid) at a heating rate of 10°C/min in a nitrogen purge at a rate of 75 mL/min. Dehydration and decarbonation reactions are marked as endothermic peaks in the DTG curve, whereas alpha to beta-form polymorphic transition of quartz is marked at the characteristic temperature around 575°C in the DSC curve.

Organic and Inorganic Phases from FTIR

FTIR analysis of pulverized (<44-micron) mortar was done to determine the presence of any organic component. Other than the three common mineral components as found in optical microscopy and XRD (quartz, calcite, and clay), no separate addition of any organic resin was found.

Water-Soluble Salts

Ion chromatography of water-soluble salts in the filtrate of deionized water digested mortar shows negligible but detectable chloride (56 ppm), nitrate (34 ppm), and sulphate (88 ppm) from the environment.

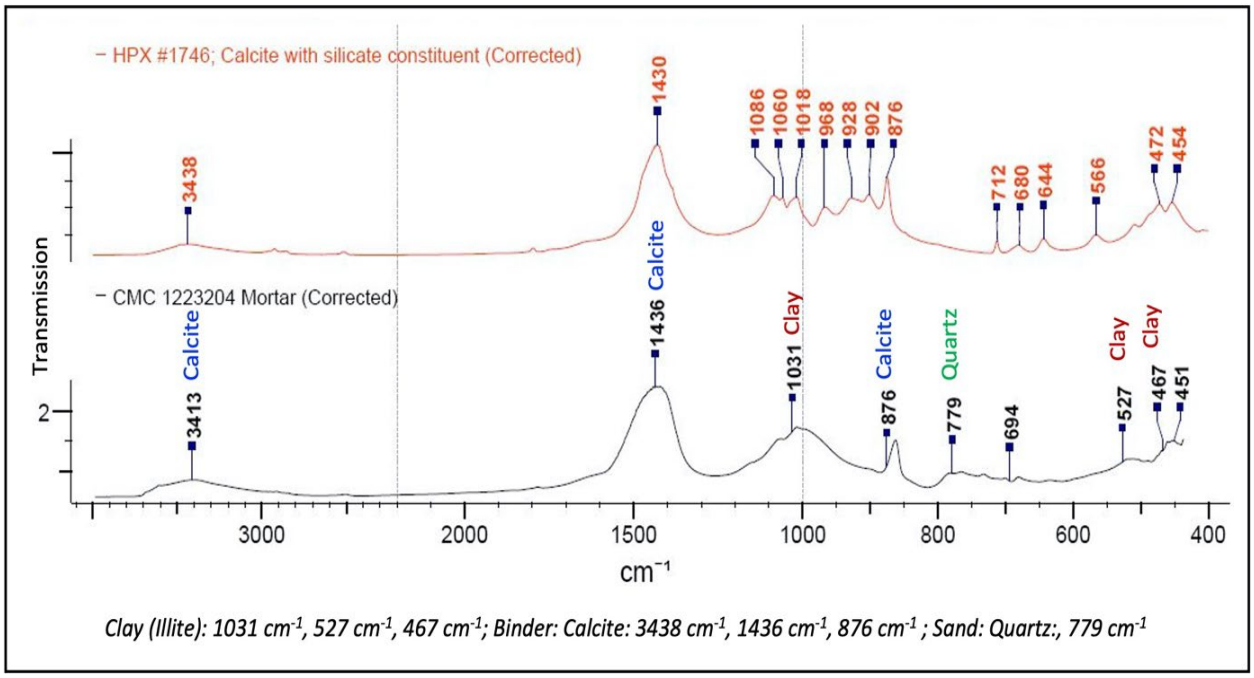

Figure 11 - FTIR spectra of mortar and a comparable calcite in silicate standard showing characteristic transmission bands along with the peaks for calcite and illitic clay, which are all consistent with the results obtained from optical microscopy and XRD studies.

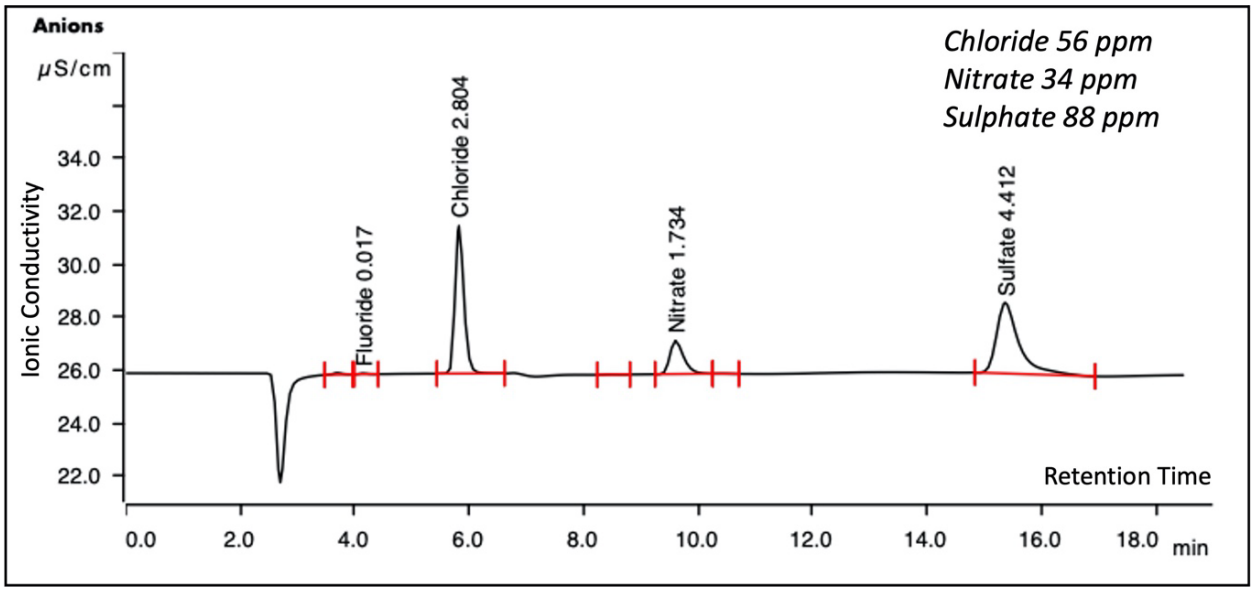

Figure 12 - Ion chromatogram of water-soluble chloride, nitrate, and sulphate extracted after digesting a gram of pulverized mortar in deionized water for 24 hours. Filtrate showed negligible contents of measured ions despite its 200 years of exposure to a moist outdoor environment indicating lack of any dissolved chloride or sulfate salts in the mortar.

DISCUSSION

Mortar Composition and Alterations

Information obtained from petrography (optical microscopy), SEM-EDS studies, mineralogical (XRD), chemical (XRF, gravimetry), and thermal (TGA/DSC) analyses are all consistent with each other, all indicated the mortar to be composed of a non-hydraulic, dolomitic lime produced from calcination of a relatively pure dolomitic limestone without any clay-based impurity to form any hydraulic phases, and fine, disseminated subangular to rounded nodules or grains of ferruginous clay, which has imparted the overall brown color tone of mortar similar to the appearance from iron-oxide-based pigmented lime mortars. Many coarser-than-sand size lumps of unmixed lime particles provided information about the composition and hydraulicity of the original binder along with potential manufacturing process not only in the traditional aged putty form but might also from hot-mixing process of calcined quicklime with wet sand.

Difficulty in Mix Calculations of Historic Mortars

Due to the presence of clay as an integral part of the examined mortar, along with historic lime-binder based composition, traditional (i.e., ASTM C 1324) method of determination of sand and binder proportions, e.g., from acid insoluble residue content (for sand content), soluble silica content (for hydraulic binder content), loss on ignition (for combined water and carbonate contents) from assumed compositions and dry densities of binder components applied for determination of mix proportions of modern cement-lime or masonry cement mortars are not possible. In fact, due to the unknown and rather wide compositional range of historic binders, e.g., for hydraulic lime and natural cements without any tight control on their raw feeds being calcined (unlike well-proportioned limestone-shale mix in the modern Portland cement manufacturing) ASTM C 1324 method of mix proportion calculation cannot be extended for historic mortars.

The philosophy of mix calculation, however, can still be extended to historic mortar wherever possible. For example, since sand is determined to be siliceous in composition, sand content is essentially determined from the acid-insoluble residue content of mortar, which is 65.9 percent. Assuming a dry density of sand as 80 lbs./ft^3 (1280 kg/m^3), sand volume is then calculated to be 0.82. Due to the non-hydraulic composition of dolomitic lime (e.g., as seen from SEM-EDS studies of lime lumps) and unknown contribution of clay components in the paste, traditional binder content determination from soluble silica content of binder with an assumed binder composition as prescribed in ASTM C 1324 cannot be used for historic mortars. XRD analysis showed an illitic clay content of 13.8% by mass of mortar. Assuming a non-hydraulic dolomitic lime composition consisting of 41% CaO and 29% MgO (i.e., 42% brucite since ratio of molecular weights of brucite to MgO is 1.447) and a dry density of dolomitic lime to be 40 lbs//ft^3 (640 kg/m^3) dolomitic lime content can be determined either from the brucite content from thermal analysis, or, from the MgO content of mortar (assuming there is no other contributor for MgO beside lime, since neither siliceous sand nor illitic clay has magnesia). For XRF-determined 8.8% MgO, dolomitic lime content corresponds to 30.34%, or 0.75, by volume. Lime-to-sand volumetric ratio from this approach is then 1:1 (i.e., without incorporating the clay content), which is rather high for many historic lime mortars, though not uncommon where high-lime content could have been contributed from the unmixed lime lumps, or from disturbance in original binder chemistry from subsequent leaching and alterations during service (Leslie and Hughes (2001)).

Microscopical examinations provided a more powerful and reasonable assessment of binder-to-sand ratio than ASTM C 1324-style estimation of mix proportions. From a combined approach of microscopy and sand content from gravimetry, volumetric proportions of binder (i.e., lime plus clay) and sand content are estimated to be roughly 1-part binder (lime plus clay) to maximum 2-part sand, by volume. The estimated proportion is not equivalent to any modern-day ASTM C 270 cement-lime or masonry cement mortars, but, indeed, a very common mix used in many historic lime mortars.

Suitable Replacement Mortar

Based on: (i) the determined non-hydraulic dolomitic lime and clay mixed binder composition from optical microscopy and SEM-EDS studies, (ii) fine (< 1 mm size) siliceous sand composition from optical microscopy, (iii) chemical (XRF and gravimetric) analyses of lime-silica-magnesia-alumina compositions, loss on ignition, and (iv) estimated rough volumetric proportions of examined clay-lime mortar, a suitable replacement mortar is recommended for initial trial mock-up mixes consisting of 1-part NHL 2 or NHL 3.5 and 2-part silica sand with appropriate dosage of an iron oxide pigment to impart the color tone of the original mortar (instead of using ferruginous illitic clay), as long as it is tested in a small area and found satisfactory to the adjacent masonry unit. Clay though might have provided some pozzolanic benefit to the lime paste if it were partly calcined or contained an amorphous phase but should preferably be avoided and substituted with mineral oxide pigment for the color match to avoid unwanted moisture absorption at plastic or hardened states and related performance and/or durability concerns especially when lime in the modern mix will probably be used in powder hydrate form (ASTM C 207) rather than putty (ASTM C 1489) form. The use of aged lime putty, however, was the recommended choice of practice in the old days because this viscous form with higher plasticity and water-retention capacity, results in mortars of higher strength that carbonate faster (Hughes et al. (2001), Leslie and Hughes (2001)). Either lime putty as specified in ASTM C 1489 or hydrated lime (ASTM C 207) can be used. ASTM

C 1713 specification for mortars for repair of historic masonry is a recommended practice for mortar restoration.

The overall appearance of the final mortar would depend on a match on sand, which constitutes the dominant proportion of the mortar. Sand should be:
(a) siliceous (crushed silica sand) type, (b) matched in color to the color of sand in the examined mortar, (c) from a similar source, (d) free of any debris, unsound, clay particles, or any potentially deleterious constituents in the sand, (e) similar to the size requirements of ASTM C 144 for masonry sand having maximum 2.5- times sand to the volume of lime, and (f) durable.

CONCLUSIONS

The historic mortar fragment was examined by a plethora of analytical techniques under ASTM C 1324 and RILEM methods including: (1) optical microscopy of as-received, polished solid, and light-transparent 30-micron thin sectioned pieces of mortar with stereomicroscope and petrographic microscope for the type, condition, and composition of sand, binder, overall mortar type used, along with evidence of any distress and alterations from almost 200 years of exposure to a moist outdoor environment, (2) SEM-EDS of interstitial paste fraction to further determine the type and potential hydraulicity of the lime binder, (3) extraction of acid-insoluble (i.e., siliceous) component of sand by dilute (1+7) HCl digestion followed by sieve analyses of extracted sand for grain-size distribution, (4) gravimetric analysis for soluble silica content from cold-acid digestion of mortar followed by hot-alkali digestion of the residue, (5) free water, combined water and carbonate contents from step-wise loss on ignition at 110°C, 550°C, and 950°C respectively, (6) XRF for major element oxide compositions, (7) XRD for mineralogical compositions, (8) thermal analysis for the hydrous, sulfate, and carbonate phases and the binder composition, (9) FTIR for the organic and inorganic phases, and (10) ion chromatography of water-soluble anions in the filtrate after digesting the mortar in deionized water to determine potentially deleterious soluble salts (e.g., of chloride, sulfate, etc.) in the mortar.

Based on optical microscopy and SEM-EDS studies, the original ingredients of the mortar, besides the omnipresent sand, are found to be (a) non-hydraulic dolomitic lime produced from calcination of a relatively pure dolomitic/magnesian limestone without any silica/clay-based impurity to form any hydraulic phases, which was mixed either in matured putty form and/or as hot mix lime mixed with (b) fine, disseminated subangular to rounded nodules or grains of ferruginous illitic clay, which has imparted the overall brown color tone of mortar similar to the appearance from iron-oxide-based pigmented lime mortars.

Mortar showed typical microstructure of a historic clay-lime mortar in having very fine (< 1 mm in size), well-graded, well-distributed crushed siliceous sand that remained in sound condition without any deleterious reactions. Sand particles extracted from mortar by acid digestion showed a fineness modulus of only 1.08 (73% retained on 0.15 mm and 0.3 mm sieves) with a noticeably finer size distribution comparable to a modern ASTM C 144 masonry sand. Sand particles are scattered in an overall fine-grained, porous, carbonated lime matrix with occasional angular to rounded lumps of unmixed lime, short, discontinuous shrinkage microcracks, and ultrafine particles to sand-size angular to rounded reddish-brown clay lumps, which have imparted to overall brown color tone of the mortar.

Lime lumps occur as coarse angular lime clasts (commonly seen in higher abundance in hot mix mortar) as well as rounded massive to mottled-texture mass that are noticeably coarser than sand (up to 10 mm in size) and free of any residual hydraulic phases (cementation index is mostly < 0.5) to indicate a relatively pure dolomitic/magnesian limestone feed used during calcination. Abundance of lime lumps indicate possible hot mixing process of mortar (adding quicklime to sand, clay, and water during mixing) and/or addition in traditional putty form. Reaction rims (outer shells) and fine shrinkage microcracks in the interior core of hot-mixed lime clast found in some Roman mortars (Seymour et al. (2023)), however, are not found.

SEM-EDS analysis of paste showed high-magnesian, relatively non-hydraulic composition dolomitic lime. An excellent linear trend in EDS oxide compositions were found when lime plus magnesia contents were plotted against silica plus alumina contents of various binder, clay, and sand phases where dolomitic lime lump and clay (plus sand) occupied the end members with a large range of paste compositions in between from various proportions of clay in the fine-grained, porous, carbonated lime matrix. XRF chemical analysis showed (in decreasing abundance of oxides) of 48.4% Si, 17.6% volatiles (from balance), 11.5% Ca, 8.8% Mg, 7.2% Al, 3.6% Fe, 1.3% K, and <1% of Na, Ti, and P. Gravimetric analyses showed 65.9% insoluble residue corresponding to siliceous sand, and 15.5% total weight losses during stepwise heating with similar loss (of 7.5%) at 550°C and 950°C indicating similar contents of clay and carbonate. XRD studies showed 52.2% quartz and 21.2% feldspar (albite) from sand, 13.8% illitic clay, and 12.8% calcite from carbonated lime matrix. Thermal analysis produced results comparable to gravimetric weight losses from loss of water, dehydroxylation of clay and lime, and decarbonation of carbonated lime paste.

Based on the determined composition and calculated proportions of dolomitic lime mixed with reddish-brown ferruginous clay and crushed sand, a suitable repointing mix of *1-part natural hydraulic lime (NHL 3.5) color-matched to the existing mortar with appropriate dosage of an iron oxide-based pigment (instead of ferruginous clay) to 2-part sand* was suggested as the best starting choice for the mock-up trial mixes. Use of any modern Portland cement or

Portland cement-based blended cement or masonry cement should be completely avoided for gross mismatch with the existing mortar. Instead of ferruginous clay in the original mortar for imparting the color, clay should be avoided and replaced with an iron oxide-based pigment for better durability of the new mortar. Due to atmospheric weathering and alterations, however, an exact match in color to the existing mortar may not be possible, which, even, if possible, could still alter in future due to continued atmospheric weathering in the presence of oxygen, moisture, salt solutions, and other elements.

ACKNOWLEDGMENTS

D. Jana acknowledges 4 years of various discussions on historic mortar testing during late 90s with the late Bernard Erlin, his last mentor before starting CMC, who has drafted the petrography portion of ASTM C 1324. Amanda Edwards at MTFA Architecture is acknowledged for providing the sample.

REFERENCES

ASTM C 144 (2017). ASTM C 144, "Standard Specification for Aggregate for Masonry Mortar;" Annual Book of ASTM Standards; Section Four Construction, Vol. 04.05 Chemical-Resistant Nonmetallic Materials; Vitrified Clay Pipe; Concrete Pipe; Fiber-Reinforced Cement Products; Mortars or mortars and Grouts; Masonry; Precast Concrete; ASTM Committee C12 on Mortars or mortars for Unit Masonry, ASTM International; West Conshohocken, PA; 2017.

ASTM C 207 (2011). ASTM C 207, "Standard Specification for Hydrated Lime for Masonry Purposes," Annual Book of ASTM Standards, Section Four Construction, Vol. 04.01; ASTM Subcommittee C07.02, ASTM International; West Conshohocken, PA; 2011.

ASTM C 270 (2017). ASTM C 270, "Standard Specification for Mortar for Unit Masonry," In Annual Book of ASTM Standards, Section Four Construction, Vol. 04.05 Chemical-Resistant Nonmetallic Materials; Vitrified Clay Pipe; Concrete Pipe; Fiber-Reinforced Cement Products; Mortars or mortars and Grouts; Masonry; Precast Concrete; ASTM Committee C12 on Mortars or mortars and Grouts for Unit Masonry, ASTM International; West Conshohocken, PA; 2017.

ASTM C 1324 (2017). ASTM C 1324, "Standard Test Method for Examination and Analysis of Hardened Masonry Mortar," In Annual Book of ASTM Standards, Section Four Construction, Vol. 04.05 Chemical-Resistant Nonmetallic Materials; Vitrified Clay Pipe; Concrete Pipe; Fiber-Reinforced Cement Products; Mortars or Mortars and Grouts; Masonry; Precast Concrete; ASTM Committee C12 on Mortars or Mortars for Unit Masonry, ASTM International; West Conshohocken, PA; 2017.

ASTM C 1489 (2015). ASTM C 1489, "Standard Specification for Lime Putty for Structural Purposes," In Annual Book of ASTM Standards, Section Four Construction, Vol. 04.01; ASTM Subcommittee C07.02, ASTM International; West Conshohocken, PA; 2015.

ASTM C 1713 (2017). ASTM C 1713, "Standard Specification for Mortars or mortars for the Repair of Historic Masonry," In Annual Book of ASTM Standards, Section Four Construction, Vol. 04.05 Chemical-Resistant Nonmetallic Materials; Vitrified Clay Pipe; Concrete Pipe; Fiber-Reinforced Cement Products; Mortars or mortars and Grouts; Masonry; Precast Concrete; ASTM Committee C12 on Mortars or Mortars and Grouts for Unit Masonry, ASTM International; West Conshohocken, PA; 2017.

ASTM C 1723 (2017). ASTM C 1723, "Standard Guide for Examination of Hardened Concrete Using Scanning Electron Microscopy;" Annual Book of ASTM Standards, Section Four Construction, Vol. 04.02; ASTM Subcommittee C 9.65, ASTM International; West Conshohocken, PA; 2017.

Bartos, P. et al. (2000). Bartos, P, Groot, C, Hughes, JJ (eds.), *Historic Mortars or mortars: Characteristics and Tests*, Proceedings PRO12, RILEM Publications, France, 2000.

Doebley, C.E., and Spitzer, D. (1996). Doebley, C.E. and Spitzer D.; "Guidelines and Standards for Testing Historic Mortars or Mortars"; Standards for Preservation and Rehabilitation; *ASTM STP 1258*; S.J. Kelley, ed., pps. 285-293; ASTM International; West Conshohocken, PA; 1996.

Eckel, E. C. (1922). Eckel, E.C.; *Cements, Limes, and Plasters*; 655 pp; John Wiley & Sons Inc.; Hoboken, NJ; 1922.

Elsen, J. et al. (2012). Elsen, J., Van Balen. K. and Mertens. G.; "Hydraulicity in Historic Lime Mortars or Mortars: A Review"; Valek, J, Hughes, J.J., and Groot, W.P. (Eds.); *Historic Mortars Characterization, Assessment and Repair*; RILEM Book series, Volume 7, pps. 125-139; Springer; Berlin, Germany; 2012.

Elsen, J. (2006). Elsen, J.; "Microscopy of Historic Mortars or Mortars – A Review"; *Cement and Concrete Research,* 36, pps. 1416-1424; ScienceDirect: Elsevier; Amsterdam, The Netherlands; 2006.

Erlin, B., and Hime, W.G. (1987). Erlin, B. and Hime, W.G.; "Evaluating Mortar Deterioration;" *APT Bulletin*, Vol. 19, No. 4, pps. 8-10; Applied Technology Council; Redwood City, CA; 1987.

Goins, E.S. (2004). Goins, E.S.; "Standard Practice for Determining the Components of Historic Cementitious Materials;" *National Center for Preservation Technology and Training, Materials Research Series*; NCPTT; Natchitoches, La; 2004.

Groot, C. et al. (2004). Groot, C., Ashall, G. and Hughes, J.; "Characterization of Old Mortars or Mortars with Respect to Their Repair"; *State-of-the-art Report of RILEM Technical Committee 167-COM*; RILEM; France; 2004.

Hughes, J.J. et al. (2001). Hughes, J.J., Leslie, A.B. and Callebaut, K.; "The Petrography of Lime Inclusions in Historic Lime-Based Mortars;" *Annales Geologiques des pays Helleniques, Edition Speciale*, ISSN: 1105-004, pps. 359-364, Laboratoire De Geologie De L'Universite; Paris, France; 2001.

Jana, D. (2005). Jana, D.; "Application of Petrography in Restoration of Historic Masonry Structures"; Hughes, J.J., Lesie, A.B. and Walsh, J.A., Eds; *Proceedings of 10th Euroseminar on Microscopy Applied to Building Materials*; Paisley Publishing Ltd.; Edinburgh, Scotland; 2005.

Jana, D. (2006). Jana, D.; "Sample Preparation Techniques in Petrographic Examinations of Construction Materials: A State-of-the-art Review"; *Proceedings of the 28th Conference on Cement Microscopy,* pps. 23-70; International Cement Microcopy Association; Denver, CO; 2006.

Jedrzejewska, H. (1960). Jedrzejewska, H.; "Old Mortars or Mortars in Poland: A New Method of Investigation"; *Studies in Conservation* 5, pps. 132-138; Taylor & Francis; London, Great Britain; 1960.

Leslie, A.B., and Hughes, J.J. (2001). Leslie, A.B. and Hughes, J.J.; "Binder Microstructure in Lime Mortars: Implications for the Interpretation of Analysis Results"; *Quarterly Journal of Engineering Geology & Hydrogeology*, V. 35, No. 3, pps. 257-263; Geological Society of London; London, Great Britain; 2001.

Middendorf, B. et al. (2000). Middendorf, B., Baronio, G., Callebaut, K. and Hughes, J.J., "Chemical-Mineralogical and Physical-Mechanical Investigation of Old Mortars or Mortars; Proceedings of the International RILEM workshop *Historic Mortars or Mortars: Characteristics and Tests*, pps. 53-61; Paisley Publishing Ltd.; Edinburgh, Scotland; 2000.

Middendorf, B. et al. (2005a). Middendorf, B., Hughes, J.J., Callebaut, K., Baronio, G. and Papayanni, I.; "Investigative Methods for the Characterization of Historic Mortars or Mortars – Part 1: Mineralogical Characterization;" *Materials and Structures*; Vol. 38; Springer; Berlin, Germany; 2005a.

Middendorf, B. et al. (2005b). Middendorf, B., Hughes, J.J., Callebaut, K., Baronio, G. and Papayanni, I.; "Investigative Methods for the Characterization of Historic Mortars or Mortars – Part 2: Chemical Characterization;" *Materials and Structures*, Vol. 38, pps. 771-780; Springer; Berlin, Germany; 2005b.

Middendorf, B. et al. (2004b). Middendorf, B., Hughes, J.J., Callebaut, K., Baronio, G. and Papayanni, I.; "Chemical Characterization of Historic Mortars or Mortars"; Groot, C., et al. (Eds.); *Characterization of Old Mortars or Mortars with Respect to Their Repair*; State-of-the-art Report of RILEM Technical Committee 167-COM, pps. 37-53; RILEM; France; 2004b.

Middendorf, B. et al. (2004a). Middendorf, B., Hughes, J.J., Callebaut, K., Baronio, G. and Papayanni, I.; "Mineralogical Characterization of Historic Mortars or Mortars"; Groot, C., et al. (Eds.); *Characterization of Old Mortars or Mortars with Respect to Their Repair*; State-of-the-Art Report of RILEM Technical Committee 167-COM, pps. 21-36; RILEM; France; 2004a.

Sarkar, S.L. et al. (2000). Sarkar, S.L., Aimin, X. and Jana, D.; "Scanning Electron Microscopy and X-ray Microanalysis of Concretes"; Ramachandran, VS and Beaudoin, J.J. (Eds.); *Handbook of Analytical Techniques in Concrete Science and Technology,* pps. 231-274; Noyes Publications; Park Ridge, NJ; 2000.

Seymour, L.M. et al. (2023). Seymour, L.M., Maragh, J., Sabatini, P., Di Tommaso, M., Weaver, J.C. and Masic, A.; "Hot Mixing: Mechanistic Insights Into the Durability of Ancient Roman Concrete"; Science Advances 9, 1602, pps. 1-13; American Association for the Advancement of Science; Washington, DC; 2023.

Stewart, J., and Moore, J. (1981). Stewart, J. and Moore, J.; "Chemical Techniques of Historic Mortar Analysis"; Proceedings of the ICCROM Symposium: *Mortars, Cements, and Grouts used in the Conservation of Historic Buildings*; pps. 297-310; ICCROM; Rome, Italy; 1981.

Valek, J. et al. (2012). Valek, J., Hughes, J.J. and Groot, C. (Eds.); *Historic Mortars or Mortars: Characterization, Assessment and Repair*; RILEM Book series Vol. 7, 464 p; RILEM; France; 2012.

Valek, J., and Matas, T. (2010). Valek, J. and Matas, T.; "Experimental Study of Hot Mixed Mortars in Comparison with Lime Putty and Hydrate Mortars"; *2nd Historic Mortars Conference HMC2010 and RILEM TC 203-RHM Final Workshop* 22-24 September; pps. 1229-1240; Prague, Czech Republic; 2010.

NOTATION

< = Less than
> = Greater than
θ = Angle of diffraction
PPL = Plane polarized light
XPL = Cross polarized light

Laboratory Testing of Historic Mortars: Part 2 – Microstructure of a Historic Feebly-Hydraulic Lime Mortar Containing Silica Flour

Dipayan Jana [1] and Shubham N. Mahajan [2]

INTRODUCTION

Clay and lime are two essential binders of most historic mortars where the former often provided a pozzolanic character when added to an essentially lime-based mortar. A variety of lime binders from non-hydraulic (calcitic to dolomitic) to variably hydraulic lime was used. Nonhydraulic lime (e.g., lime putty) sets in air from carbonation, whereas depending on the degree of hydraulicity, hydraulic lime sets mostly in air from carbonation for feebly hydraulic ones to water from hydration with increasing hydraulicity from increasing aluminosilicate impurities in the calcined feed. Masons often added fibers, brick dusts, microfiller like silica flour, etc. for added strength and durability. Various organic or inorganic pigments were occasionally added to bring an aesthetic dimension to the adjacent masonry units.

A microstructural atlas is presented here on a 190-year-old mortar from the historic Manor House (built circa 1834, Figure 1A) in the Clifton historic farm in Clarke County Virginia, located in the northern end of the Shenandoah Valley, 60 miles west of Washington DC. Clifton Farm has played a significant role in American history for over two hundred years notably, from its close association with George Washington, who walked its rolling fields as a youth in the 18th century.

SAMPLE

As part of renovation, a dusty fragmented piece of a beige/tan colored mortar weighing 45 grams and measuring 40 mm × 30 mm × 15 mm in lateral dimensions for the largest fragment was provided (Figure 1B) to determine the composition and mix proportion of the mortar so that a suitable repointing mortar could be formulated. Scattered throughout are white, angular, soft, unmixed lumps of lime (Figure 1C), many noticeably coarser than sand (up to 10 mm) to immediately confirm its lime-based binder composition consistent with its age. The brown color tone indicated potential presence of an iron oxide-based pigment or some other ferruginous components in the lime.

1. TMS Member, President and Petrographer, Construction Materials Consultants, Inc., Greensburg, PA, info@cmc-concrete.com.

2. Petrographer, Construction Materials Consultants, Inc., Greensburg, PA, info@cmc-concrete.com.

ANALYTICAL TECHNIQUES

The mortar was analyzed by following the procedures of: (a) ASTM C 1324 "Standard Test Method for Examination and Analysis of Hardened Masonry Mortar," and (b) the RILEM method, described in Middendorf et al. (2000), (2004 a), (2004 b), (2005 a), (2005 b), (Valek et al. (2012), and Bartos et al. (2000). Steps followed during examinations include: (1) detailed optical microscopy of as-received, polished solid and thin (30-µm thick) sectioned pieces of sample with stereo-zoom microscope, and petrographic microscope to determine the type, condition, and composition of sand, binder, and overall mortar; (2) scanning electron microscopy and energy-dispersive X-ray microanalyses (SEM-EDS) of interstitial paste fraction of mortar to ascertain the binder composition determined from optical microscopy; (3) extraction of acid-insoluble (e.g., siliceous) component of sand by acid (HCl) digestion, followed by sieve analysis of extracted sand to determine the grain-size distribution of sand; (4) chemical (gravimetric) analysis to determine siliceous sand content from hydrochloric-acid insoluble residue content, (5) free and combined water and carbonate contents from loss on ignition at 110°C, 550°C, and 950°C, respectively, (6) X-ray fluorescence spectroscopy (XRF) to determine chemical (oxide) composition, (7) X-ray diffraction (XRD) study to determine the mineralogical composition, (8) thermal analysis to determine the hydrous, sulfate, and carbonate phases, and (9) water-soluble chloride and sulfate contents in the filtrates after digesting mortar in deionized water to determine the presence of potentially deleterious soluble salts (e.g., of chloride, sulfate, etc.). Based on all these comprehensive analyses, the overall condition, extent of deterioration, and composition of the sample can be assessed, from which suitable replacement for the examined sample can be evaluated. Details of analytical techniques are provided in the Part 1 of this series by Jana and Mahajan (2024).

Optical Microscopy

Epoxy-impregnated polished solid sections and thin sections (25-to-30-micron thickness, 50 × 75 mm size) of mortar were prepared following procedures mentioned in Jana (2006). Prepared sections were examined in Nikon SMZ 1500 stereozoom and Olympus BX-51 petrographic microscopes (both equipped with transmitted and reflected plane-polarized, cross-polarized, and fluorescent light facilities).

SEM-EDS

Following optical microscopy, features of interest for further exploration of polished solid and thin sections were examined in two SEMs (Camscan Series II and Jeol Neoscope JCM-7000) both equipped with secondary electron, backscatter electron, and EDS detectors for observations of microstructures at high-resolution, compositional analysis, and quantitative determinations of major element oxides from various areas of interest, respectively. Procedures for SEM examinations are described in ASTM C 1723.

Gravimetric Analysis

Acid digestion was done to (a) extract insoluble component of sand for grain-size distribution and (b) determine insoluble (siliceous) sand content from 1.00 gram of pulverized sample (finer than 0.3 mm size) digested in 50-ml dilute (1+3) HCl (heated rapidly but below boiling for 15 min). Losses in weight of 1.00 gram of pulverized mortar (less than 0.3 mm size) in a muffle furnace at a heating rate of 10°C/min on stepwise heating from ambient to 110°C, 550°C, and 950°C temperatures determine free water by 110°C, combined water from dehydration/dehydroxylation of various hydrous phases by 550°C, and degree of carbonation from decomposition of carbonated paste by 950°C, respectively.

X-ray Fluorescence Spectroscopy (XRF)

An energy-dispersive bench-top X-ray fluorescence unit from Rigaku Americas Corporation (NEX-CG) was used, which was calibrated by using various certified (CCRL, NIST, GSA, and Brammer) reference standards of cements and rocks. The less than 44-micron pulverized fraction of mortar was pressed into a pellet with a 15-ton Spex hydraulic press for XRF.

X-ray Diffraction (XRD)

X-ray diffraction was done on the pulverized (to finer than 45-micron size) fraction of mortar in a Bruker D2 Phaser benchtop powder diffractometer equipped with a Lynxeye 1D detector, a θ-θ goniometer, a Cu X-ray tube (Cu k-alpha radiation of 1.54 angstroms), a primary slit of 1 mm, a receiving slit of 3 mm, a position sensitive 1D Lynxeye XE-T detector, generator settings used are 30 kV and 10mA (300 watt, scanned at 2θ from 4° to 64° with a step of 0.05° 2θ integrated at 0.05 sec. step^{-1} dwell time). The resulting diffraction patterns are collected by Bruker Diffrac. Suite software and analyzed by MDI Jade with ICDD PDF4 Minerals database of diffraction data. Phase identification and quantitative analyses were carried out with MDI Jade's Search/Match with Rietveld Whole Pattern Fitting.

Thermal Analyses

Simultaneous thermogravimetric analyses (TGA) and differential scanning calorimetry (DSC) analyses were done in a Perkin Elmer STA 6000 unit on 30-70 mg of finely ground (less than 45-micron) sample in alumina crucible (70 µl, no lid) from 30°C to 1000°C at a heating rate of 10°C/min with high purity nitrogen as purge gas at a flow rate of 75.0 ml/min, from which first derivative of TGA curves (DTG) were presented as superposed patterns to compare bulk mortar with lime lump and finest fractions.

Potentiometric Titration and Ion Chromatography (IC)

Water-soluble chloride ions are determined by titration using silver nitrate titrant following ASTM C 1218, and both chloride and sulfate by IC following ASTM D 4327. About a gram of pulverized mortar finer than 200-µm is digested in deionized water at near-boiling temperature for 15 minutes followed by 24-hour digestion at room temperature after which the solution was passed through two 0.2-micron filter paper, under vacuum, to collect the filtrate for analyses.

RESULTS

Mortar Sand and Silica Flour

The composition, mineralogy, grain size, shape, color variations, distribution, gradation, and soundness of sand were examined from (a) thin section microscopy of as-received mortar fraction, and (b) a portion extracted from as-received mortar after hydrochloric acid digestion. Both methods showed three distinct populations of sand based on grain size and angularity, which are:

(a) A coarse fraction, greater than 0.6 mm in size, present in minor (~10 percent) proportion, present mostly in rounded, equant shape, probably sourced from the nearby Shenandoah River.

(b) An intermediate fraction, less than 0.6 mm to 0.15 mm in size, present as the dominant proportion (~50 percent), mostly subangular to rounded grains probably representing the same provenance as the coarser grains.

(c) A finest fraction, less than 0.1 mm in size, ~40 percent, which is mostly angular, and probably represent a separate addition as a silica flour (for its characteristic crushed and ultrafine nature compared to rounded river sand) to fill the interstitial spaces left from packing of coarser and finer sand grains. The silica flour component has provided a gritty, granular fritstone-type texture of the interstitial mass between medium-to-coarse sand grains.

Relative proportions of these populations are determined from percent acid-insoluble residues retained at various sieves (Figure 2), whereas their *in situ* spatial distribution are displayed in thin section micrographs in Figures 3 to 6. Acid-washed sand fraction constituted 85.4

percent of mortar, by mass, which contained clear, colorless, transparent to translucent, subangular to rounded, mostly equant-shaped, dense, hard, subtranslucent vitreous lustered, well-graded grains having 93.1 percent quartz, 6.9 percent K-feldspar (microcline), and no clay residue as determined from Rietveld XRD analysis. Corresponding calculated chemical composition of extracted sand showed 97.6 percent SiO_2, 1.3 percent Al_2O_3, and 1.2 percent K_2O. Grain size distribution in Figure 2 showed overall very fine size fractions of sand compared to modern ASTM C 144 natural sand with a fineness modulus of only 1.06, mostly contributed from the ultrafine silica flour, which must have had a negative impact on increasing the water requirement of mortar mix during placement at a given workability. Compared to acid-washed fraction, however, polished sections of mortar as received showed some darker ferruginous-argillaceous-carbonaceous grains (e.g., boxed in Figures 1E, 1F) mostly in the 0.6-to-0.15 mm size fractions. Figure 3 shows type, size, shape, and distribution of sand in blue or clear epoxy-impregnated thin (30-µm thick) section of three fragments in plane polarized light (PPL) and corresponding cross polarized light (XPL) modes. Thin section micrographs in Figures 4 to 7 showed siliceous mineralogies and textures of sand grains. No calcareous component was found, which has helped straightforward determination of sand content from the acid-insoluble residue content. Sand was present in sound condition without any evidence of potentially deleterious physical or chemical (e.g., alkali-aggregate) reactions. Despite soundness, however, based on the abundance (e.g., greater than 85 percent by mass) and mainly fineness (fineness modulus less than 2, probably for derivation from extensively abraded bank of river) sand is judged unsuitable compared to a modern-day ASTM C 144 sand to restrict its straightforward incorporation in a pointing mortar mix.

Binder Compositions and Microstructure

Perhaps the most unusual aspect of the mortar compared to other traditional historic lime mortars is in the microstructure of interstitial paste fraction between sand grains, which are neither straightforward (i) porous, fine-grained carbonated lime, which is a telltale sign of a nonhydraulic lime mortar, nor (ii) a carbonated paste with occasional denser regions of residual hydraulic phases as seen in many hydraulic lime mortars, or (iii) variably carbonated and hydrated matrix with scattered residual cement and calcined feeds seen in many natural (Roman) cement mortars. The difficulty is partly due to the low volume of paste, mostly from the use of finest (less than 0.1 mm size) silica grains at 40 percent abundance (as silica flour) to fill most of the interstitial spaces, which would have been otherwise filled with paste.

The only direct evidence of use of lime, mostly in the putty form (commensurate with its 1830's derivation) came not from the interstitial paste fraction but from the scattered soft white lumps of unmixed lime, which are present at wide size ranges, e.g., from noticeably coarser than even the coarsest sand grains to variably finer to ultrafine dusty forms mostly present in the interstitial paste fraction. Many lime lumps contained tiny grains of residual hydraulic phases and associated hydration products, which are described under the section dedicated to lime lump.

The interstitial paste fraction showed a distinct potassium-aluminum-silicate composition, which is characteristically depleted in lime compared to a traditional lime-dominant composition of paste in a historic mortar. Source of silica and alumina in the interstitial paste fraction are partly derived from (i) the carbonated lime that contained silica-alumina impurities from hydration of residual hydraulic phases (RHPs) from the calcined limestone feed, and partly from (ii) the finest (less than 0.1 mm size) fraction of sand (probably added as silica flour) that contained quartz and K-feldspar.

Thin section micrographs in Figures 6A to 6D show optically isotropic nature of a lime lump (in Figures 6A, 6B) and interstitial paste fraction (in Figures 6A to 6D) interstitial paste fractions due to variable leaching of lime. Figures 6E to 6H show the paste fraction at higher magnifications in PPL and XPL modes, where relatively high birefringence of paste is noted from the carbonated nature even though carbonated lime content is noticeably lower than that of a traditional lime mortar.

Both the lime lump and carbonated lime in the interstitial paste fraction are porous where pore spaces are highlighted in micrographs of thin sections prepared with a blue dye-mixed epoxy for the very purpose (Figures 5 to 7), along with highlighting fine hairline carbonation shrinkage microcracks seen in many coarse lumps (Figure 8E).

SEM-EDS analyses of interstitial paste fraction in Figures 12, 13, and 16 showed overall depletion in Ca from lime leaching and corresponding enrichment in silica-alumina, which were derived partly from the hydraulic phases in lime and partly from quartz-feldspar grains in the finest fraction of added silica flour. Cvbhngmj,l.m

Lime Lump

Lime lumps can have multiple origins and modes of occurrences all of which are commonly found in many historic lime mortars (Hughes et al. (2001)), e.g.,

(a) As unburnt or overburnt lime often occur in darker black or brown color tones, respectively, where former can potentially permit identification of limestone provenance.

(b) As dense, massive-textured unmixed clumps of very fine-grained slaked lime from traditional matured lime putty (which may also occur in dry hydrated lime), now variably carbonated during service. These lumps often maintain distinct rounded to subrounded to angular shapes with distinct boundaries or may have partially or completely diffused boundary to the surrounding lime matrix. They may

show massive to pelleted or clotted appearance or texture with internal porosity, or concentric color zoning over distinct granular texture with silicate inclusions from original limestone feed, sometimes contain pseudomorphs of original limestone texture to help potential detection of limestone provenance, or residual hydraulic phases if original calcined limestone was impure.

(c) As lime clasts as subangular to angular coarse-grained aggregates from slaked quicklime left from hot mixing process.

All modes and origins of lime lumps/clasts can show fine discontinuous shrinkage microcracks developed either during initial stage from loss of moisture or during subsequent carbonation. Microcracks in clasts from hot-mixed mortar are more common as also in matured lime putty than dry hydrated lime (Valek and Matas (2010)).

Lime lumps free of any RHPs indicate non-hydraulic nature of the original lime binder produced from calcination of a relatively pure calcitic/dolomitic/magnesian limestone feed. RHPs (e.g., commonly belite and/or Ca-Si-Al-based crystalline and/or amorphous phases) are commonly found within the unmixed lumps if the original limestone feed used for calcination contained clay and/or silica impurities.

Scattered soft, white, angular lumps of unmixed lime as seen in Figure 1C is the most characteristic telltale sign of incorporation of the traditional lime binder in putty form. Lime lumps are clearly seen in many thin section micrographs in PPL and corresponding XPL images, e.g., in Figures 5C to 5F, 6A, 6B, 7C to 7H, and 8E to 8H. Four microstructural features are noted in many of these lumps: (a) overall *fine-grained, porous nature* as highlighted by absorption of blue epoxy during impregnation in PPL images, (b) overall *carbonated nature* in XPL images from prolonged interaction with atmospheric CO_2, Figures 7D, 7H, 8B, 8F), (c) fine hairline *carbonation shrinkage microcracks* in PPL images (Figure 8H); and (d) variable degrees of *leaching of lime*, which has increased the overall porosity of lump as seen in the PPL images (Figure 8A) and turned the overall lump optically isotropic as seen in the XPL images (Figures 5F, 6B).

Residual Hydraulic Phases (RHPs) in Lime Lump

Despite using the lime in the traditional putty form, the feebly hydraulic nature of lime imparted from the presence of minor impurities in the calcined calcitic limestone feed is revealed from scattered very fine grains of RHPs within lime lump, which provide direct microstructural evidence of the nature of hydraulic phases formed during the calcination process. RHPs are seen in thin section micrographs in Figures 6A, 7E, 8E, 8G, and 9A to 9D. SEM-EDS analysis of RHPs within lime lump are shown in Figure 14.

Thin section micrographs in Figures 9E to 9J show lump size optically isotropic grain of separate RHP in the mortar matrix, not necessarily within a lump, where isotropic nature was partly derived from the amorphous aluminosilicate phase formed from calcination and partly from subsequent leaching of lime during service.

Residual Hydraulic Phases and Hydration Products in Incompletely Calcined Limestone Feed

Thin section micrographs in Figure 10A and 10B showed an incompletely calcined calcitic limestone feed in mortar having abundant fine disseminated grains of RHPs as cores and associated hydration products (HPs) in the overall mosaic-textured calcite grains of limestone, which is the gold mine in finding hydraulic phases formed from calcination process of feed. Figures 10C to 10F show the typical core and rim microstructure of RHPs and HPs, respectively at PPL and XPL. Associated top-right column photos in Figure 10 show backscatter electron (BSE) image and elemental maps of cores and rims depicting typical K-Al-Si compositions of RHPs in cores and Ca-Si-Al compositions of hydration rims in the overall calcite matrix of limestone. Figure 10 bottom images further explored the core-rim microstructure and microchemical variations by pinpointing analyses at various regions of RHPs and hydration products to reveal their inherent difference in compositions, e.g., aluminosilicate-based compositions of RHPs versus calcium-silicate-aluminate compositions of hydration products. The core-vs-rim compositional difference became distinct in the cluster phase map analysis in Figure 11 where Ca-rich HPs versus Si-Al-rich cores are clear.

Cluster Phase Map – A Powerful Tool for Analysis of Microchemical Variations in Historic Mortar

Figures 11 through 17 provided eight SEM-EDS cluster phase map analyses of mortar to reveal following microchemical features:

(a) RHPs and associated HPs within calcined limestone feed (Figure 11).

(b) Si (quartz) and K-Al-Si (K-feldspar) sand grains, voids and pore spaces (highlighted by C map from epoxy), and interstitial paste between sand grains having disseminated Ca-rich and Ca-poor K-Al-Si-rich areas (Figure 12 left).

(c) Compositional variation of interstitial paste fraction at high magnification showing Ca-depleted K-Al-Si-rich regions having variable Si-Al ratios and scattered Si (quartz) and K-Al-Si (K-feldspar) grains (Figure 12 right).

(d) Lime lumps (highlighted in Ca-map) scattered throughout the matrix of Si (quartz) and K-Al-Si (K-feldspar) sand grains, and interstitial paste of variable degrees of Ca-leaching and variable Si/Al ratios

(Figure 13 left at low and right a high magnification of a boxed area from left).

(e) RHPs within a carbonated lime lump showing compositional zonation from core to rim from variable Ca/Si and Si/Al ratios in RHPs (Figure 14 left).

(f) RHPs within the same lime lump at lower magnification showing scattered silica grains from silica impurity in the original feed (sometimes form a thin melted rim around cristobalite), rounded K-Al-Si grains from RHPs, thin rims of Ca-K-Al-Si of variable Ca/Si and Si/Al ratios from HPs of RHPs, and overall Ca-K-Ai-Si matrix of a leached lime lump (Figure 14 right).

Many such maps provide important details on microchemical variations of RHPs in SEM-EDS studies, which are otherwise impossible to determine from traditional optical microscopy even though thin section examination in a traditional petrographic microscope can easily detect RHPs within lime lump or in the paste fraction of mortar for further exploration in SEM. Degree of hydraulicity of lime is usually assessed from the proportions of RHPs scattered through the paste fraction revealed through optical microscopy.

Finest Fraction (less than 44-µm) Before and After Acid Digestion

The finest fraction of the dusty mortar sample passed through US 325 (44-micron opening) sieve is analyzed by XRD for detection of potential addition of clay, and SEM-EDS before and after hydrochloric acid digestion to determine elements that are contributed from sand versus paste. Results are presented in Figure 15, which shows expected disappearance of calcite in XRD pattern of acid-digested residue leaving finest sand fraction of quartz and K-feldspar as also seen in the bulk mortar but no clay residue either in the undigested or in digested residue. SEM-EDS analyses of fractions before and after digestion showed noticeable loss of Ca, Mg, and Fe in the residue due to their adherence to the acid-soluble (lime) fractions. Iron in the lime putty was present as minor impurity in limestone that has imparted the beige color tone of mortar without any separate addition of a pigment (which would have been detected in the acid-insoluble residue).

Air

Mortar is non-air-entrained, which is typical of most historic mortars formulated before the advent of air entrainment. Air content is estimated to be 4 to 6 percent, which are coarse, irregular-shaped entrapped voids best depicted in thin section scans in PPL in Figure 3.

Salt Crystallization and Sulfate Ingress

SEM-EDS chemical analyses of interstitial paste fractions in Figure 16 showed high levels of sulfur and chlorine, which are commonly penetrated from the external environment and can potentially cause chloride attack from salt crystallization and sulfate attack, respectively. BSE image and Na-Cl elemental maps in Figure 17 showed spectacular development of cubic crystals of halite, which if occurs in a confined space in mortar can cause cracking. Distress from salt crystallization, however, is not found due to the overall porous nature of the matrix. Potentiometric titration of a filtrate from deionized water digested pulverized mortar showed 1237-ppm water-soluble chloride whereas ion chromatography of another filtrate from a separate aliquot showed 1250-ppm chloride and 9450-ppm sulfate.

Mineralogy and Chemistry from XRD-XRF-DTG

Figure 18 shows superposed XRD patterns of bulk mortar, lime lumps, acid-washed sand, and finest (less than 44-micron) fraction depicting: (a) dominant quartz and subordinate K-feldspar composition of sand after acid digestion, (b) overall similarities in patterns of extracted sand and bulk mortar for dominant (greater than 85 percent) volume proportion of sand, (c) absence of any characteristic clay peaks and dominance of ultrafine quartz in the finest fraction (less than 44-µm) of mortar, and (d) calcite mineralogy of carbonated lime lump indicating calcination of a calcitic limestone feed. Rietveld mineral percent of bulk mortar showed 70 percent quartz, 25 percent K-feldspar (microcline), and 10 percent calcite. Chemical composition by XRF and gravimetric (acid-insoluble residue content and losses on ignition at 110°C, 550°C, and 950°C) results are shown in a Table inside Figure 18. Finally, superposed DTG curves of bulk mortar, lime lump, and finest (less than 44-µm) fraction showed characteristic endotherms from (a) loss of free water, (b) dehydration of hydration products of RHPs, (c) various dehydroxylation reactions, (d) decomposition of calcium hydroxide component of lime, and (e) decarbonation of lime lumps and interstitial carbonated lime products in paste.

DISCUSSIONS

Importance of Microscopy in Determining Binder Type of Historic Mortar

Of all the analytical techniques described, optical microscopy in combination with SEM-EDS are the most powerful methods, which provide first-hand information about the original lime binder from its calcitic versus low-magnesian versus dolomitic composition to latent hydraulicity (Elsen (2006), Elsen et al. (2012), Erlin and Hime (1987), Goins (2004), Groot et al. (2004)) to composition of the original feed used in the calcination process for production of first quicklime and subsequently lime putty. Although white lumps of unmixed lime scattered

throughout the mortar provided straightforward clue on use of lime binder but the hydraulicity and dominantly calcitic composition of lime with minor silica, alumina, iron impurities in original limestone feed became apparent from subsequent microscopy. Information obtained from acid-washed sand on its type, composition, fineness, gradation, etc. are already confirmed from optical microscopy of thin sections. XRD provided an additional tool to check for the finest fractions, especially for presence of clay with lime in binder, which are usually present at ultrafine sizes unresolvable in optical microscopy. SEM-EDS studies may not confirm the clay mineralogy if clay is consumed by pozzolanic reaction with lime except only suspecting its presence from its characteristic elemental peaks (Al, Si). Al-Si peaks, however, can also come from hydraulic phases especially after leaching. Calcitic versus dolomitic composition of lime is confirmed from magnesia content of paste in EDS analysis along with possible presence of brucite and/or hydromagnesite endotherms in DSC/DTG curves. BSE images show spectacular evidence of salt crystallization along with the identification of salt, whereas IC provides concentration of water-soluble salts.

Difficulty in Mix Calculations of Historic Mortars

Beyond microscopy, supplemental tests from traditional gravimetric analyses to XRF, XRD, and TGA provide additional information needed for calculation of proportions of various binder components and sand used in the original mortar mix so that a suitable pointing mortar for restoration can be formulated.

Historic mortars, however, offer various levels of difficulties from unrestricted chemistries/hydraulicities of lime mortars used to unknown degrees of alterations during service where traditional (i.e., ASTM C 1324) method of determination of sand and binder proportions of modern cement-lime or masonry cement mortars, e.g., from acid insoluble residue content (for sand content), soluble silica content (for hydraulic binder content), loss on ignition (for combined water and carbonate contents) from assumed compositions and dry densities of binder components applied for determination of mix proportions are impossible. In fact, due to the unknown and rather wide unrestricted compositional range of historic binders, e.g., for hydraulic lime having wide range of hydraulicities and natural cements without any tight control on their argillaceous dolomitic limestone feeds being calcined (unlike well-proportioned limestone-shale mix in the modern Portland cement manufacturing), ASTM C 1324 method of mix proportion calculation cannot be extended for historic mortars.

The underlying philosophy of mix calculation, however, can still be exercised to historic mortar, wherever possible. For example, since sand here is determined to be siliceous in composition with no calcareous component, sand content is essentially determined from the acid-insoluble residue content of mortar, which is 85.4 percent, a majority of which (almost 35.4 percent) is from addition of ultrafine (less than 0.1 mm size) crushed silica sand as silica flour. Such an excess fine fraction can increase the water requirement of mortar mix at a given workability. Assuming a dry density of sand as 80 lbs./ft^3, sand volume with or without the finest (less than 0.1 mm) fraction is then calculated to be either 1.06 or 0.62, respectively, which including the finest fraction is representative of a grossly over-sanded mortar for a modern mix. Due to the feebly hydraulic composition of calcitic lime binder as assessed from a few RHPs mostly within the lime lumps, traditional binder content determination from soluble silica content of binder with an assumed binder composition as prescribed in ASTM C 1324 cannot be used for historic mortars. Since carbonation of mortar is mostly confined to the lime (left after the mass already leached) a minimum lime content can be assessed from degree of carbonation from 2.3 percent loss on ignition at 950ºC, which corresponds to 3.87 percent lime. Assuming a dry density of lime to be 40 lbs//ft^3, lime volume is estimated to be 0.096. Lime-to-sand volumetric ratio from this approach is then 1:11 including the finest fraction of sand, or 1:6.5 without the finest fraction, both of which are noticeably higher than most modern mortars used for repointing purposes.

Suitable Replacement Mortar

Microscopy provided more straightforward approach for selection of a suitable NHL binder and silica sand type pointing mortar than mix calculations including the three populations of sand and binder. Final mix can be selected from initial mock-up mixes of 1-part NHL 2 or NHL 3.5 and 2-part silica sand as long as it is tested in a small area and found satisfactory to the adjacent masonry unit. The use of aged lime putty, however, was the recommended choice of practice in old days because this viscous form with higher plasticity and water-retention capacity, results in mortars of higher strength that carbonate faster (Hughes et al. (2001), Leslie and Hughes (2001)). Either lime putty as specified in ASTM C 1489 or hydrated lime (ASTM C 207) can be tried in case of NHL. Initial rate of absorption of adjacent masonry units is also important for mortar selection. ASTM C 1713 specification for mortars for repair of historic masonry is a recommended practice for mortar restoration. Overall appearance of the final mortar would depend on a match on sand, which constitutes the dominant proportion of the mortar. Sand should be siliceous (river sand) except perhaps without adding the finest fraction, match in color to the color of sand in the examined mortar, from a similar source, free of any debris, unsound, clay particles, or any potentially deleterious constituents, similar to the size requirements of ASTM C 144 for masonry sand having maximum 2.5- times sand to the volume of lime, and durable.

CONCLUSIONS

A rather unusual historic mortar is found being used in the 1830s Manor house showing the addition of very fine (0.1 mm size) silica flour in a feebly hydraulic calcitic lime putty binder where the color tone of mortar was imparted mostly from the sand and secondarily from the lime fraction. Optical microscopy showed unmixed lumps of carbonated lime (many containing very fine RHPs and hydration rims) scattered throughout a matrix of coarse (greater than 0.6 mm) to intermediate (0.6 to 1.5 mm) size siliceous sand of dominant quartz and subordinate K-feldspar and a finest (less than 0.1 mm size) fraction of angular silica flour all constituting greater than 85 percent mass of mortar and rest interstitial variably leached, porous, and carbonated paste and voids. Paste showed an overall lime-depleted dominantly aluminosilicate composition derived partly from the finest (less than 0.1 mm size) fraction of sand (dominant quartz, subordinate K-feldspar, mostly as silica flour) and partly from hydration (and carbonation) products of RHPs in lime. Feebly hydraulic nature of lime putty binder is confirmed from minor occurrence of RHPs in carbonated lime lump along with some Si-Al found in the lime lump.

Historic mortars were traditionally prepared using nonhydraulic to hydraulic lime-based or mixed lime-natural cement or natural cement-based binders of unrestricted compositions that are inherently different from modern Portland (or blended) cement-hydrated lime or masonry cement-based binders produced under strict quality controls. This difference in binder type and chemistry along with prolonged environmental effects make proper identifications and mix proportions of historic mortars difficult. Microscopy is the best tool available that not only evaluates historic mortars from sand to binder(s) types and proportions, extent of distress from exposure conditions, but also the original feed and slaking/calcination processes followed, and eventually to assess the most suitable replacement mortar to use for restoration projects.

ACKNOWLEDGMENTS

D. Jana acknowledges 4 years of various discussions on historic mortar testing during late 90s with late Bernard Erlin, his last mentor before starting CMC, who has drafted the petrography portion of ASTM C 1324.

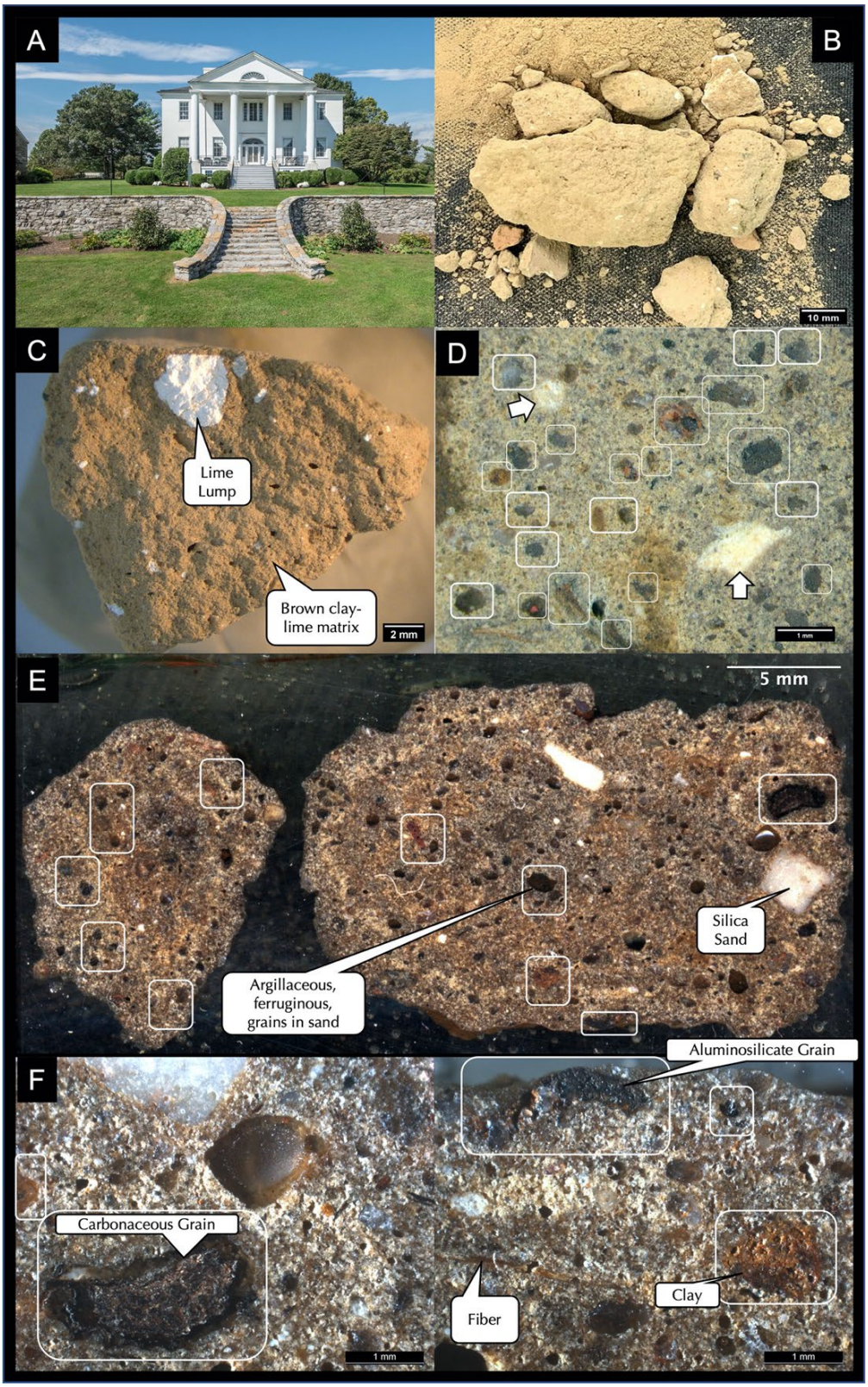

Figure 1 - A: The historic Clifton Manor house, from where the mortar sample was collected. B: Fragmented, dusty brown mortar sample, as received. C: White lumps of unmixed lime scattered throughout the mortar. D: Lapped section of a clear epoxy-impregnated fragment showing dark-gray sand-size argillaceous/ferruginous particles in sand (boxed) and a few off-white coarse sand grains (arrows). E: Polished section of two epoxy-impregnated fragments showing scattered dark-brown grains (boxed), a few off-white coarse sand, and other finer darker grains in an overall brown-toned matrix. F: Micrographs of polished section showing dark-gray carbonaceous, dark-brown ferruginous, some dark aluminosilicate grains (boxed), and occasional fibers (scale bars are 1 mm).

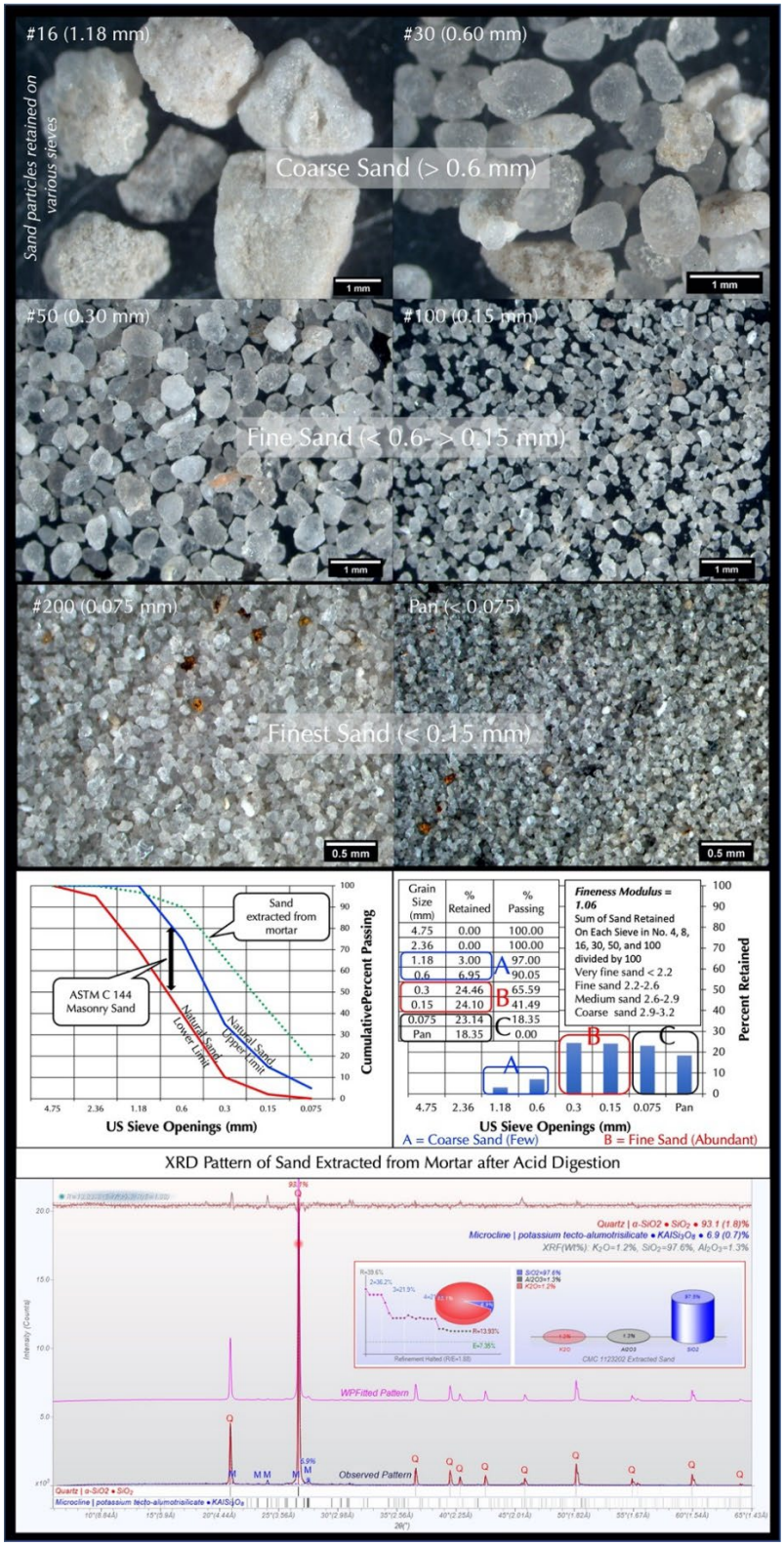

Figure 2 - Grain-size distribution of sand extracted from mortar after acid digestion and retained on various US sieves showing overall very fine grain size of sand compared to the size distribution of modern ASTM C 144 sand. Fineness modulus is only 1.06. Majority (greater than 90 percent) of sand grains are finer than 0.6 mm (41.5 percent are less than 0.1 mm), and only a few (less than 10 percent) are coarse. Particles are clear, transparent to translucent, subangular to rounded, mostly equant shaped, and well-graded. XRD (Rietveld) analysis showed 93.1 percent quartz and 6.9 percent K-feldspar (microcline). No clay residue was found after acid digestion. Acid-insoluble residue content of quartz and feldspar was 85.4 percent. Corresponding calculated chemical composition showed 97.6 percent SiO_2, 1.3 percent Al_2O_3, and 1.2 percent K_2O from sand.

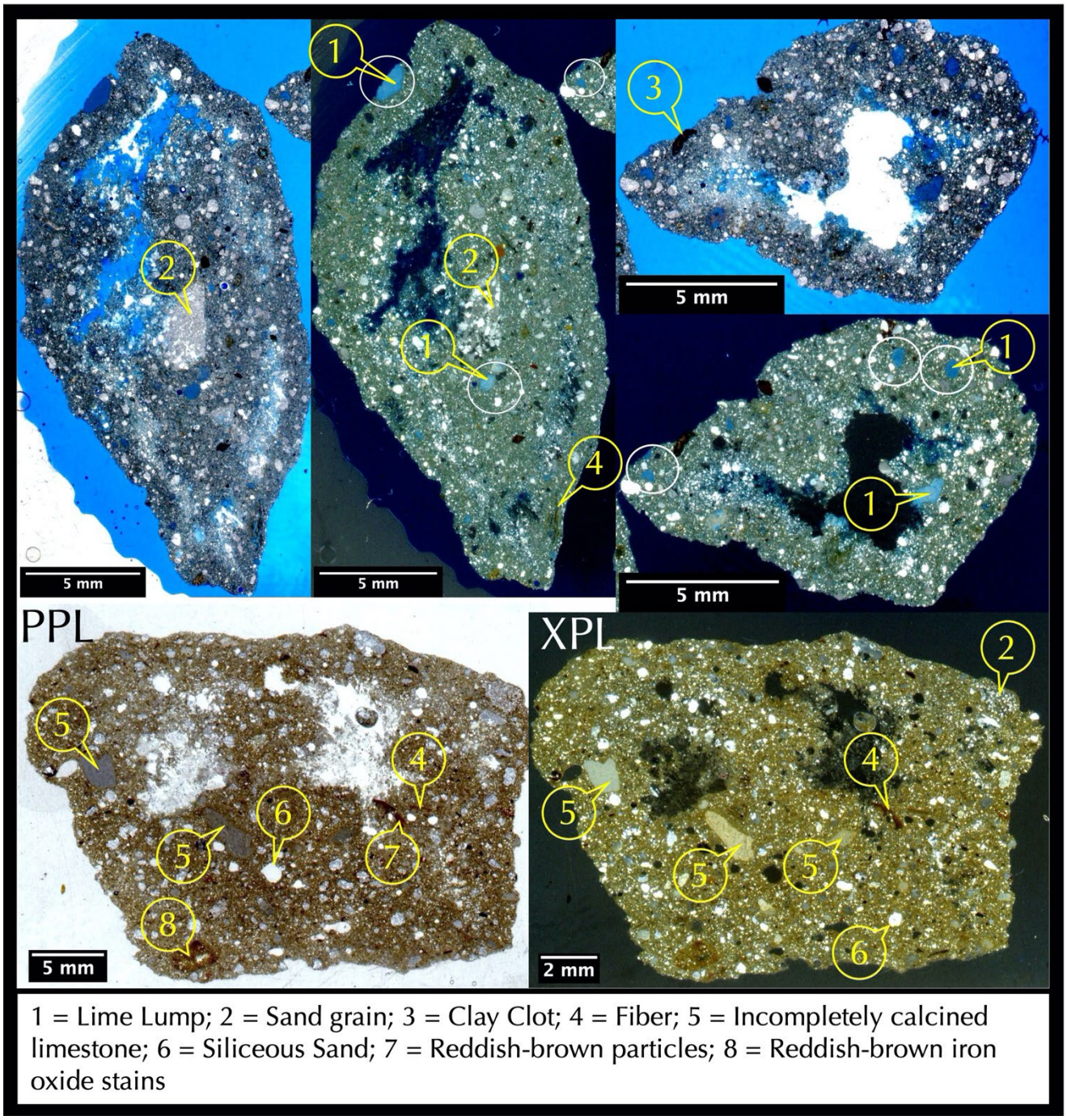

Figure 3 - Thin sections prepared from epoxy-impregnated polished block of mortar (top row blue dye-mixed epoxy and bottom row clear epoxy) showing overall very fine grain-size and uniform distribution of sand with occasional coarser (greater than 0.6 mm size) grains. Thin sections are scanned on flatbed transparency scanner with one on top or sandwiched between two perpendicular polarizing filters to recreate plane and cross polarized modes (PPL and XPL), respectively. Various features of interest are marked in 1 through 8. Many details are shown in Figures 4 to 9.

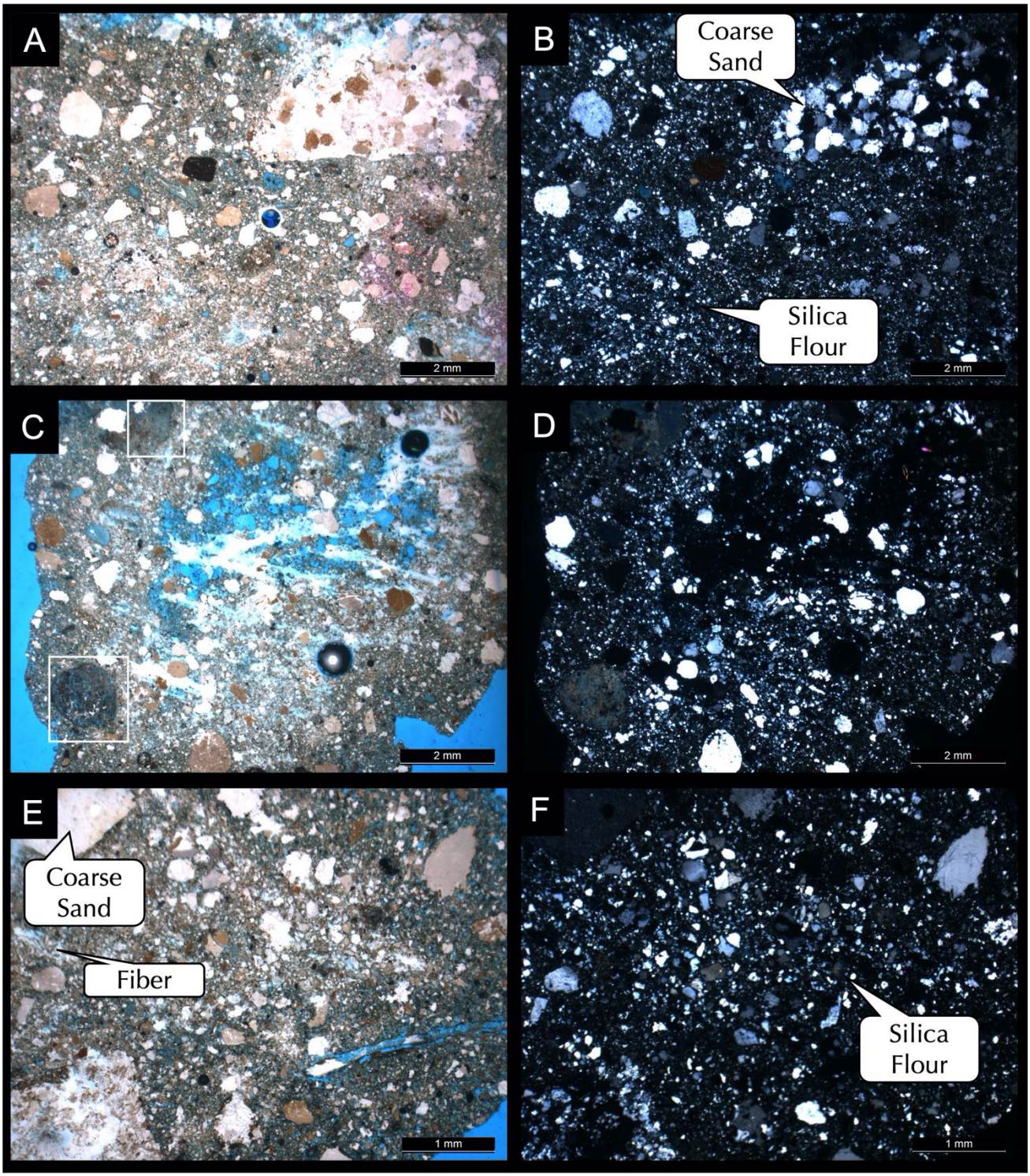

Figure 4 - Thin section micrographs showing A-B: three populations of silica – a coarse (greater than 0.6 mm size) mostly rounded silica sand, a finer subangular to rounded silica sand (less than 0.6 mm), and a finest (less than 0.1 mm) crushed angular silica flour addition as microfiller. C-D: isolated lumps of unmixed lime (boxed). E-F: Coarse to fine sand, silica flour, and occasional fibers. All thin section micrographs from Figures 4 through 9 are shown in pairs of PPL and corresponding XPL images.

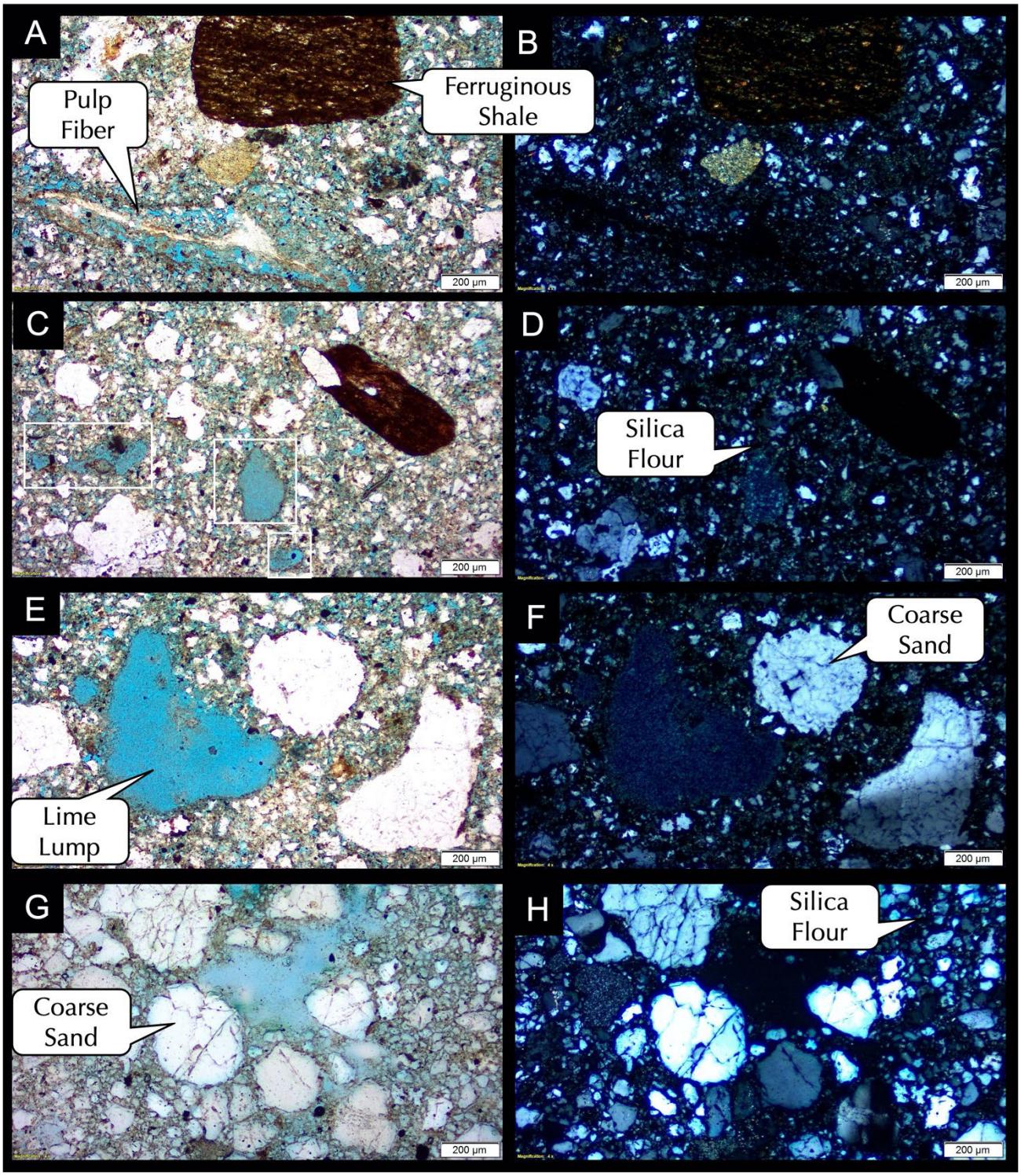

Figure 5 - Thin section micrographs showing trace amount of dark-brown ferruginous shale particle in sand, isolated lumps of unmixed lime, trace pulp fiber, coarse to fine sand, silica flour, and interstitial paste.

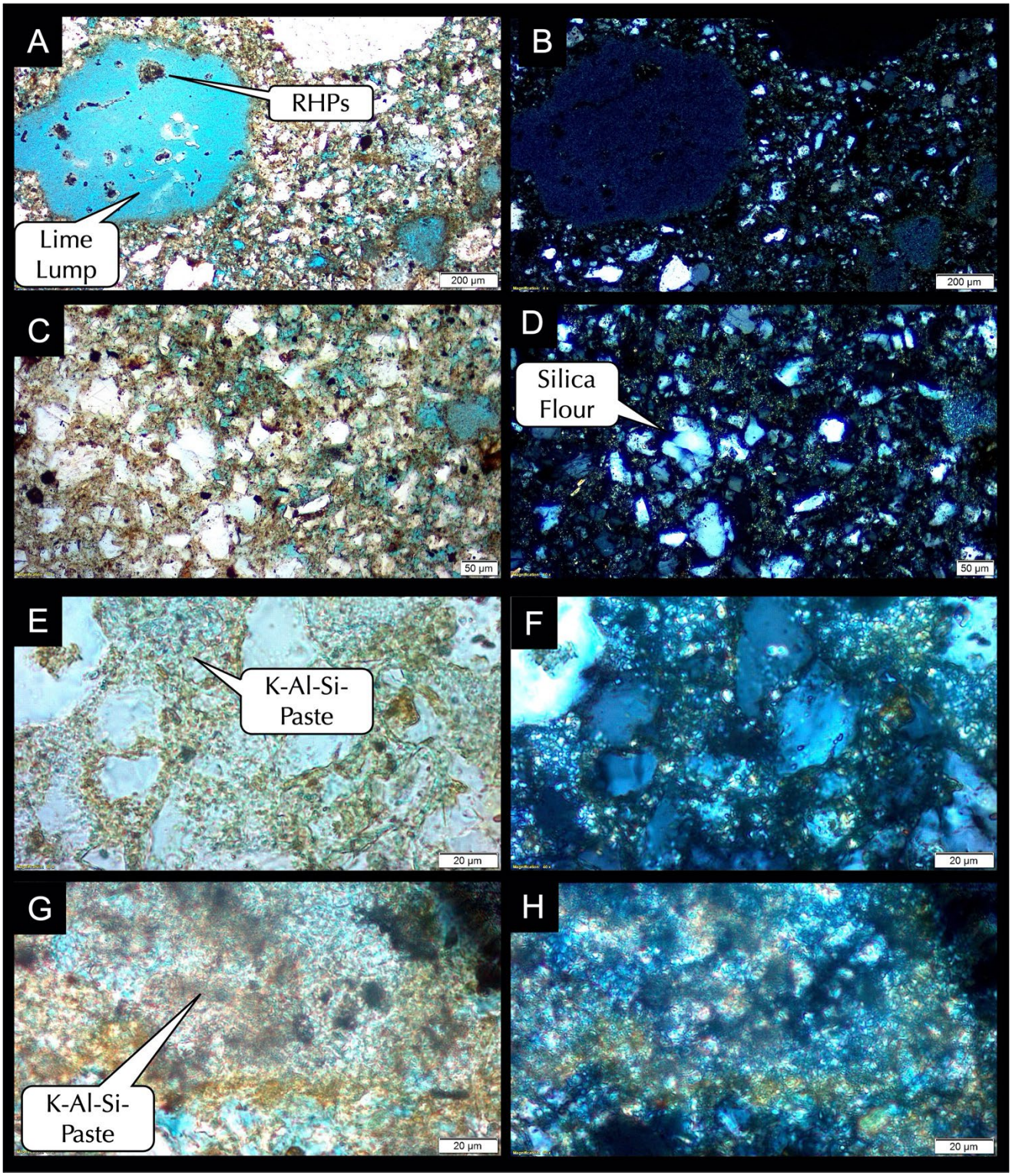

Figure 6 - Thin section micrographs showing interstitial paste fraction between finest silica grains that show carbonated nature from high birefringence of paste (bottom two rows). Subsequent SEM-EDS analyses showed K-Al-Si with variable lime contents of paste, along with heterogeneous distribution of chloride and sulfur from ingress from the environment.

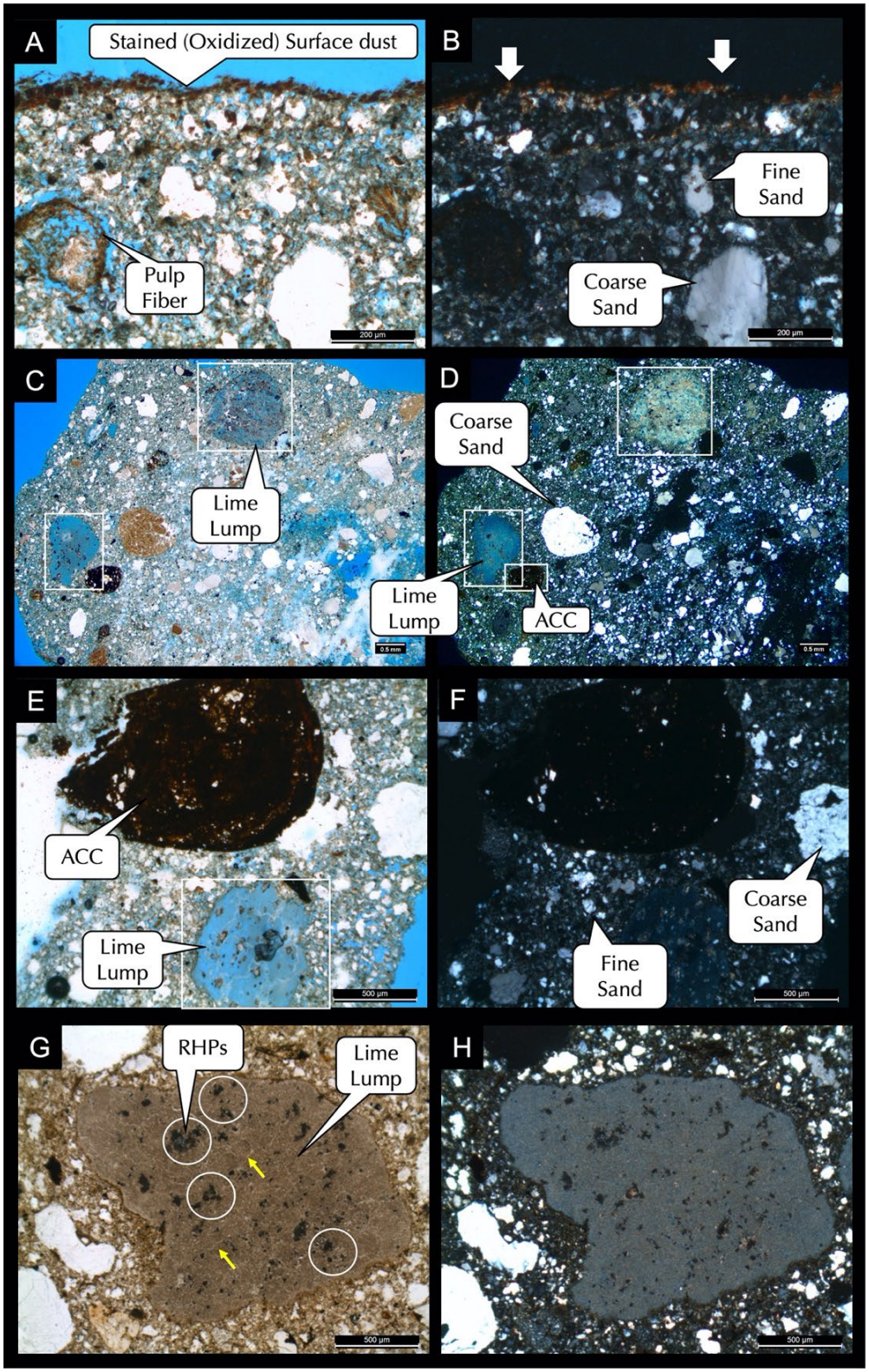

Figure 7 - Thin section micrographs showing A-B: reddish-brown oxidized stains at surface region of the porous mortar where interstitial pore spaces between sand grains are highlighted in blue epoxy in PPL image; XPL image shows overall dark isotropic nature of paste region between the dominant quartz grains in sand. C-D: occasional lime lumps scattered throughout the mortar that are noticeably coarser than even coarser sand grains. E-F: occasional dark-brown argillaceous clay clots (ACCs, e.g., ferruginous shale) and coarse unmixed lime lump (latter contain occasional scattered grains of residual hydraulic phases, RHPs). G-H: A carbonated lime lump at the center having many very fine RHPs (circled) and a few fine hairline carbonation shrinkage microcracks (arrows in 'G').

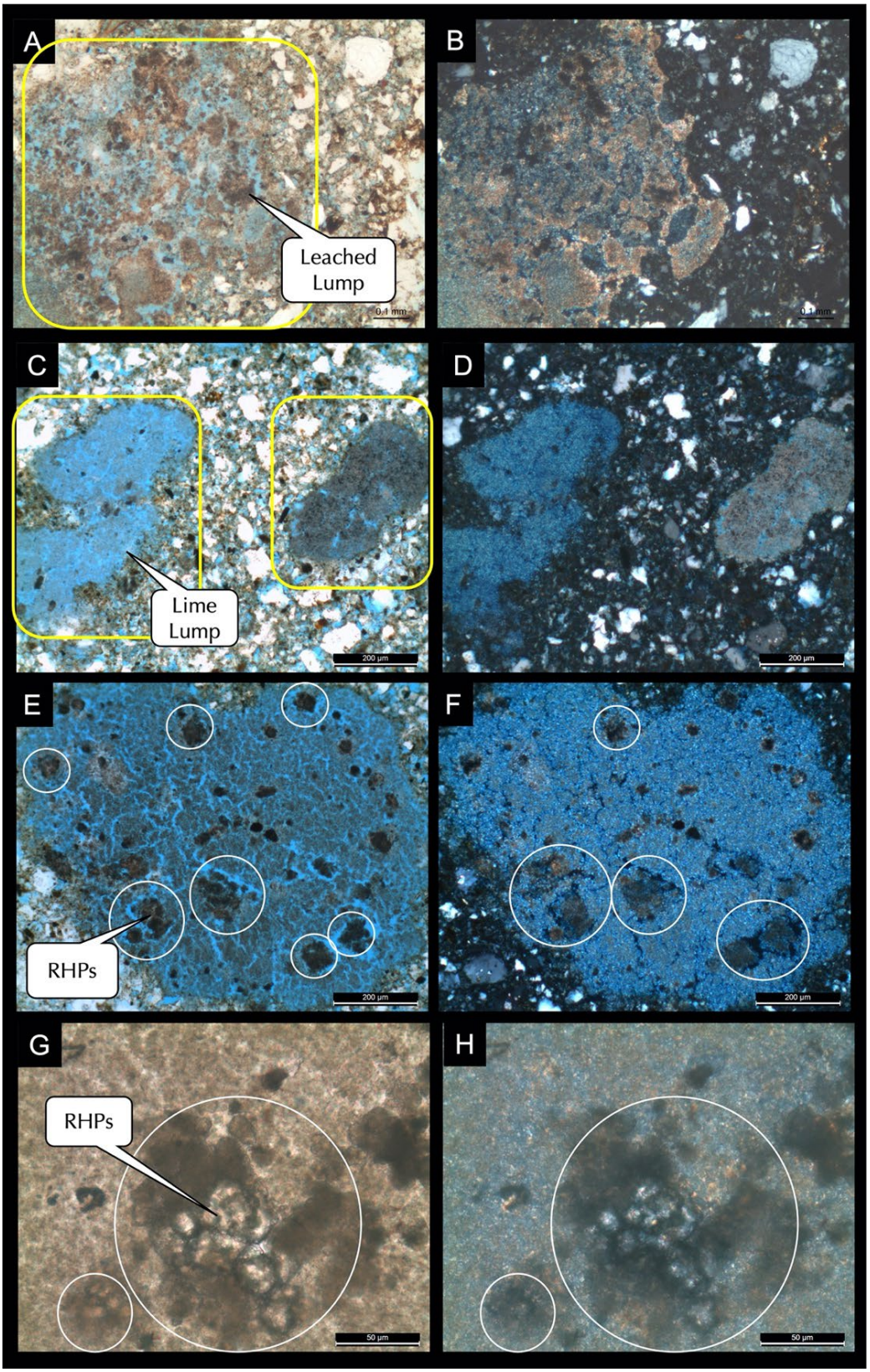

Figure 8 - Thin section micrographs showing A-B: a leached and carbonated lump of lime where most of the lime has leached out leaving a porous skeletal mass. C-D: not so leached or porous lumps of lime as seen in A-B that show characteristic porous, fine-grained, carbonated nature. E-F: RHPs in a lime lump (circled). G-H: RHPs in the same lump showed in E-F but at higher magnification showing residual belite-like granular microstructure of calcium silicate grains and darker rims and interstitial phase.

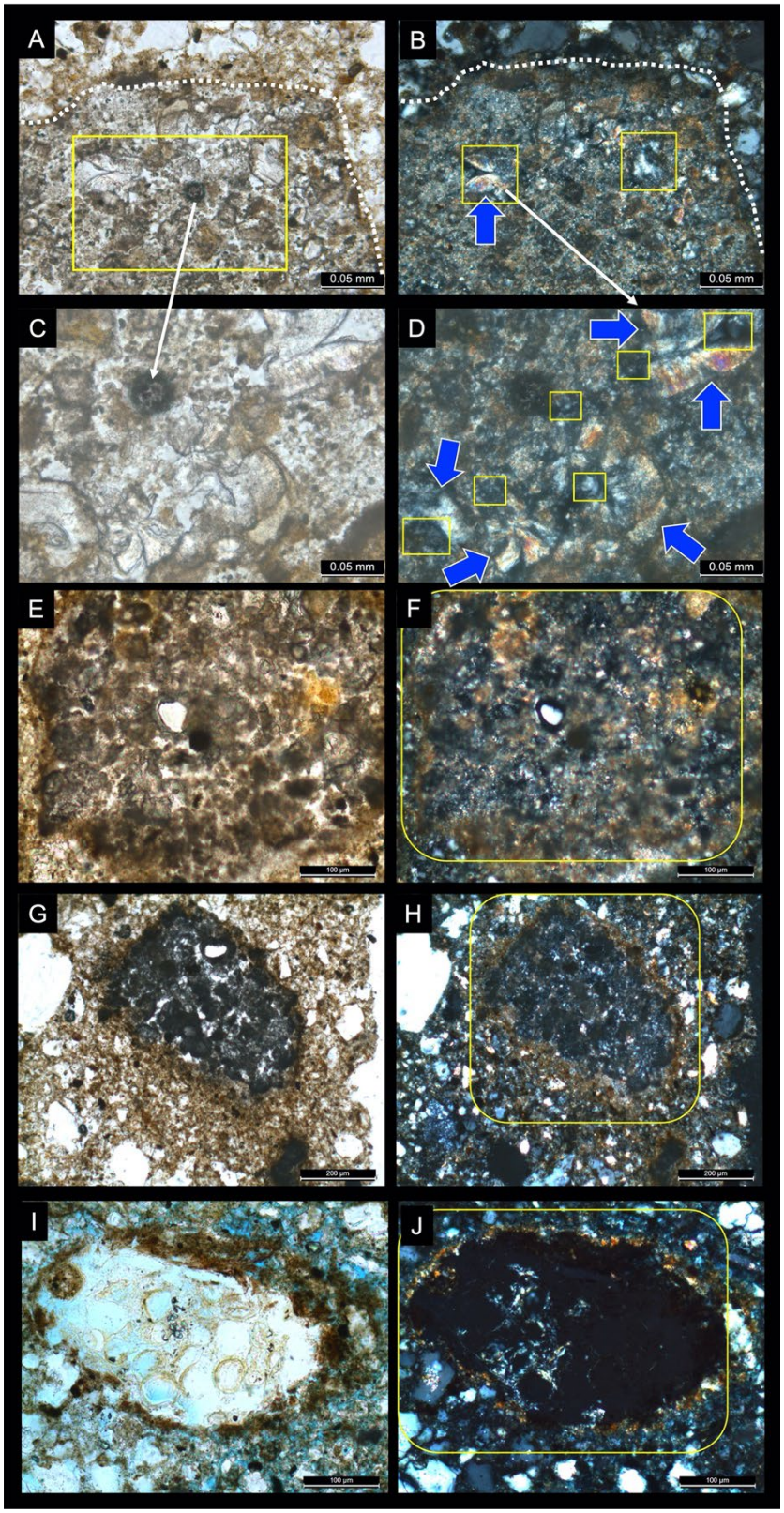

Figure 9 - Thin section micrographs showing A-B: RHPs in a lime lump (separated from the rest of the matrix by dotted line). C-D: At higher magnification showing fibrous, low birefringent nature of hydration products (HPs, occasionally showing higher golden yellow birefringence, arrows) of RHPs. E-F: A leached lump of lime. G-H: A calcined lime showing isotropic amorphous interior surrounded by reddish-brown oxidized rim. I-J: A leached, calcined lime where optically isotropic interior in XPL is from amorphous nature of interior followed by leaching of mass. Various degrees of leaching (leading to increased porosity) and calcination (leading to optically amorphous nature) are seen in many coarse lime grains.

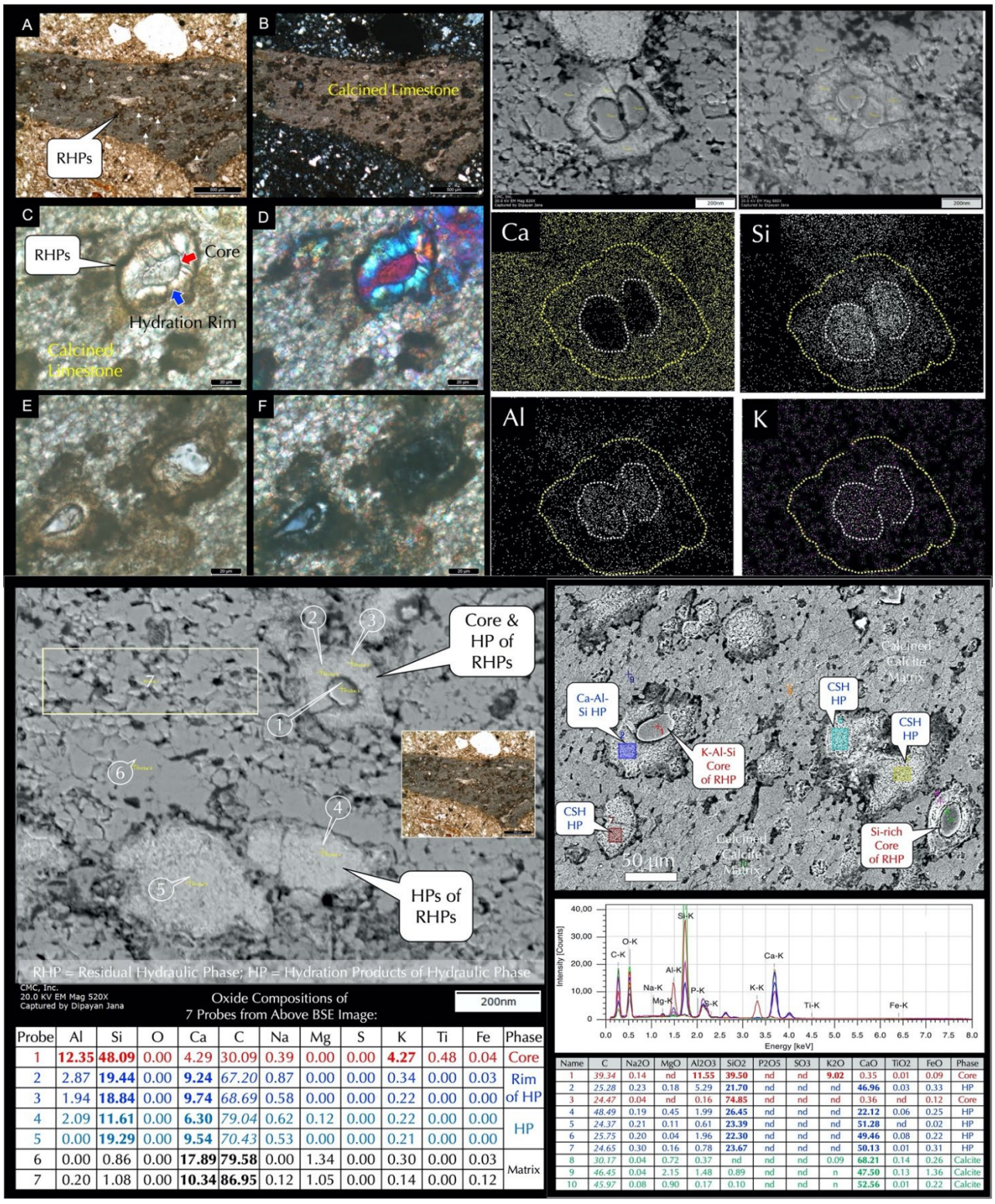

Probe	Al	Si	O	Ca	C	Na	Mg	S	K	Ti	Fe	Phase
1	**12.35**	**48.09**	0.00	4.29	30.09	0.39	0.00	0.00	**4.27**	0.48	0.04	Core
2	2.87	**19.44**	0.00	**9.24**	*67.20*	0.87	0.00	0.00	0.34	0.00	0.03	Rim of HP
3	1.94	**18.84**	0.00	**9.74**	*68.69*	0.58	0.00	0.00	0.22	0.00	0.00	
4	2.09	**11.61**	0.00	**6.30**	*79.04*	0.62	0.12	0.00	0.22	0.00	0.00	HP
5	0.00	**19.29**	0.00	**9.54**	*70.43*	0.53	0.00	0.00	0.21	0.00	0.00	
6	0.00	0.86	0.00	**17.89**	**79.58**	0.00	1.34	0.00	0.30	0.00	0.03	Matrix
7	0.20	1.08	0.00	**10.34**	**86.95**	0.12	1.05	0.00	0.14	0.00	0.12	

Name	C	Na2O	MgO	Al2O3	SiO2	P2O5	SO3	K2O	CaO	TiO2	FeO	Phase
1	*39.34*	0.14	nd	**11.55**	**39.50**	nd	nd	**9.02**	0.35	0.01	0.09	Core
2	*25.28*	0.23	0.18	5.29	**21.70**	nd	nd	nd	**46.96**	0.03	0.33	HP
3	*24.47*	0.04	nd	0.16	**74.85**	nd	nd	nd	0.36	nd	0.12	Core
4	*48.49*	0.19	0.45	1.99	**26.45**	nd	nd	nd	**22.12**	0.06	0.25	HP
5	*24.37*	0.21	0.11	0.61	**23.39**	nd	nd	nd	**51.28**	nd	0.02	HP
6	*25.75*	0.20	0.04	1.96	**22.30**	nd	nd	nd	**49.46**	0.08	0.22	HP
7	*24.65*	0.30	0.16	0.78	**23.67**	nd	nd	nd	**50.13**	0.01	0.31	HP
8	*30.17*	0.04	0.72	0.37	nd	nd	nd	0.09	**68.21**	0.14	0.26	Calcite
9	*46.45*	0.04	2.15	1.48	0.89	nd	nd	n	**47.50**	0.13	1.36	Calcite
10	*45.97*	0.08	0.90	0.17	0.10	nd	nd	n	**52.56**	0.01	0.22	Calcite

Figure 10 - Left column A-F: Thin section micrographs showing an incompletely calcined limestone feed left in the mortar containing many scattered RHPs (A and B), many of which show distinct rounded cores surrounded by fibrous hydration rims (C-F). Right column shows corresponding backscatter and secondary electron images and X-ray elemental maps of central RHPs having K-Al-Si-rich cores surrounded by Ca-Si-Al-rich hydration rims in the overall granular mosaic-textured calcite matrix of limestone. Source of K, Al, and Si in RHPs are probably from calcination of minor K-feldspar impurities in the limestone feed. Bottom: BSE images of calcined limestone showing many scattered RHPs having cores and surrounding hydration products (HPs), or just the HPs showing characteristic chemical variations between potassium aluminosilicate cores and calcium silicate HPs from overall outer calcite matrix presented in the oxide composition Tables (carbon in the analyses is from epoxy used in impregnation, and/or carbonates).

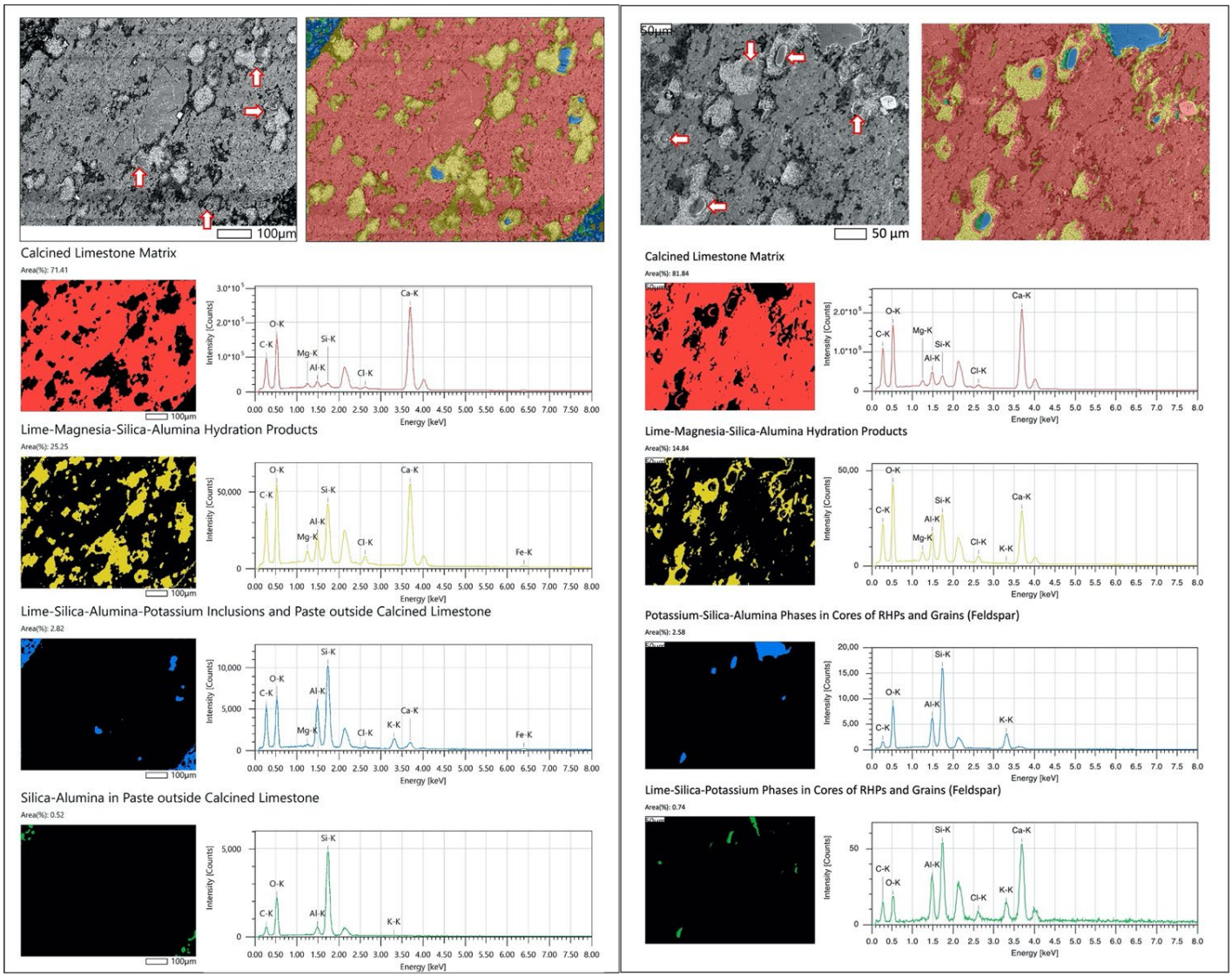

Figure 11 - Cluster phase maps of calcined limestone from two previous Figures containing scattered RHPs and HPs where various color segmented maps are produced depending on variations in overall potassium aluminosilicate compositions of RHPs and lime-rich compositions of HPs in overall calcite matrix. Blue spots in the rounded cores of RHPs are from calcination of K-feldspar impurities in lime. Arrows in BSE images show these cores of RHPs.

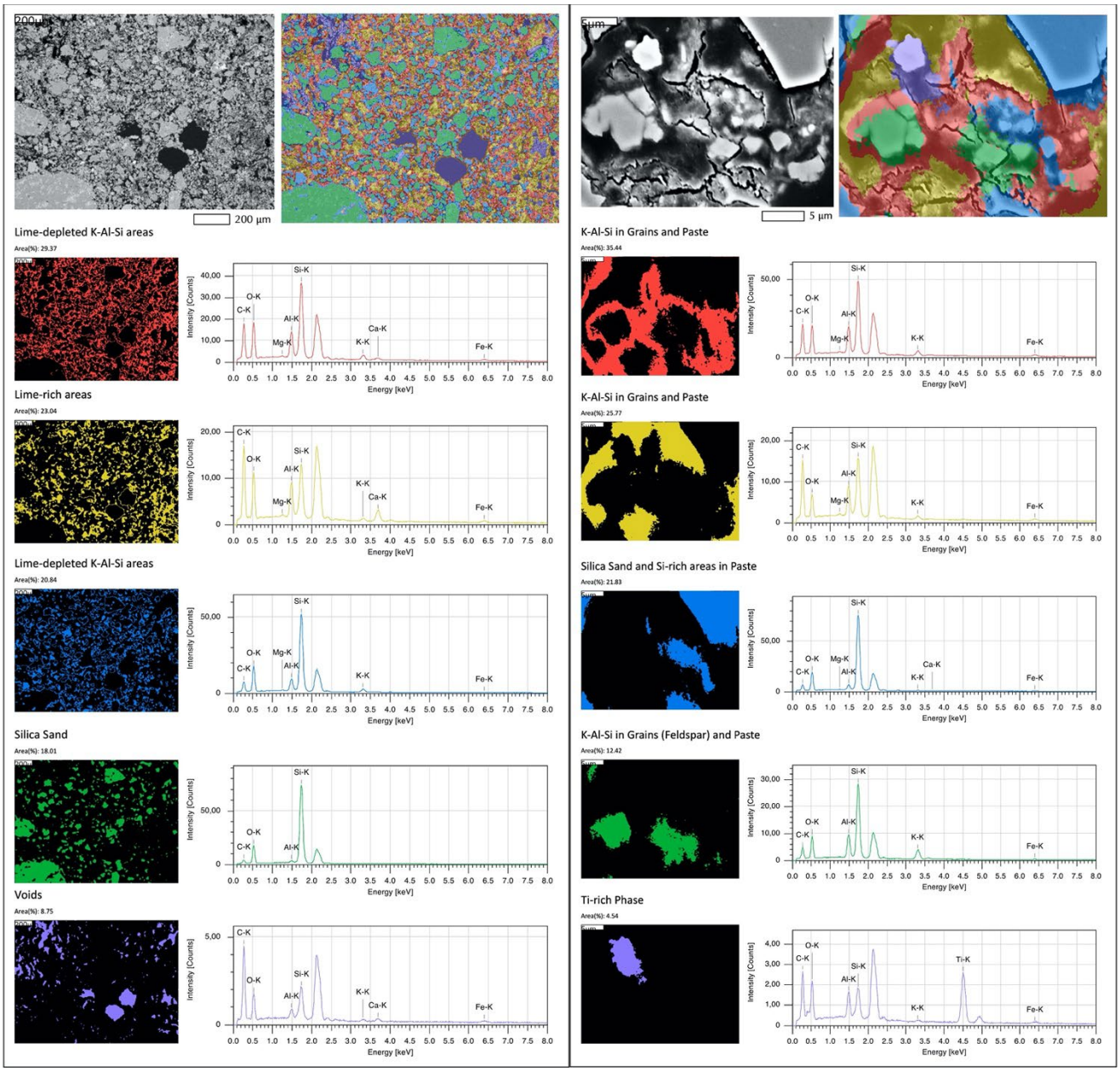

Figure 12 - Cluster phase maps of interstitial paste region between sand grains at low (left) and high (right) magnifications showing overall lime-depleted K-Al-Si-based paste fraction containing patchy areas of lime, silica sands, K-rich areas in paste and in grains (K-feldspar), interstitial voids (8.75 percent area), and trace Ti-rich phase in sand. Various color tones in the paste depicting shrinkage microcracks at right are from variations in lime-depleted potassium-aluminosilicate compositions of paste.

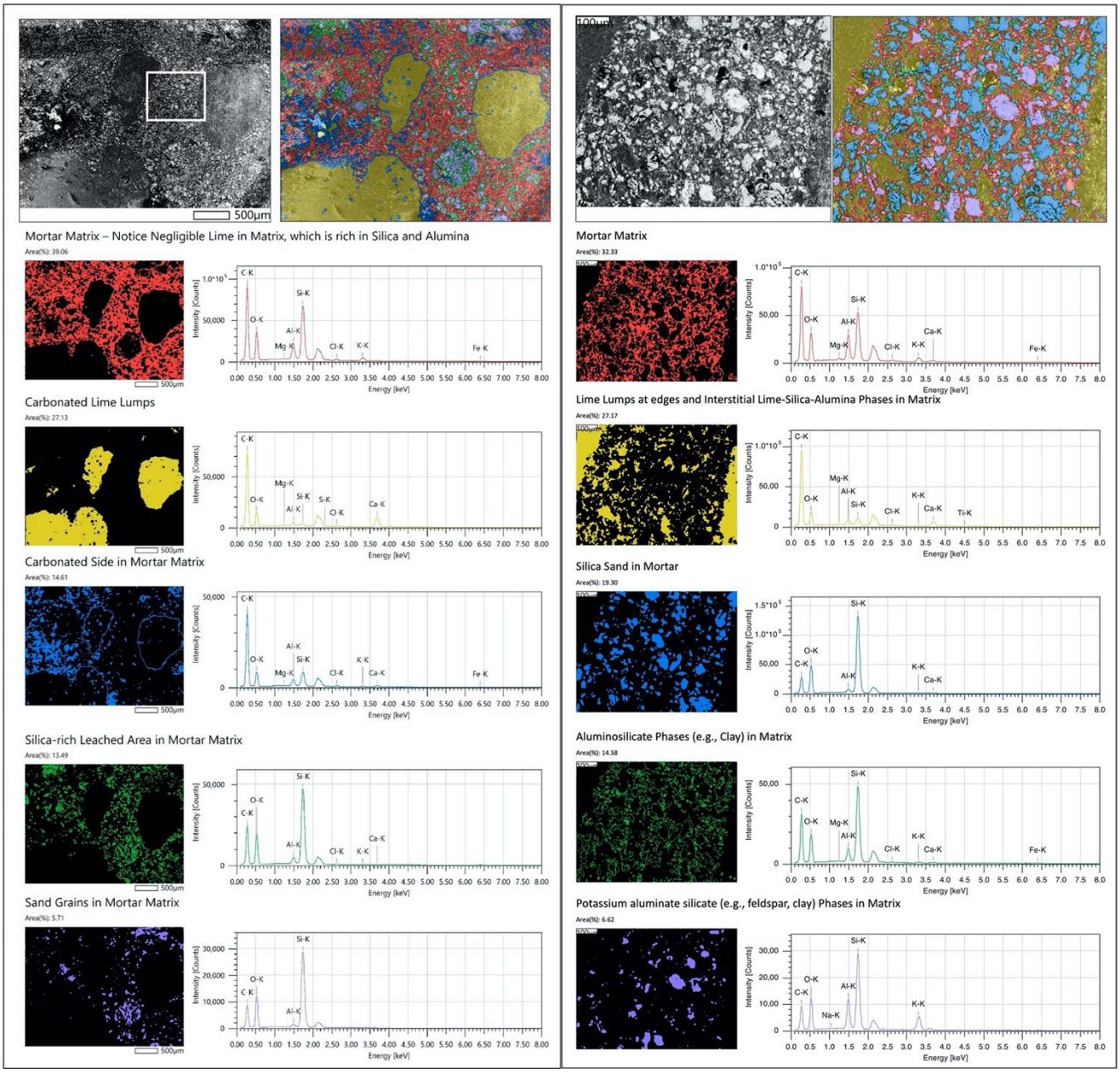

Figure 13 - Cluster phase maps of carbonated lime lumps scattered in lime-depleted aluminosilicate mortar matrix which shows silica sand grains, silica-rich leached areas of paste, and aluminosilicate (possibly from clay) areas in paste. Potassium-rich areas are from K-feldspar grains in sand and K-Al-Si-rich areas in paste. Boxed area at left BSE image is enlarged at right.

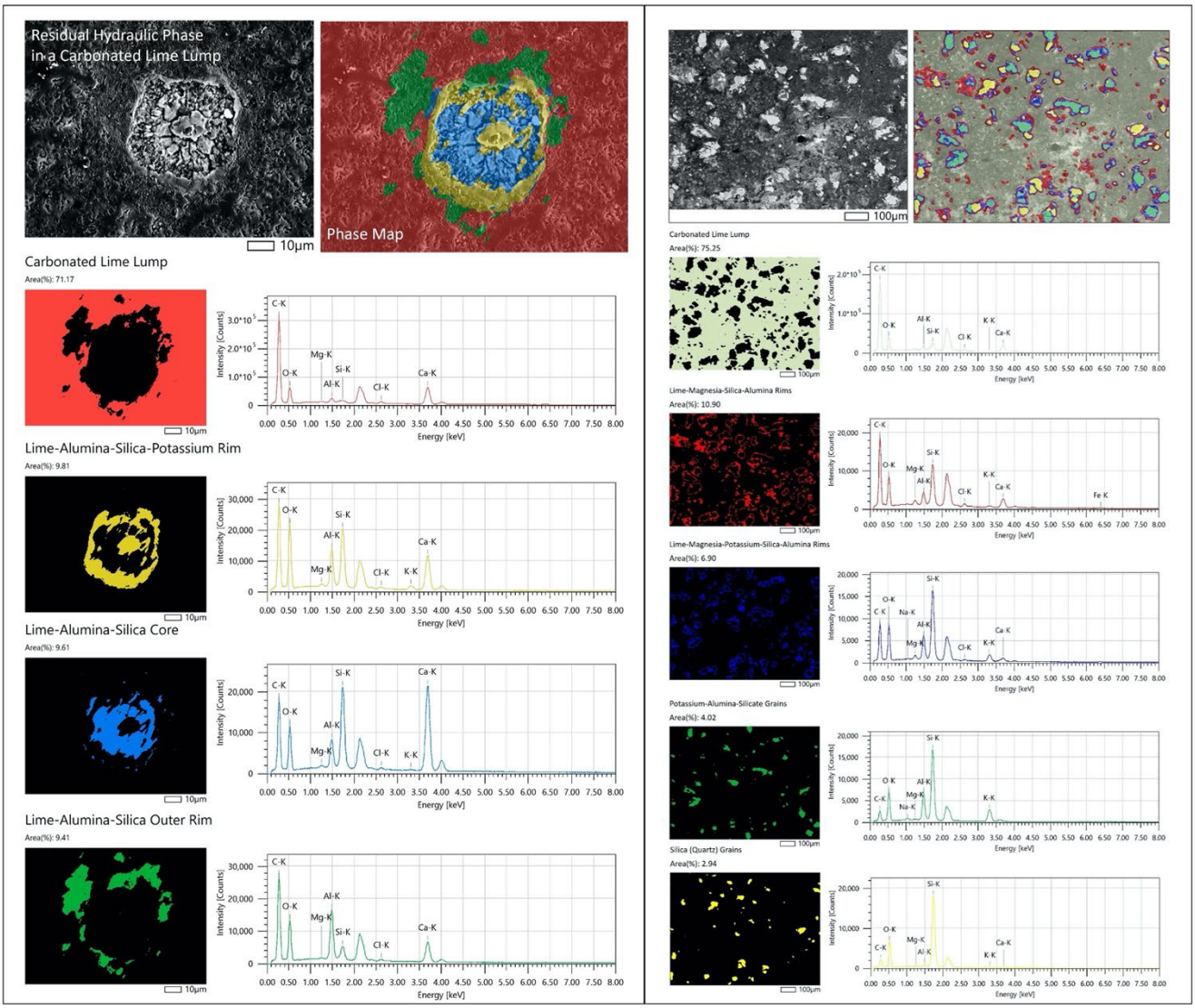

Figure 14 - Left: Anatomy of an infinitesimally small RHP in a carbonated lime lump showing chemical variations from different proportions of Ca-K-Al-Si-Mg produced from hydration and carbonation of original hydraulic phases. Notice concentric zonation in chemistry of hydration products in the color maps from variations in Si/Al and Ca/Si ratios. Right: At a lower magnificent of the same lime lump showing many scattered grains of RHPs and fine silica grains in lump representing original impurities in the calcined limestone feed. Notice small chlorine peaks from chloride ingress in mortar.

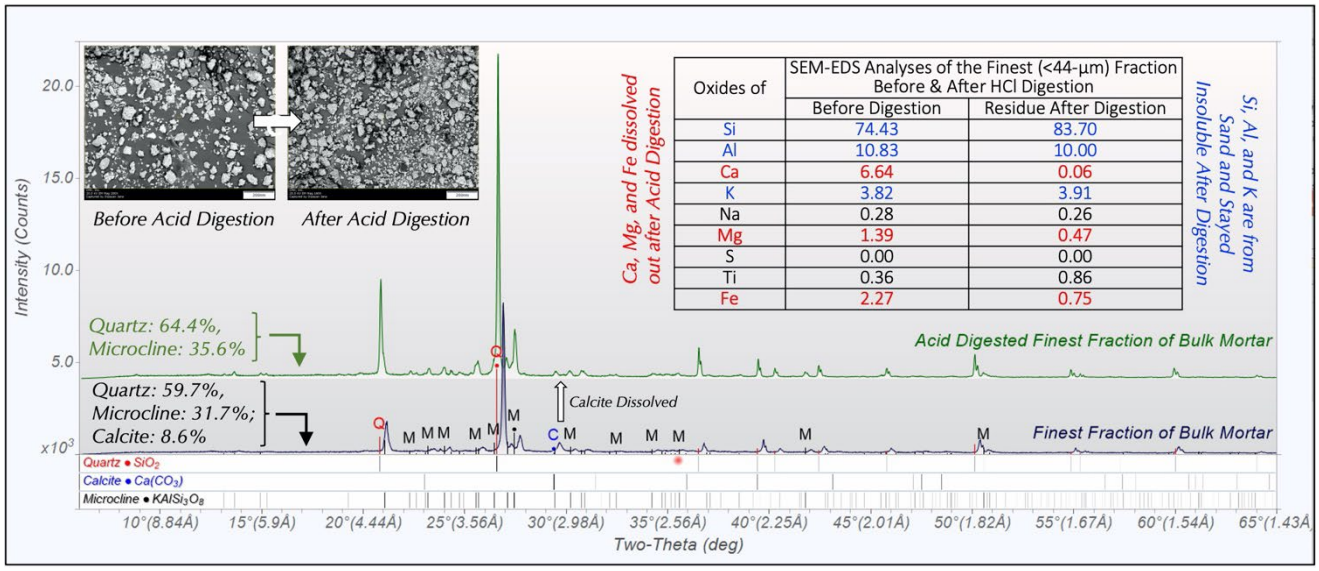

Oxides of	SEM-EDS Analyses of the Finest (<44-μm) Fraction Before & After HCl Digestion	
	Before Digestion	Residue After Digestion
Si	74.43	83.70
Al	10.83	10.00
Ca	6.64	0.06
K	3.82	3.91
Na	0.28	0.26
Mg	1.39	0.47
S	0.00	0.00
Ti	0.36	0.86
Fe	2.27	0.75

Figure 15 - In search of the source of the beige color tone, potential presence of clay, and acid soluble components of the mortar, the finest (less than 44-μm) fraction and its residue after hydrochloric acid digestion were analyzed by XRD and SEM-EDS to determine the elements/minerals that were dissolved out. Results showed the dominance of quartz and subordinate K-feldspar in the finest fraction as well as in its residue (as also seen in the bulk mortar after digestion, shown in next Figure) except disappearance of calcite in the residue and hence severe loss of Ca along with Mg and Fe in the residue indicating their presence in the lime (i.e., the acid-soluble component) as opposed to sand (i.e., the acid insoluble component, which contained Si, Al, and K from quartz and K-feldspar).

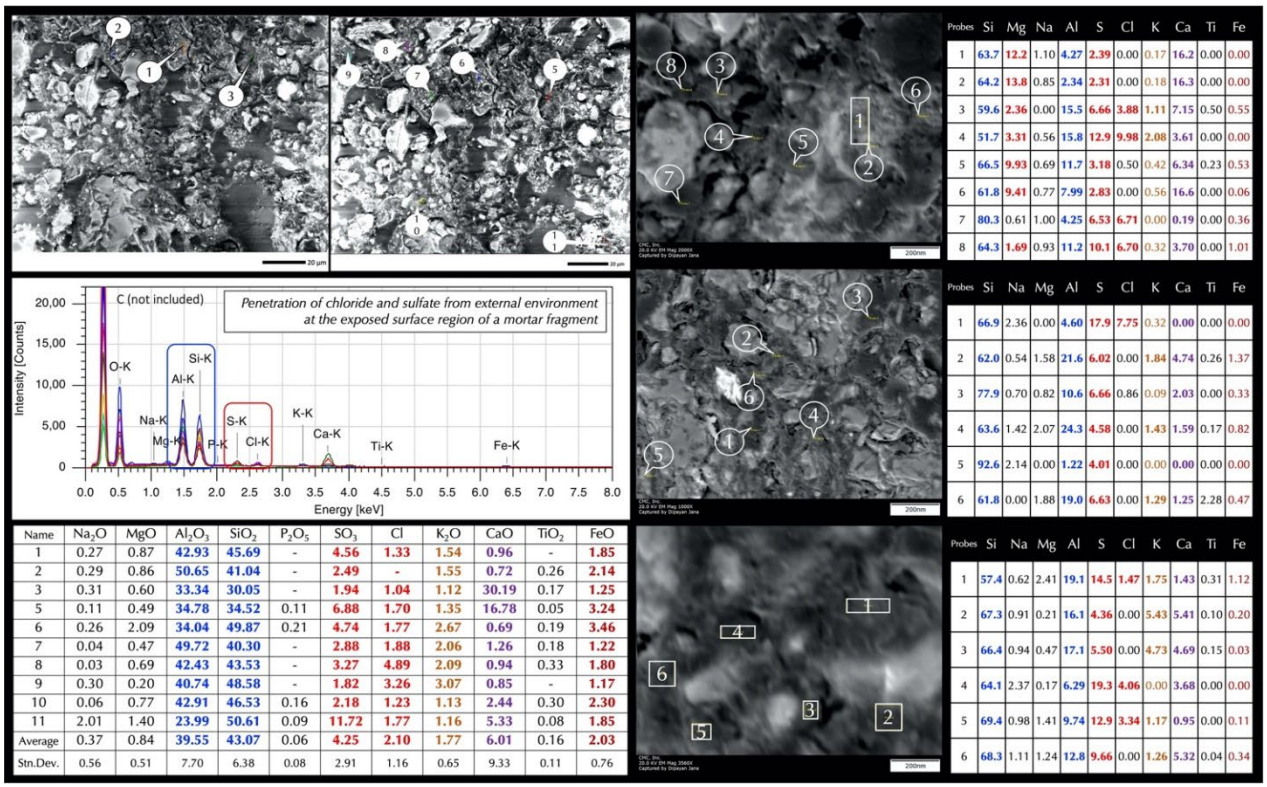

Probes	Si	Mg	Na	Al	S	Cl	K	Ca	Ti	Fe
1	63.7	12.2	1.10	4.27	2.39	0.00	0.17	16.2	0.00	0.00
2	64.2	13.8	0.85	2.34	2.31	0.00	0.18	16.3	0.00	0.00
3	59.6	2.36	0.00	15.5	6.66	3.88	1.11	7.15	0.50	0.55
4	51.7	3.31	0.56	15.8	12.9	9.98	2.08	3.61	0.00	0.00
5	66.5	9.93	0.69	11.7	3.18	0.50	0.42	6.34	0.23	0.53
6	61.8	9.41	0.77	7.99	2.83	0.00	0.56	16.6	0.00	0.06
7	80.3	0.61	1.00	4.25	6.53	6.71	0.00	0.19	0.00	0.36
8	64.3	1.69	0.93	11.2	10.1	6.70	0.32	3.70	0.00	1.01

Probes	Si	Na	Mg	Al	S	Cl	K	Ca	Ti	Fe
1	66.9	2.36	0.00	4.60	17.9	7.75	0.32	0.00	0.00	0.00
2	62.0	0.54	1.58	21.6	6.02	0.00	1.84	4.74	0.26	1.37
3	77.9	0.70	0.82	10.6	6.66	0.86	0.09	2.03	0.00	0.33
4	63.6	1.42	2.07	24.3	4.58	0.00	1.43	1.59	0.17	0.82
5	92.6	2.14	0.00	1.22	4.01	0.00	0.00	0.00	0.00	0.00
6	61.8	0.00	1.88	19.0	6.63	0.00	1.29	1.25	2.28	0.47

Probes	Si	Na	Mg	Al	S	Cl	K	Ca	Ti	Fe
1	57.4	0.62	2.41	19.1	14.5	1.47	1.75	1.43	0.31	1.12
2	67.3	0.91	0.21	16.1	4.36	0.00	5.43	5.41	0.10	0.20
3	66.4	0.94	0.47	17.1	5.50	0.00	4.73	4.69	0.15	0.03
4	64.1	2.37	0.17	6.29	19.3	4.06	0.00	3.68	0.00	0.00
5	69.4	0.98	1.41	9.74	12.9	3.34	1.17	0.95	0.00	0.11
6	68.3	1.11	1.24	12.8	9.66	0.00	1.26	5.32	0.04	0.34

Name	Na_2O	MgO	Al_2O_3	SiO_2	P_2O_5	SO_3	Cl	K_2O	CaO	TiO_2	FeO
1	0.27	0.87	42.93	45.69	-	4.56	1.33	1.54	0.96	-	1.85
2	0.29	0.86	50.65	41.04	-	2.49	-	1.55	0.72	0.26	2.14
3	0.31	0.60	33.34	30.05	-	1.94	1.04	1.12	30.19	0.17	1.25
5	0.11	0.49	34.78	34.52	0.11	6.88	1.70	1.35	16.78	0.05	3.24
6	0.26	2.09	34.04	49.87	0.21	4.74	1.77	2.67	0.69	0.19	3.46
7	0.04	0.47	49.72	40.30	-	2.88	1.88	2.06	1.26	0.18	1.22
8	0.03	0.69	42.43	43.53	-	3.27	4.89	2.09	0.94	0.33	1.80
9	0.30	0.20	40.74	48.58	-	1.82	3.26	3.07	0.85	-	1.17
10	0.06	0.77	42.91	46.53	0.16	2.18	1.23	1.13	2.44	0.30	2.30
11	2.01	1.40	23.99	50.61	0.09	11.72	1.77	1.16	5.33	0.08	1.85
Average	0.37	0.84	39.55	43.07	0.06	4.25	2.10	1.77	6.01	0.16	2.03
Stn.Dev.	0.56	0.51	7.70	6.38	0.08	2.91	1.16	0.65	9.33	0.11	0.76

Figure 16 - EDS chemical (oxide) variations in paste fraction showing characteristic aluminosilicate composition and excess sulfate and chloride contents at the surface region from influence of environment during service. Notice large variation in lime contents from combined actions of carbonation and leaching, overall depletion in Ca and enrichment in Si-Al in paste from lime leaching. Potassium and iron oxides are from RHPs/HPs/K-feldspar and an iron oxide-based component in the original lime (not a separate pigment) responsible for imparting the brown color tone, respectively. Low magnesia content indicates use of a calcite lime binder.

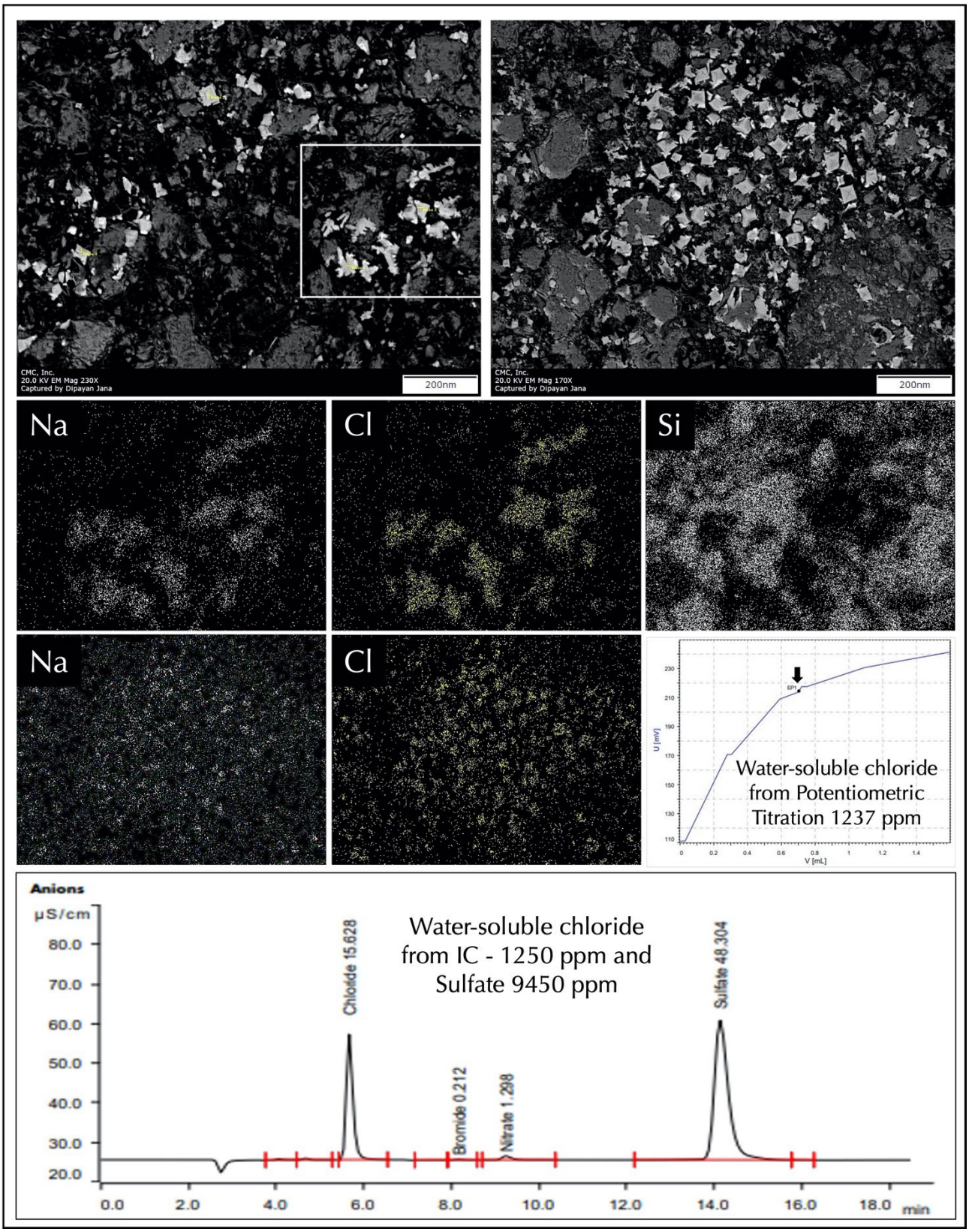

Figure 17 - Evidence of chloride contamination in mortar and subsequent salt crystallization in the BSE images depicting perfect cubic shape of halite crystals and enriched Na and Cl grains in X-ray elementals maps. Potentiometric titration of deionized water digested pulverized mortar against silver nitrate titrant showed 1237-ppm water-soluble chloride, whereas anion chromatography of filtrate showed 1250-ppm chloride and 9450-ppm sulfate.

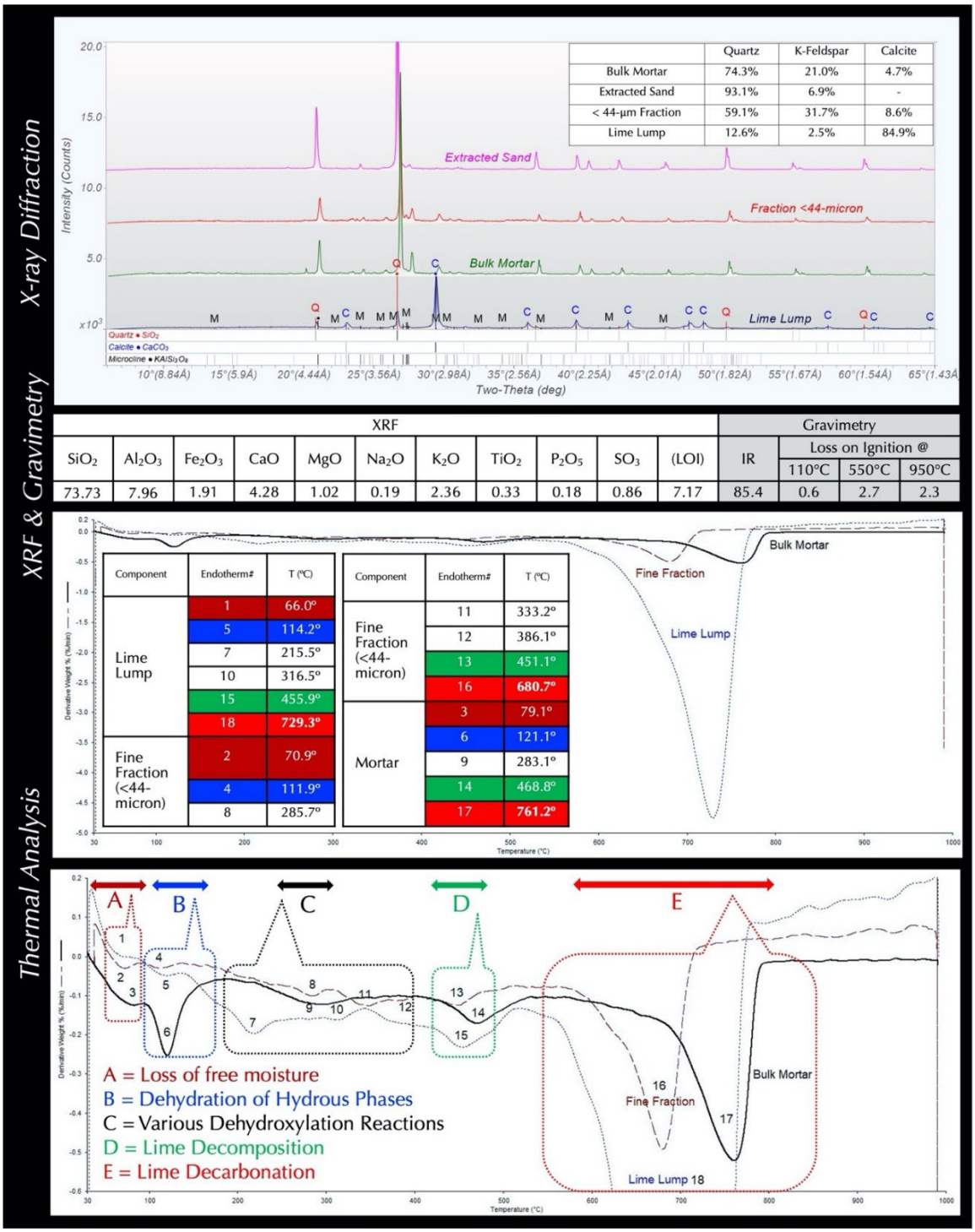

	Quartz	K-Feldspar	Calcite
Bulk Mortar	74.3%	21.0%	4.7%
Extracted Sand	93.1%	6.9%	-
< 44-µm Fraction	59.1%	31.7%	8.6%
Lime Lump	12.6%	2.5%	84.9%

XRF											Gravimetry			
SiO_2	Al_2O_3	Fe_2O_3	CaO	MgO	Na_2O	K_2O	TiO_2	P_2O_5	SO_3	(LOI)	IR	Loss on Ignition @		
												110°C	550°C	950°C
73.73	7.96	1.91	4.28	1.02	0.19	2.36	0.33	0.18	0.86	7.17	85.4	0.6	2.7	2.3

Component	Endotherm#	T (°C)
Lime Lump	1	66.0°
	5	114.2°
	7	215.5°
	10	316.5°
	15	455.9°
	18	**729.3°**
Fine Fraction (<44-micron)	2	70.9°
	4	111.9°
	8	285.7°

Component	Endotherm#	T (°C)
Fine Fraction (<44-micron)	11	333.2°
	12	386.1°
	13	451.1°
	16	**680.7°**
Mortar	3	79.1°
	6	121.1°
	9	283.1°
	14	468.8°
	17	**761.2°**

Figure 18 -Top: Superposed XRD patterns of bulk mortar, extracted white lumps of unmixed lime, extracted sand after acid digestion, and finest (less than 44-micron) fraction of mortar showing: (a) dominant quartz and subordinate K-feldspar composition of extracted sand after acid digestion, (b) overall similarities in patterns of extracted sand and bulk mortar for dominant (greater than 85 percent) volume proportion of sand, (c) absence of any characteristic clay peaks and dominance of ultrafine quartz in the finest fraction (less than 44-µm) of mortar, and (d) calcite mineralogy of carbonated lime lump indicating calcination of a calcitic limestone feed. Rietveld mineral percent of bulk mortar showed 70 percent quartz, 25 percent K-feldspar (microcline) and 10 percent calcite. Middle: XRF chemical composition and gravimetric (acid-insoluble residue content and losses on ignition at 110°C, 550°C, and 950°C) results of mortar. Bottom: Superposed DTG curves of bulk mortar, lime lump, and finest (less than 44-µm) fraction showing characteristic endotherms from (a) loss of free water, (b) dehydration of hydration products of RHPs, (c) various dehydroxylation reactions, (d) decomposition of calcium hydroxide component of lime, and (e) decarbonation of lime lumps and interstitial carbonated lime products in paste.

REFERENCES

ASTM C 144 (2017). ASTM C 144, "Standard Specification for Aggregate for Masonry Mortar:" Annual Book of ASTM Standards, Section Four Construction, Vol. 04.05: Chemical-Resistant Nonmetallic Materials; Vitrified Clay Pipe; Concrete Pipe; Fiber-Reinforced Cement Products; Mortars or Mortars and Grouts; Masonry; Precast Concrete; ASTM Committee C12 on Mortars or mortars for Unit Masonry, ASTM International; West Conshohocken, PA; 2017.

ASTM C 207 (2011). ASTM C 207; "Standard Specification for Hydrated Lime for Masonry Purposes;" Annual Book of ASTM Standards, Section Four Construction, Vol. 04.01; ASTM Subcommittee C07.02; ASTM International; West Conshohocken, PA; 2011.

ASTM C 1324 (2017). ASTM C 1324, "Standard Test Method for Examination and Analysis of Hardened Masonry Mortar;" Annual Book of ASTM Standards, Section Four Construction, Vol. 04.05; Chemical-Resistant Nonmetallic Materials; Vitrified Clay Pipe; Concrete Pipe; Fiber-Reinforced Cement Products; Mortars or mortars and Grouts; Masonry; Precast Concrete; ASTM Committee C12 on Mortars or mortars for Unit Masonry, ASTM International; West Conshohocken, PA; 2017.

ASTM C 1489 (2015). ASTM C 1489; "Standard Specification for Lime Putty for Structural Purposes;" Annual Book of ASTM Standards; Section Four Construction, Vol. 04.01; ASTM Subcommittee C07.02; ASTM International; West Conshohocken, PA;2015.

ASTM C 1713 (2017). ASTM C 1713, "Standard Specification for Mortars or mortars for the Repair of Historic Masonry;" Annual Book of ASTM Standards, Section Four Construction, Vol. 04.05 Chemical-Resistant Nonmetallic Materials; Vitrified Clay Pipe; Concrete Pipe; Fiber-Reinforced Cement Products; Mortars or mortars and Grouts; Masonry; Precast Concrete; ASTM Committee C12 on Mortars or mortars and Grouts for Unit Masonry; ASTM International; West Conshohocken, PA; 2017.

ASTM C 1723 (2017). ASTM C 1723; "Standard Guide for Examination of Hardened Concrete Using Scanning Electron Microscopy;" Annual Book of ASTM Standards; Section Four Construction, Vol. 04.02; ASTM Subcommittee C 9.65; ASTM International; West Conshohocken, PA; 2017.

Bartos, P. et al. (2000). Bartos, P, Groot, C, Hughes, JJ (Eds.); *Historic Mortars or mortars: Characteristics and Tests*, Proceedings PRO12, RILEM Publications, France, 2000.

Elsen, J. (2006). Elsen, J., "Microscopy of Historic Mortars or mortars – A Review"; *Cement and Concrete Research* 36, pps. 1416-1424; Elsevier; Amsterdam, The Netherlands; 2006.

Elsen, J. et al. (2012). Elsen, J., Van Balen. K. and Mertens. G.; "Hydraulicity in Historic Lime Mortars or mortars: A Review"; Valek, J, Hughes, J.J., and Groot, W.P. (Eds.); *Historic Mortars Characterization, Assessment and Repair*, RILEM Book series, Volume 7, pps. 125-139; Springer; Berlin, Germany; 2012.

Erlin, B., and Hime, W.G. (1987). Erlin, B. and Hime, W.G.; "Evaluating Mortar Deterioration;" *APT Bulletin*, Vol. 19, No. 4, pps. 8-10; Applied Technology Council; Redwood City, CA; 1987.

Goins, E.S. (2004). Goins, E.S., "Standard Practice for Determining the Components of Historic Cementitious Materials;" *National Center for Preservation Technology and Training, Materials Research Series*; NCPTT; Natchitoches, La; 2004.

Groot, C. et al. (2004). Groot, C., Ashall, G. and Hughes, J.; "Characterization of Old Mortars or mortars with Respect to Their Repair"; *State-of-the-art Report of RILEM Technical Committee 167-COM*; RILEM Publications; France; 2004.

Hughes, J.J. et al. (2001). Hughes, J.J., Leslie, A.B. and Callebaut, K.; "The Petrography of Lime Inclusions in Historic Lime-Based Mortars;" *Annales Geologiques des pays Helleniques, Edition Speciale*; ISSN: 1105-004, pps. 359-364; Laboratoire de géologie de l'Université; Greece; 2001.

Jana, D. (2005). Jana, D.; "Application of Petrography in Restoration of Historic Masonry Structures"; Hughes, J.J., Lesie, A.B. and Walsh, J.A., Eds.; *Proceedings of 10th Euroseminar on Microscopy Applied to Building Materials*; Paisley Publishing Ltd.; Edinburgh, Scotland; 2005.

Jana, D. (2006). Jana, D., "Sample Preparation Techniques in Petrographic Examinations of Construction Materials: A State-of-the-Art Review"; *Proceedings of the 28th Conference on Cement Microscopy;* pps. 23-70; International Cement Microcopy Association; Denver, CO; 2006.

Jana, D., and Mahajan, S.N. (2024). Jana, D. and Mahajan, S.N.; "Laboratory Testing of Historic Mortars: Part 1 - A Close Look to a 200-year-old Historic Clay-Lime Mortar"; *The Masonry Society Journal*; Vol.42, No.1; Longmont, CO; 2024.

Leslie, A.B., and Hughes, J.J. (2001). Leslie, A.B. and Hughes, J.J.; "Binder Microstructure in Lime Mortars: Implications for the Interpretation of Analysis Results"; *Quarterly Journal of Engineering Geology & Hydrogeology*; V. 35, No. 3, pps. 257-263; Geological Society of London; London, Great Britain; 2001.

Middendorf, B. et al. (2000). Middendorf, B., Baronio, G., Callebaut, K. and Hughes, J.J.; "Chemical-Mineralogical and Physical-Mechanical Investigation of Old mortars or mortars: Proceedings of the International RILEM workshop; *Historic Mortars or mortars: Characteristics and Tests*; pps. 53-61; Paisley Publishing Ltd.; Edinburgh, Scotland; 2000.

Middendorf, B. et al. (2005a). Middendorf, B., Hughes, J.J., Callebaut, K., Baronio, G. and Papayanni, I.; "Investigative Methods for the Characterization of Historic Mortars or mortars – Part 1: Mineralogical Characterization;" *Materials and Structures*; Vol. 38; RILEM Publications; France; 2005a.

Middendorf, B. et al. (2005b). Middendorf, B., Hughes, J.J., Callebaut, K., Baronio, G. and Papayanni, I.; "Investigative Methods for the Characterization of Historic Mortars or mortars – Part 2: Chemical Characterization;" *Materials and Structures*; Vol. 38, pps. 771-780; RILEM Publications; France; 2005b.

Middendorf, B. et al. (2004b). Middendorf, B., Hughes, J.J., Callebaut, K., Baronio, G. and Papayanni, I., "Chemical Characterization of Historic Mortars or mortars"; Groot, C., et al. (Eds.); *Characterization of Old Mortars or mortars with Respect to Their Repair*; State-of-the-Art Report of RILEM Technical Committee 167-COM; pps. 37-53; RILEM Publications; France; 2004b.

Middendorf, B. et al. (2004a). Middendorf, B., Hughes, J.J., Callebaut, K., Baronio, G. and Papayanni, I.; "Mineralogical Characterization of Historic Mortars or mortars"; Groot, C., et al. (Eds.); *Characterization of Old Mortars or mortars with Respect to Their Repair*; State-of-the-Art Report of RILEM Technical Committee 167-COM; pps. 21-36; RILEM Publications; France; 2004a.

Valek, J. et al. (2012). Valek, J., Hughes, J.J. and Groot, C. (Eds.); *Historic Mortars or mortars: Characterization, Assessment and Repair*; Springer, RILEM Book series Vol. 7, 464 p; RILEM Publications; France; 2012.

Valek, J., and Matas, T. (2010). Valek, J. and Matas, T.; "Experimental Study of Hot Mixed Mortars in Comparison with Lime Putty and Hydrate Mortars"; *2nd Historic Mortars Conference HMC2010 and RILEM TC 203-RHM Final Workshop* 22-24 September; Prague, Czech Republic; pps. 1229-1240; RILEM Publications; France; 2010.